COMMITTEE CERTIFICATION OF APPROVED VERSION

The committee for Norelle Christine Wildburger certifies that this is the approved version of the following dissertation:

HUMAN MESENCHYMAL STEM CELL HOMING TO GLIOMA STEM CELL XENOGRAFTS

Committee:

Carol L. Nilsson, M.D., Ph.D.

Roger A. Kroes, Ph.D.

Mark R. Emmett, Ph.D.

Charles A. Conrad, M.D.

Giulio Taglialatela, Ph.D.

Frederick F. Lang Jr., M.D.

Owen Hamill, Ph.D.

Robert L. Ullrich, Ph.D.

David Niesel, Ph.D.
Dean, Graduate School

HUMAN MESENCHYMAL STEM CELL HOMING TO GLIOMA STEM CELL XENOGRAFTS

by

Norelle Christine Wildburger
Department of Pharmacology and Toxicology, Neuroscience Graduate Program
University of Texas, Galveston Texas

Dissertation
Presented to the Faculty of The University of Texas Graduate School of
Biomedical Sciences at Galveston
in Partial Fulfillment of the Requirements
for the Degree of

Doctor of Philosophy

Approved by the Supervisory Committee

Carol L. Nilsson, M.D., Ph.D.
Mark R. Emmett, Ph.D.
Giulio Taglialatela, Ph.D.
Owen Hamill, Ph.D.
Roger A. Kroes, Ph.D.
Charles A. Conrad, M.D.
Frederick F. Lang Jr., M.D.
Robert L. Ullrich, Ph.D.

June, 2015
Galveston, Texas

Key Words: Glioblastoma, Glioma stem cells, xenografts, bone marrow-derived mesenchymal stem cells, homing, lipidomics, proteomics, transcriptomics

HUMAN MESENCHYMAL STEM CELL HOMING TO GLIOMA STEM CELL XENOGRAFTS

Norelle Christine Wildburger

Department of Pharmacology and Toxicology, Neuroscience Graduate Program
University of Texas, Galveston Texas

Abstract

Glioblastoma (GBM) is the most common adult primary brain tumor with a median survival of approximately one year. The current standard of care for GBM includes the maximal surgical resection, followed by concurrent chemotherapy, radiotherapy, and in some cases and adjuvant chemotherapy. Yet, despite this aggressive multimodal approach, GBM is a nearly universally fatal disease. The poor outcome is in large part due to the lack of effective therapeutic agents that can penetrate the blood-brain and blood-tumor barriers to deliver anti-glioma therapeutics to the whole tumor and the microsatellite populations of tumor cells scattered throughout the brain parenchyma. However, bone marrow-derived human mesenchymal stem cells (hMSCs) offer a viable alternative to enhance therapeutic delivery – one that overcomes current limitations. hMSCs are a population of cells with the capability of self-renewal and multilineage differentiation that can be safely isolated in routine clinical procedures and pose no ethical quandaries. hMSCs demonstrate an intrinsic tropism towards gliomas and are capable of migrating across the blood-brain and blood-tumor barriers. These cells have been used as delivery vehicles to convey immunotherapy, enzymes for chemotherapeutic pro-drugs, and oncolytic viruses with some success in pre-clinical models.

Despite the promise of hMSCs, previous studies have relied for the most part on xenografts derived from commercially available immortalized GBM cell lines. These cell lines poorly mimic patient tumors *in vivo* and thus do not adequately translate into the clinical setting.

Glioma stem cells (GSCs) rectify this shortcoming by faithfully recapitulating the genotype and phenotype of the human tumor from which they were isolated. However, studies from our collaborators at MD Anderson Cancer Center show that hMSCs demonstrate variable tropism towards GSC-derived tumors (GSC xenografts; GSCXs). Those GSC xenografts that attract hMSCs are referred to as 'attractors', whereas those that fail to evoke hMSC homing are designated 'non-attractors'. The underlying biological mechanism of hMSCs differential homing capacity towards GSCXs is virtually unknown.

Given the clinical potential of hMSCs as therapeutic delivery vehicles of anti-glioma agents, the rationale behind this project was to elucidate the molecular mechanisms that underlie the variable localization of hMSCs to gliomas by use of GSCXs as a clinically relevant brain tumor model. The *long-term* goal is to understand the essential factors in hMSC homing to gliomas, in order to successfully harness hMSCs for clinical use or to identify patients most appropriate for hMSC-mediated therapeutic delivery. This work is significant because the outcomes will identify differences between attractor and non-attractor GSCXs, which will be critical in advancing our knowledge for continued development of hMSCs as a viable therapeutic strategy.

TABLE OF CONTENTS

LIST OF FIGURES

LIST OF TABLES

COMMITTEE

Carol L. Nilsson, M.D., Ph.D.
Professor
Department of Pharmacology & Toxicology
Graduate School of Biomedical Sciences
University of Texas Medical Branch

Mark R. Emmett, Ph.D.
Professor
Department of Biochemistry & Molecular Biology
Graduate School of Biomedical Sciences
University of Texas Medical Branch

Giulio Taglialatela, Ph.D.
Professor
Department of Neuroscience & Cell Biology
John Sealy Professor and Vice Chair for Research, Department of Neurology
Director, Mitchell Center for Neurodegenerative Diseases
University of Texas Medical Branch

Owen Hamill, Ph.D.
Associate Professor
Department of Neuroscience & Cell Biology
Graduate School of Biomedical Sciences
University of Texas Medical Branch

Roger A. Kroes, Ph.D.
Research Associate Professor
Department of Biomedical Engineering
Associate Director
Falk Center for Molecular Therapeutics
Head, Pharmacogenomics Program
Northwestern University

Charles A. Conrad, M.D.
Professor
Department of Neuro-Oncology
Texas Oncology-Austin, Midtown

Frederick F. Lang Jr., M.D.
Professor
Department of Neurosurgery
Division of Surgery
The University of Texas MD Anderson Cancer Center

Robert L. Ullrich, Ph.D.
Professor
Department of Radiation Oncology,
University of Texas Medical Branch

ABBREVIATIONS

AGC: Automatic gain control
BBB: Blood-brain barrier
BCA: Bicinchoninic acid
BTB: Blood-tumor barrier
CID: Collision-induced dissociation
CNS: Central nervous system
DDA: Data-dependent acquisition
DHB: 2,5-Dihydroxybenzoic acid
EC: Endothelial cell
ESI: Electrospray ionization
GBM: Glioblastoma, formerly glioblastoma multiforme*
GSC: Glioma stem cell
GSCX: Glioma stem cell xenograft
H&E: Hematoxylin and eosin
hMSC: Human [bone marrow-derived] mesenchymal stem cell
MALDI-IMS: Matrix assisted laser desorbtion/ionization-imaging mass spectrometry
MGMT: O^6-alkylguanine DNA alkyltransferase
MOI: Multiplicities of infection
MS: Mass spectrometry
MS/MS: Tandem mass spectrometry
m/z: Mass-to-charge ratio
NSC: Neural stem cell
nLC-MS/MS: Nano-liquid chromatography tandem mass spectrometry
PDGF: Platlet-derived growth factor
ppm: parts per million
PUFA: Polyunsaturated fatty acid
RNA: Ribonucleic acid
ROS: Reactive oxidative species
TCGA: The Cancer Genome Atlas
TOF: Time-of-flight
WCL: Whole cell lysate
WHO: World Health Organization

* The WHO discarded the term ‘multiforme’, but for historical purposes the abbreviation remains GBM.

BACKGROUND

Glioblastoma

The World Health Organization (WHO) established standardized classification guidelines for tumors of the central nervous system (CNS) in 1979 (Zülch, 1979), most recently updated in 2007 (Louis *et al*., 2007). The classification of gliomas includes the cell type they share histological features with – not necessarily the cell type they originated from – and a consensus-derived tumor grade scale. Tumor grade (I-IV) is determined histologically and includes a malignancy scale. Grade I is largely benign, shows low proliferation, and is reliably cured by surgical resection, thus having the best prognosis. Grade IV has the worst prognosis, as these tumors are highly malignant and mitotic, and demonstrate prolific necrosis. Grade IV tumors are associated with poor survival and are typically lethal (Louis *et al*., 2007).

Gliomas account for 28% of all CNS tumors and 80% of all malignant CNS tumors (Ostrom *et al*., 2014). Glioblastoma (GBM), a Grade IV astrocytoma, accounts for nearly half (45.6%) of all malignant primary CNS tumors (Ostrom *et al*., 2014), making GBM the most common malignant primary brain tumor in adults (DeAngelis, 2001; Stupp *et al*., 2005). GBM is more frequent among men compared to women (male-to-female ratio ~3:2; DeAngelis, 2001; Ostrom *et al*., 2014, 2014). Most incidences (~90%) are primary glioblastomas – these tumors arise *de novo* with no clinical evidence of a lower grade tumor (DeAngelis, 2001; Ohgaki & Kleihues 2005; Furnari *et al*., 2007). Primary glioblastomas typically present in the fifth decade of life (DeAngelis, 2001). Secondary glioblastomas, which originate from a pre-existing lower-grade tumor, affect younger patients, typically less than 45 years of age (Kleihues & Cavenee, 2000; DeAngelis, 2001). Despite the clinical distinction between primary and secondary glioblastoma, their cellular morphology and histology are indistinguishable and their prognostic

trajectories are equally poor when adjusted for age (Furnari *et al*., 2007).

Glioblastomas are aggressive heterogeneous tumors, characterized by the hallmark features of robust vascularization and resistance to apoptosis, while paradoxically having a large number of necrotic foci (Brat & Van Meir, 2004), uncontrolled proliferation, and extensive invasion. In addition to the heterogeneous tumor histology, glioblastomas can be subdivided and characterized by variant genomic and transcriptomic aberrations, chromosomal alterations, and a largely undefined epigenetic landscape within the context of cell signaling networks. As the intricate landscape of somatic mutations in glioblastoma are outside the focus of this work, the reader is kindly referred to Phillips *et al*., (2006); Furnari *et al*., (2007); McLendon *et al*., (2008); Parsons *et al*., (2008); Verhaak *et al*., (2010); and Brennan *et al*., (2013) for review. The Cancer Genome Atlas (TCGA) provides a repository of these data available for public access (http://cancergenome.nih.gov/).

Extensive vascularization is characteristic of high-grade tumors, particularly GBM, which is one of the most vascularized solid tumors (Wesseling, Ruiter, and Burger, 1997; Kaur *et al*., 2004). The microvascular hyperplasia stems from endothelial cell outgrowth from existing parent blood vessels (Brat & Van Meir, 2001). The most extreme form of microvascular hyperplasia classically associated with GBM are glomeruloid bodies, which are florid, coiled capillary-like loops (Feigin *et al*., 1958; McComb & Bigner, 1984; Wesseling, Ruiter, and Burger, 1997; Kaur *et al*., 2004). The proliferating vasculature of GBM typically occurs adjacent to necrotic regions or at the brain-tumor interface (Feigin *et al*., 1958; McComb & Bigner, 1984; Wesseling, Ruiter, and Burger, 1997; Kaur *et al*., 2004) and marks the beginning of aggressive tumor growth (Brat & Van Meir, 2001).

Despite the accelerated growth of new vasculature, the vessels are often tortuous

compromising blood flow and oxygen delivery (Kaur *et al*., 2004; Furnari *et al*., 2007). The poor vascular architecture is further compounded by the lack of proper tight junction formation (Kaur *et al*., 2004; Furnari *et al*., 2007), which results in increased susceptibility to thrombosis, microhemorrhages, and interstitial edema that further compromises blood flow, promoting hypoxia and ultimately necrosis (Kaur *et al*., 2004; Furnari *et al*., 2007). Hypercellular zones of pseudopalisading cells often surround the necrotic foci (Baily & Cushing, 1926; Brat & Van Meir, 2004; Rong *et al*., 2006). Pseudopalisading necrosis is a unique feature to GBM that, even independent of microvascular hyperplasia, is a marker for poor prognosis (Brat & Van Meir, 2001; Brat & Van Meir, 2004). Pathologically, pseudopalisades are linked to adjacent microvascular hyperplasia (Brat & Van Meir, 2001; Brat & Van Meir, 2004). These cells are hypoxic, producing in high levels of hypoxia-inducible factor 1 (HIF-1), a mediator of VEGF and IL-8 gene transcription (Brat & Van Meir, 2004; Rong *et al*., 2006). Secreted pro-angiogenic factors VEGF and IL-8 result in hypoxia-mediated angiogenesis (Brat & Van Meir, 2004; Rong *et al*., 2006) linking GBM vascular pathology, hypoxia, pseudopalisade formation, and necrosis.

The uncontrolled proliferation characteristic of tumor cells can be attributed to three major signaling pathways, typically but not invariably mutated, in GBM i) retinoblastoma (RB) (78%), ii) p53 (87%), and iii) receptor tyrosine kinases (RTK) (88%) (Cancer Genome Atlas Research Network, 2008; Dunn *et al*., 2012; **Fig 1.1**). The RB tumor suppresor protein sequesters transcription factor E2F in a RB-E2F dimer. Upon phosphorylation by cyclin-dependent kinase complexes (cyclin D1 with CDK4/6), E2F is released from the dimer and transcribes its gene targets, which advance the cell to the S-phase of mitosis (Frolov & Dyson, 2004). In GBM, control of the RB pathway is circumvented by either one or more of these events: loss of tumor suppressor and cyclin inhibitor CDK2 ($p16^{Ink4a}$) (Serrano, Hannon, and

Beach, 1993), amplification of CDK4 (Reifenberger *et al*., 1994), or amplification of CDK6 (Costello *et al*., 1997) resulting in constitutively active E2F. Inactivation of the RB pathway occurs in the majority of GBMs (Ueki *et al.,* 1996). Another tumor suppressor responsible for cell cycle arrest and apoptosis of genetically altered or unstable cells, p53, is frequently mutated or lost in gliomas (*see* Furnari *et al*., 2007 *for review*). RTKs, particularly EGFR and PDGFR, are overexpressed in GBM. The binding of their respective ligands in an autocrine and paracrine manner leads to receptor autophosphorylation and activation of Ras signaling cascades, resulting

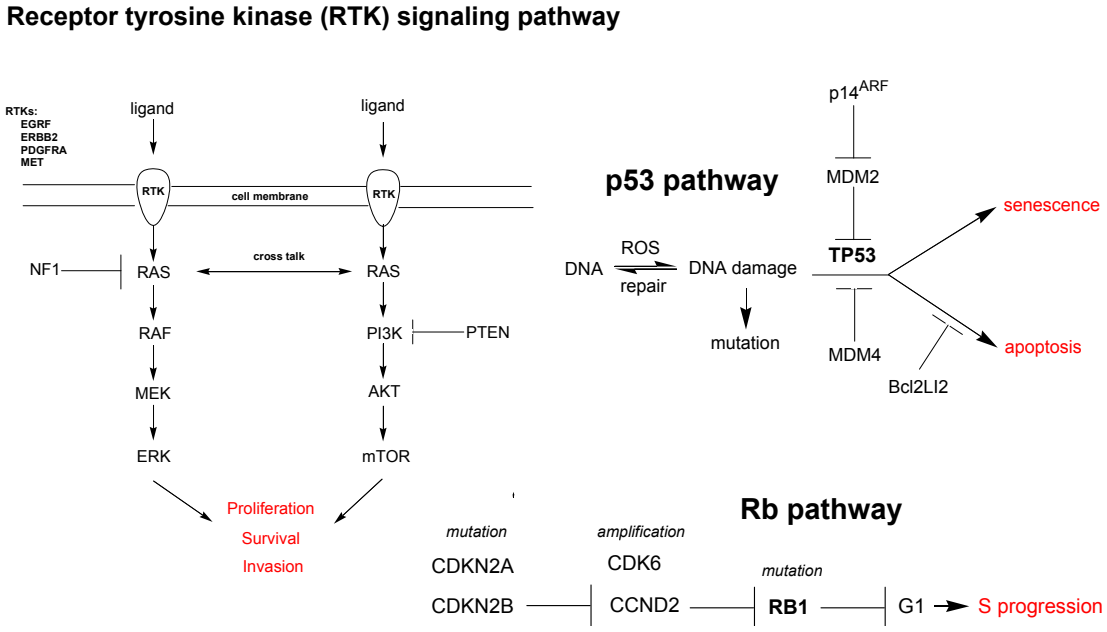

Figure 1.1: Signaling pathways commonly perturbed in GBM. Adapted from Sowers *et al*., Adv Exp Med Biol. 816: 75-105, pg. 78. Reprinted with permission.

in constitutive proliferation signals (*see* Furnari *et al*., 2007; Dunn *et al*., 2012; Sowers *et al*., 2014 *for review*). As tumor cells rapidly proliferate due to escape from cell cycle control and mitogenic signaling, they undergo a shift in metabolism towards glycolysis, a phenomenon known as the Warburg effect (Warburg, 1925; DeBerardinis *et al*., 2007; DeBerardinis *et al*., 2008). The hypoxic environment of GBM is also hypothesized to contribute to this metabolic

shift (Gatenby & Gillies, 2004; Xie, Mittal, and Berens, 2014).

Independent, but not mutually exclusive of proliferation (Bernstein *et al*., 1991; Xie, Mittal, and Berens, 2014), the mechanism of invasion requires cell-matrix and cell-cell adhesion, integrins (including CD44), and degradation of the basement membrane and extracellular matrix with matrix metalloproteases (*see* Grobben, De Deyn, and Slegers, 2002 *for review*). The local acidic conditions produced by excess lactate from tumor glycolysis complement invasion by inducing cell death of neurons and glia, which are susceptible to low pH (Xie, Mittal, and Berens, 2014). In contrast to most tumors, GBM does not spread hematogenously (i.e. through the blood stream or the lymphatic system), thus metastasis outside the CNS is virtually impossible (Kleihues & Cavenee, 2000). In fact, GBM cells are unable to penetrate the basement membrane of blood vessels (Bernstein & Woodard, 1995) or the calvarium (Bellail *et al*., 2004). However, GBM cell invasion is diffuse, rather than limited and localized as in other tumors, which contributes to the therapeutic limitations.

Therapeutic Limitations

The current standard of care for GBM is a multimodal therapeutic approach encompassing maximally allowable surgical resection, radiotherapy, chemotherapy, and in many cases adjuvant chemotherapy with the alkylating agent temozolomide (Stevens & Newlands, 1993; Newlands *et al*., 1997; Stupp *et al*., 2005; Stupp *et al*., 2006). Despite this aggressive therapeutic approach, recurrence is inevitable (Scherer, 1940; Giese *et al*., 2003; Stupp *et al*., 2005; Stupp *et al*., 2006) usually within < 2 cm of resection margin (Hochberg & Pruitt, 1980; Gaspar *et al*., 1992; **Fig. 1.2**). As a result, the median survival is 14-15 months, making GBM a nearly universally fatal disease (Berens & Giese, 1998; Stupp *et al*., 2005; Louis *et al*., 2007).

The poor clinical prognosis of glioblastoma is largely due to the nature of the tumor itself and the limited efficacy of current therapeutics.

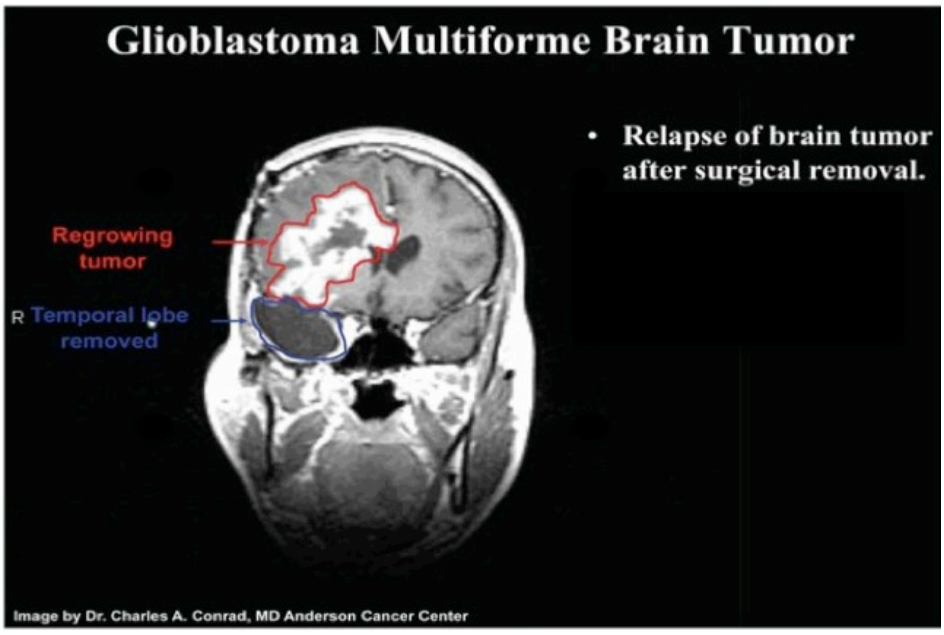

Figure 1.2: T1 gadolinium-enhanced MRI of a patient with GBM. The original tumor as removed from the temporal lobe (*blue*) followed by multimodal therapy. Tumor recurred ~6 months later < 2 cm from the original tumor margin (*red*). Image courtesy of Dr. Charles A. Conrad.

The introduction of temozolomide (Stevens & Newlands, 1993; Newlands *et al*., 1997; Stupp *et al*., 2005; Stupp *et al*., 2006) in the 1990s impacted the field of neuro-oncology by becoming a component of the current standard of care for GBM. Stupp *et al*. (2005) demonstrated that radiotherapy with concomitant and adjuvant temozolomide provided a modest survival benefit (~3 months) with minimal adverse effects compared to patients who received only radiotherapy. Temozolomide is an oral alkylating agent that methylates the O^6 position of guanine (Pegg, 1990). The O^6-methyl guanine mismatches with thymine during DNA replication ultimately leading to cell death (Stupp *et al*., 2007). Though the methyl adduct may be removed by DNA repair enzyme, O^6-methyl guanine methyltransferase (MGMT) (Pegg, 1990), methylation of the *MGMT* promoter epigenetically silences this DNA repair gene (Harris *et al*.,

1991; Costello *et al.,* 1994; Esteller *et al*., 1999). Patients who received temozolomide and had a methylated *MGMT* promoter benefited by longer survival (Hegi *et al*., 2005). While the benefits of temozolomide are clearly evident, the variable methylation status of patients presents a disparity in the patient population for temozolomide treatment benefit. This warrants either patient screening prior to initiation of GBM treatment and possibly the addition of MGMT inhibitors with temozolomide to enhance treatment response (Wedge *et al*., 1997; Chakravarti *et al*., 2006; Stupp 2007).

Nonetheless, patients, even after initial tumor control, relapse and disease progression continues, indicating that the tumors developed temozolomide-acquired resistance. The mechanisms of temozolomide-acquired resistance are not fully understood, but many patients do not change in *MGMT* promoter methylation status (Brandes *et al*., 2010; Felsberg *et al*., 2011). Accumulating evidence indicates that there may be a varied number of molecular mechanisms, which contribute to temozolomide-acquired resistance in GBM cells. Resistance may involve MGMT re-expression (Zhang *et al*., 2010) or instead of *de novo* re-expression of MGMT, a down-regulation of DNA mismatch-repair proteins (Curtin *et al*., 2004; Happold *et al*., 2012). Other implicated mechanisms include miRNA (Ujifuku *et al*., 2010), p21 (Happold *et al*., 2012), reduction of pro-apoptotic proteins (Ma *et al*., 2002), and glutamate transporters and AKR1C proteins (Le Calvé *et al*., 2010). Resistance presents obstacles to successful GBM treatment. Further reasons for the overall failure of conventional therapy include: the limitations of surgery, residual microsatellite populations of tumor cells, chemotherapy and radiotherapy efficacy, and the presence of glioma stem cells (GSCs).

Therapeutically, the extent of tumor resection is the primary factor that can be influenced (Jackson *et al*., 2001). The goal is to achieve the maximally safe surgical resection of the tumor

volume without compromising brain function any further than what the tumor has accomplished through relentless growth. However, the foremost limitation of surgical resection is the location of the tumor. Tumor location is classified into three categories: eloquent (e.g. motor/sensory cortex, speech center, visual center, brain stem), near-eloquent (e.g. near speech center, motor/sensory cortex, brain stem; and corpus callosum), and non-eloquent (e.g. cerebellar hemisphere, right parietal occipital) (Sawaya *et al*., 1998). Eloquent and near-eloquent locations make it difficult for complete surgical resection and re-operation only confers a modest survival benefit (Dirks *et al*., 1993). Patients with tumors in eloquent or near-eloquent brain regions acquire more neurological deficits than patients with tumors in non-eloquent areas and such complications are more prevalent among older patients (Sawaya *et al*., 1998). Surgically acquired deficits in language or motor skills are associated with a decrease in post-operative survival (McGirt *et al*., 2009).

The shortcoming of even total surgical resection is highlighted by a series of surgeries performed by Walter Dandy, M.D., on a cohort of GBM patients. After a complete hemispherectomy, the tumor recurred in the contralateral hemisphere (Dandy, 1928). This is due to the extensive, diffuse migration or microscopic invasion of tumor cells that are virtually beyond detection by the surgical operator and by modern diagnostic techniques (Salazar & Rubin, 1976; Burger *et al.*, 1988). The microsatellite population of tumor cells scattered throughout the brain parenchyma can occur via contiguity or seeding (Bryan, 1974; Salazar & Rubin, 1976). GBM cells are highly invasive and actively migrate long distances (Kleihues & Cavenee, 2000) along [white matter] nerve fibers (e.g. corpus callosum) (Laerum *et al*., 1984; Rutka *et al*., 1988; Pedersen *et al*., 1995; Furnari *et al*., 2007) blood vessels (Laerum *et al*., 1984; Furnari *et al*., 2007) and some substrates (Giese *et al*., 1994) disseminating through the narrow

extracellular spaces of the brain parenchyma. Whether these routes function as guided paths via biochemical substrates or simply offer the least resistance or both is unclear, but the migrant microsatellite population of cells have the potential to proliferate and give rise to tumors in other brain regions (Scherer, 1940; Bryan, 1974; Salazar & Rubin, 1976).

Chemotherapy and radiotherapy are the next obvious choice to combat GBM due to the limitations of complete and effective surgical resection. However, using chemotherapy and radiotherapy to destroy the tumor and the diffusely infiltrating tumor cells and preserve the surrounding brain parenchyma has proven difficult to achieve. Further limitations to chemotherapy and radiotherapy include systemic toxicity and neurotoxicity, low drug penetration through the blood brain and blood-tumor barrier (BBB and BTB, respectively), drug half-life, and the inability to destroy *all* infiltrative tumor cells (Groothuis, 2000; Lang *et al*., 2003; Pardridge, 2003; Yong *et al*., 2009; Shinojima *et al*., 2013). Even newer therapies such as oncolytic viruses, anti-sense oligonucleotides and immunotherapy (Groothuis, 2000; Kosztowski, Zaidi, and Quiñones-Hinojosa, 2009) are hindered by these factors. The BBB and the BTB have long been recognized as obstacles to effective therapeutic delivery and tumor treatment. As a result, a number of innovated methods have been developed to increase drug delivery (*see* Groothuis, 2000 *for review*). Each has its relative advantages and disadvantages, but few – if any – have proven superior over another method, and none have been translated into successful increases in patient survival.

Chemotherapeutic delivery can be divided into two classes: intravenous (IV) and local delivery by intracerebroventricular (ICV) or intracerebral (IC) injection. Immediately after IV injection, the drug is diluted several-fold by the total blood volume of the patient in a ‘washout’ effect, after which it is distributed everywhere (Groothuis, 2000). Throughout its distribution to

all body tissues, the drug is eliminated by first order metabolism and inactivation via a series of half-life cycles (Groothuis, 2000; Pardridge, 2003; Meyer & Quenzer, 2005). Other factors to consider are the blood-to-tissue transfer constant, which is limited in the brain, and the tissue efflux constant, and the variable spatial distribution and function of brain tumor capillaries (Groothuis, 2000; Pardridge, 2003; Meyer & Quenzer, 2005). All of these factors make it nearly impossible for drugs to cross the BBB and BTB in pharmacologically significant amounts; typically < 1% of an intravenously delivered drug – regardless of solubility, permeability, and capillary permeability – will reach the tumor (Groothuis, 2000). Effectively, the administered dose needed to reach the brain and ensure a clinically meaningful effect would result in systemic toxicity (Groothuis, 2000).

An alternative to systematic drug delivery is a more localized approach by IC or ICV injection. Drugs delivered by IC administration typically diffuse only 2-3 mm from the injection site (Krewson, Klarman, and Saltzman, 1995; Pardridge, 2003). As a consequence, delivery must be nearly directly at the tumor site for maximal efficacy, which may come at the expense of compromising healthy brain tissue. Delivery of the drug during surgical resection of the bulk tumor would offer the ideal opportunity for IC administration, but at the exclusion of repeated dosing and with the possibility of neurotoxicity. Similarly, ICV administration has limited drug penetration into the brain parenchyma – typically the ependyma – and neurotoxicity may present (Pardridge, 2003). ICV administration is usually best suited for treatment of carcinomatous meningitis, which is situated within the subarachnoid space (Groothuis, 2000).

Drug distribution throughout the brain is diffusional and declines exponentially as a function of distance from the brain surface (Blasberg, 1977; Blasberg, Patlak, and Shapiro, 1977; Groothuis, 2000). Approximately < 1% of drug volume, delivered by either IC or ICV, would

effectively treat the tumor (Pardridge, 2003). A *transvascular* route of drug delivery, on the other hand, would be so highly efficient that all parts of the brain could be treated simultaneously due to the rich surface area of the brain capillary network (Groothuis, 2000). Though the excessive focus on the BBB and BTB has detracted from the study of drug uptake by tumor cells and metabolic fate (Groothuis, 2000).

Given the recognized infiltrative and diffuse nature of GBM cells, curative resection was not possible. Thus post-operative radiation treatment was given to patients to prolong survival (Salazar & Rubin, 1976; Hochberg & Pruitt, 1980). Initially, whole-brain radiation treatment was used, but with the introduction of imaging technologies, such as computerized tomography, localized radiation treatment has been used. Early reports suggested that high doses of radiation were critical to prolong patient survival (Onoyama *et al*., 1976). In an evaluation of standard (60 Gy) or short-course (40 Gy) radiotherapy, Minniti *et al.* (2014) found no difference in overall survival and progression-free survival, though the standard course of treatment was associated with higher neurotoxicity. These results are similar to phase III studies of low-grade glioma wherein high-dose radiotherapy resulted in higher incidence of radiation toxicity and lower survival (Shaw *et al*., 2002). Newer strategies such as brachytherapy (Selker *et al*., 2002) or stereotactic radiosurgery (Tsao *et al*., 2005) have failed to improve survival.

GBMs have long been recognized as resistant to radiation treatment (Kramer, 1969; Salazar & Rubin, 1976). Current evidence now suggests that like many other cancers, GBMs contain a small sub-population (< 1%) of cells, which are resistant to radiotherapy and chemotherapy. The characteristics of these cells parallel that of endogenous neural stem cells (NSCs) (Reya *et al.*, 2001; Ignatova *et al*., 2002; Singh *et al*., 2003; Singh *et al*., 2004; Yuan *et al*., 2004; Galli *et al*., 2004; Nduom, Hadjipanayis, and Van Meir, 2012). They possess similar

morphology and the stem-like properties of unlimited self-renewal (Singh *et al*., 2003; Singh *et al*., 2004) and multi-lineage differentiation (i.e. potency). These cells, termed glioma stem cells (GSCs), are hypothesized to promote relapse due to their therapeutic resistance (Bao *et al*., 2006; Liu *et al*., 2006; Kang & Kang, 2007; Hadjipanayis & Van Meir, 2009; Facchino *et al*., 2010). Alarmingly, studies suggest that radiotherapy and chemotherapy results in de-differentiation and acquisition of stem cell properties (Charles & Holland, 2009; Dahan *et al*., 2014; Auffinger *et al*., 2014). Other studies have shown that radiation treatment enriches the existing population of GSCs (Bao *et al*., 2006; Charles & Holland, 2009).

Bone Marrow-Derived Human Mesenchymal Stem Cells

Despite clinical shortcomings, recent developments in molecular biology and stem cell therapy have provided us with the opportunity to improve therapeutic outcomes with human mesenchymal stem cells (hMSCs). These non-hematopoietic cells exist postnatally and have the capacity for self-renewal and multilineage differentiation to form adipocytes, chondrocytes, and osteocytes (Friedenstein *et al*., 1976; Bianco *et al*., 2001; Dominici, *et al*., 2006; Motaln, Schichor, and Lah, 2010). They may be safely isolated in routine clinical procedures (Bianco *et al*., 2001; Motaln, Schichor, and Lah, 2010) expanded *in vitro,* and used for autologous transplantation (Lazarus *et al*., 1995; Bianco *et al*., 2001), which negates any potential immunological rejection. Evidence suggests their potential use in allogenic transplantation (Koç *et al*., 2002; Aggarwal & Pittenger, 2004; Motaln, Schichor, and Lah, 2010) due to their low immunogenicity (i.e. ability to provoke an immune response) and immunosuppressive properties (Le Blanc *et al*., 2003; Le Blanc *et al*., 2004; Zhang *et al*., 2004; Motaln, Schichor, and Lah, 2010). This feature of hMSCs generates a viable opportunity for the use of banked donor cells in

the clinical setting for patient therapy. An additional benefit of hMSCs is that, due to their sources, they pose no ethical quandaries (Bianco *et al*., 2001).

Neural stem cells (NSCs) are another source of stem cells used as therapeutic delivery vehicles (Aboody *et al*., 2000; Benedeti *et al*., 2000; Kosztowski, Zaidi, and Quiñones-Hinojosa, 2009). However, we limit this chapter to discussion of hMSCs as i) the endogenous population of NSCs declines with age (Gage, 2000). ii) NSCs are localized in the dentate gyrus of the hippocampus and subventricular zones of the lateral ventricles – difficult areas to reach and surgically high risk particularly in regard to the hippocampus (Sawaya *et al*., 1998; Gage, 2000). iii) Existing human NSC lines are under tight regulation as a result of serious ethical concerns (Young, 2000; Perry, 2000; Kennedy, 2000; The NIH Guidelines on Stem Cell Research) and iv) the necessity for allogenic rather than autologous transplantation. Due to these limitations, NSCs are not actively used by our team and will not be discussed further; for an extensive review the reader is kindly guided to Kosztowski, Zaidi, and Quiñones-Hinojosa (2009).

The origin of hMSCs varies (Aggarwal & Pittenger, 2004; Kern *et al*., 2006; Rebelatt *et al*., 2008; Lepperdinger *et al*., 2008), but three important sources are umbilical cord blood (Erices *et al*., 2000; Lee *et al.,* 2004; Kern *et al*., 2006), adipose tissue (Zuk *et al*., 2002), and bone marrow (Pittenger *et al*., 1999). Umbilical cord blood has been posited as an attractive source of hMSCs since the method of isolation is less invasive (Erices *et al*., 2000; Lee *et al.,* 2004; Kern *et al*., 2006), though there is some controversy as to whether umbilical cord blood can serve as a source of fully multipotent cells (Mareschi *et al*., 2001; Wexler *et al*., 2003). In a comparative analysis of hMSCs from these three sources, Kern *et al*., (2006) discerned that the success of isolating hMSCs was highest in bone marrow and adipose tissue (100%) and lowest in umbilical cord blood (~63%). Rebelatt *et al*., (2008) achieved similar results, except with much

lower isolation from umbilical cord blood (~30%). Colony formation frequency was lowest in umbilical cord blood cells (Kern *et al*., 2006). In contrast, bone marrow-derived mesenchymal stem cells (hMSCs) had the lowest proliferation capacity, followed by those derived from adipose tissue. Length of culture period followed the same pattern, bone marrow-derived hMSCs had the shortest culture period and umbilical cord blood hMSCs the longest (Kern *et al*., 2006), though another study by Colter *et al*., (2000) demonstrated significantly longer culture periods with bone marrow-derived hMSCs.

Phenotypically, hMSCs from all three sources have similar immune profiles (Kern *et al*., 2006; Rebelatto *et al*., 2008). The low immunogenicity of all these cells offers the potential for allogenic transplantation, though it is generally best to err on the side of caution; therefore, autologous transplantation would be the most clinically viable – and likely to achieve FDA approval – course of treatment. Assuming autologous transplantation only, the most practical source of stem cells would be bone marrow. Umbilical cord blood-derived hMSCs require long-term storage, which is cost prohibitive and requires the forethought by the patient that these cells need to be saved in the event of GBM decades later. Observations by Bieback *et al*., (2004) found that isolation of hMSCs from umbilical cord blood declined markedly after cryostorage. It also limits therapy to females when GBM affects males more frequently than females (DeAngelis, 2001; Ostrom *et al*., 2014). Arguments in favor of umbilical cord blood-derived hMSCs mainly point to their longer culture period, which would hypothetically translate to higher overall number of cells (Kern *et al*., 2009). An associated risk with extensive culture periods is mutations that alter the phenotype of the cells (Lepperdinger *et al*., 2008; Motaln, Schichor, and Lah, 2010). Adipose tissue volume varies greatly particularly with patients undergoing chemotherapy and enduring cancer cachexia (Fearon & Moses, 2002) affecting

adipose hMSC recovery potential. Though one proposed counter-argument is that with the success of isolation of hMSCs from adipose, small amounts of this tissue would be sufficient (Kern *et al*., 2006).

The population of hMSC declines with age (Nishida *et al*., 1999; Stenderup *et al*., 2003; Kern *et al.,* 2006) and GBM typically affects individuals in mid-life. The practical and medical concerns with acquisition of umbilical cord blood and adipose tissue hMSCs (*as described above*), and the routine use of bone marrow extraction as an outpatient procedure makes bone marrow-derived hMSCs an attractive cell-based therapeutic delivery vehicle (Caplan & Bruder, 2001; Bianco *et al*., 2001). It is also important to note that many research studies acquire hMSCs from donations, and the age range of normal donors is quite wide. Thus, within this text and our previous studies, hMSCs specifically refer to the non-hematopoietic mesenchymal stem cells derived from the bone marrow.

The growing interest in hMSCs for cell-mediated therapy originates from observations that endogenous hMSCs actively migrate to sites of injured or stressed tissue (Pittenger & Martin, 2004; Kidd *et al*., 2009). For instance, it has been demonstrated by several groups that hMSCs migrate or home to the heart after myocardial infarction (Bittira *et al*., 2003; Wu *et al*., 2003), and the brain after stroke (Li *et al*., 2000) or traumatic brain injury (Mahmood *et al*., 2001). Tumors display many microenvironmental similarities to injured or severely stressed tissue. The parallels to injured tissue tumors present have led investigators to consider tumors as "wounds that do not heal" (Dvorak, 1986). As such, hMSCs have an intrinsic tropism for tumor cells (Nakamura *et al*., 2004; Nakamizo *et al*., 2005; Kosztowski, Zaidi, and Quiñones-Hinojosa, 2009).

The unique ability of hMSCs to actively localize or home to tumors, migrating long

distances and even transversing the BBB and BTB (Nakamura *et al*., 2004; Nakamizo *et al*., 2005; Yong *et al*., 2009; Kosztowski, Zaidi, and Quiñones-Hinojosa, 2009), offers a viable solution to the long sought after *transvascular* route of drug administration (see *Therapeutic Limitations* above) (Groothius, 2000). We and others have utilized hMSCs for the targeted delivery of anti-glioma agents due to the intrinsic tropism of these cells for gliomas. hMSCs are capable of homing to xenografts of human gliomas from commercially available cell lines (Nakamizo *et al*., 2005; Nakamura *et al*., 2004**;** Yong *et al*., 2009), glioma stem cells (Shinojima *et al*., 2013), or syngenic models (Doucette *et al*., 2011). Though the mechanisms that underlie homing remains largely undefined (see *Homing* below), these cells possess tremendous clinical potential as a transvascular carrier for anti-glioma therapeutics, due to their innate tropism for gliomas and high migratory capacity. hMSCs have been found to home to gliomas after injection into either the ipsilateral or contralateral hemisphere, migrating across the corpus callosum (Nakamura *et al*., 2004) or after injection into either the ipsilateral or contralateral internal carotid artery (Nakamizo *et al*., 2006; Yong *et al*., 2009; Kosztowski, Zaidi, and Quiñones-Hinojosa, 2009; Doucette *et al*., 2011) (**Fig. 1.3**). The fact that these are living cells means that they are capable of full transcriptional, translational, and post-translational expression and modification of transduced or transfected genetic material for secretion into the tumor microenvironment (Kosztowski, Zaidi, and Quiñones-Hinojosa, 2009). In a rational clinical approach, several groups have used hMSCs for delivery of immunotherapeutics such as IL-2 (Nakamura *et al*., 2004) and IFN-β (Nakamizo *et al*., 2005) or enzymes for chemotherapeutic pro-drugs (Miletic *et al*., 2007).

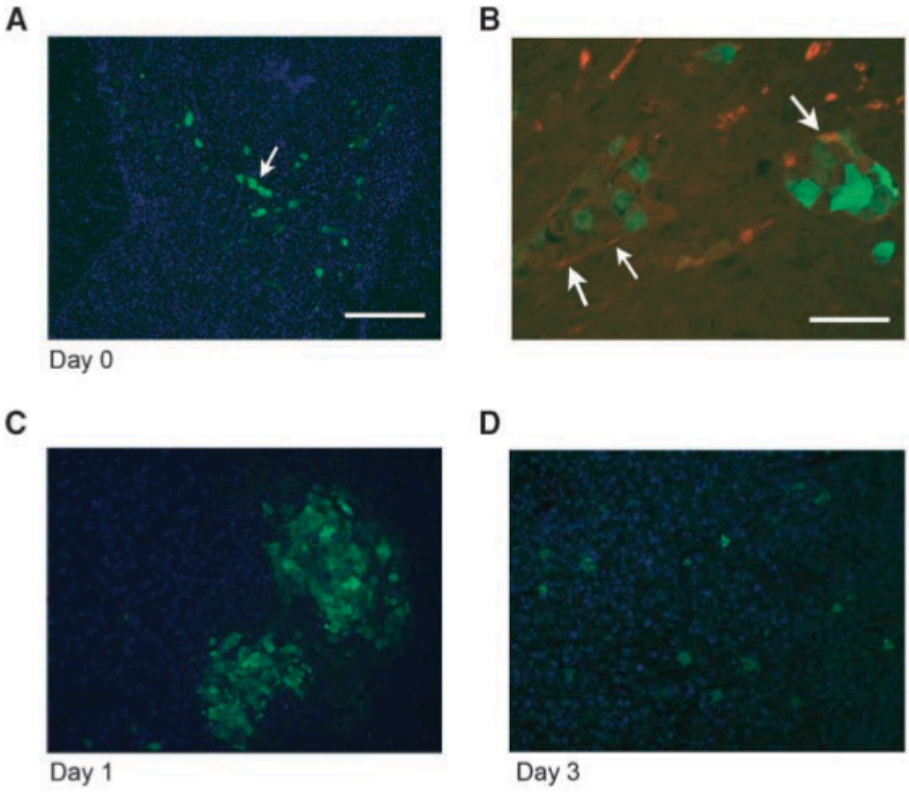

Figure 1.3: Transvascular delivery of hMSCs. **A**. GFP-labeled hMSCs (*green*) are shown in a linear arrangement suggesting they are within the blood vasculature; *Bar*, 200 μm. **B**. hMSCs co-localize with endothelial cell marker CD31 (*red*) confirming their presence within blood vessels. Arrows point to where CD31+ cells surround hMSCs; *Bar*, 50 μm **C**. One day after delivery of hMSCs to the right internal carotid artery the cells are present within the tumor mass of a U87 xenograft; nuclear stain DAPI (*blue*). **D**. Three days after intravascular delivery, GFP-labeled hMSCs are widely dispersed in the xenograft. Adapted from Yong *et al*., Cancer Res. 69: 8932-8940, pg. 8934. Reprinted with permission.

However, the overall goal is to use hMSCs to deliver oncolytic virus Delta-24 RGD developed by a team at MD Anderson Cancer Center, which is now in phase II clinical trials. Delta-24 RGD is a tumor-selective, replication-competent adenovirus with enhanced infectivity due to the insertion of Arg-Gly-Asp (RGD) motif for integrin-mediated infection in the absence of the cocksackie-adenovirus receptor (Dmitriev *et al*., 1998; Fueyo 2000; Fueyo 2003). The virus also contains a 24-bp deletion in the E1A region that is responsible for Rb protein binding (Fueyo 2000; Fueyo 2003). The mutation renders the virus unable to bind Rb due to compromised E1A (Fueyo 2000; Fueyo 2003). The result of this mutation is that Delta-24 is capable of replication in cells were the Rb protein is inactivated a characteristic feature of GBM (see *Glioblastoma* above). Studies have demonstrated that this virus is incapable of replication in cells where Rb is intact and that it inhibits tumor cell growth *in vitro* and *in vivo* (Fueyo 2000; Fueyo 2003) – particularly with repeated dosing, which is feasible in this context (see *Therapeutic Limitations* above). Another advantage to viral-mediated therapy is its widespread distribution throughout the tumor after lysing hMSCs (Yong *et al*., 2009). In some cases, large numbers of cells need to be expanded *in vitro* in order to ensure successful cell-based therapy with for example immunotherapeutics; this is accompanied by the risk of genetic alteration or cell senescence (Lepperdinger *et al*., 2008; Motaln, Schichor, and Lah, 2010). However, in our hands, delivery of 1 x 10^6 hMSCs transduced with 50-100 MOI of Delta-24 RGD is sufficient for homing to the tumor, inhibition of tumor growth, and improving overall survival, thus negating the need for high levels of *in vitro* cell expansion (Yong *et al*., 2009).

Homing

Cellular homing is the migration of cells to their organ of origin. Homing also constitutes

the migration of cells to sites of injured or damaged tissue from either their organ of origin or injection site. By understanding the critical events and factors that take place during homing, we can enhance our knowledge of hMSC-mediated therapeutic delivery and find ways to further improve this process in the clinical setting (see *Current State of the Problem* below).

The homing process entails cell-cell signaling followed by an intricate and complex series of coordinated events between the blood-borne cells and the blood vessel endothelium (Lapidot, Dar, and Kollet, 2005). This process is perhaps best characterized within the field of microbiology and immunology with the study of leukocyte migration to infected tissue as a component of the innate immune response (Moser, 2001). Injured or stressed tissue elicit pro-inflammatory signals in the form of cytokines, chemokines, and growth factors to which blood-borne cells respond and migrate to arrive at the appropriate site guided by these chemoattractants (Moser, 2001; Honczarenko *et al*., 2006; Ponte *et al*., 2007; Kosztowski, Zaidi, and Quiñones-Hinojosa, 2009). Examples of soluble chemoattractants implicated in hMSC homing to gliomas include TGF-β (Shinojima *et al*., 2013), PDGF-BB (Hata *et al*., 2010), and SDF-1 (Son *et al*., 2006; Ponte *et al*., 2007).

Once cells within the blood vessel are nearest the site of injury, they must cross the blood vessel epithelium to reach the damaged tissue. The process whereby circulating cells in the blood vasculature exit the circulatory system to migrate towards sites of damaged of infected tissue is called extravasation. Similarly, hMSCs must extravasate from the blood vessel endothelium to localize to the tumor mass though the precise mechanisms are not fully known (**Fig. 1.3**). Here we outline the process of extravasation and the concerted sequence of events it entails based largely on knowledge of mature leukocyte extravasation, though we present hMSCs-specific data throughout as available (**Fig. 1.4**).

In response to soluble factors released when tissue is injured or stress, the blood vessel endothelium becomes "activated" (Wright & Cooper, 2014). Activated endothelium express cell surface receptors not normally present in quiescent cells such as P-selectin and E-selectin (Hattori *et al*., 1989; Wright & Cooper, 2014) in preparation for the first of extravasation. In the first step, free-flowing cells in the bloodstream, such as hMSCs, must slow down and begin rolling along the inner surface of the vessel wall. The carbohydrates on the hMSC cell surface (glycolipids and glycoproteins) are captured by carbohydrate-binding proteins (predominantly selectins) on the endothelial cell (EC) surface in a step known as rolling adhesion (Wright & Cooper, 2014). Rüster *et al*. (2006) demonstrated *in vitro* with EC-containing parallel flow plates that hMSCs bind in a P-selectin-dependent manner and confirmed these results *in vivo* with P-selectin knockout mice. Furthermore, treatment of hMSCs with TNF-α – a cell signaling cytokine – enhanced binding to ECs (Rüster *et al.,* 2006 Segers *et al.,* 2006).

In the second step, complementary pairs of adhesion molecules (which, may be glycosylated, e.g. integrins) on opposing cell surfaces strengthen the rolling adhesion interaction. N-linked glycosylation of the various adhesion proteins is thought to play an important role in modulating tight binding between the endothelial and leukocyte cell surfaces (Wright & Cooper, 2014) though the nature of N-linked glycosylation remains unexamined at present in relation to the interaction between hMSCs and ECs. Data support the EC/hMSC interaction between VCAM-1/VLA-4 (Rüster *et al*., 2006; Segers *et al*., 2006) and β1 integrin (Steingen *et al.,* 2008; Ip *et al*., 2007), but not ICAM-1 (Segers *et al*., 2006) as is typical for leukocytes (Wright & Cooper, 2014). Next, cells begin the process of squeezing between the ECs (i.e. diapedesis) to enter the target tissue (Schmidt *et al.,* 2006; Yong *et al*., 2009) after which they are free to disseminate throughout the tissue or in our studies the brain parenchyma and tumor mass.

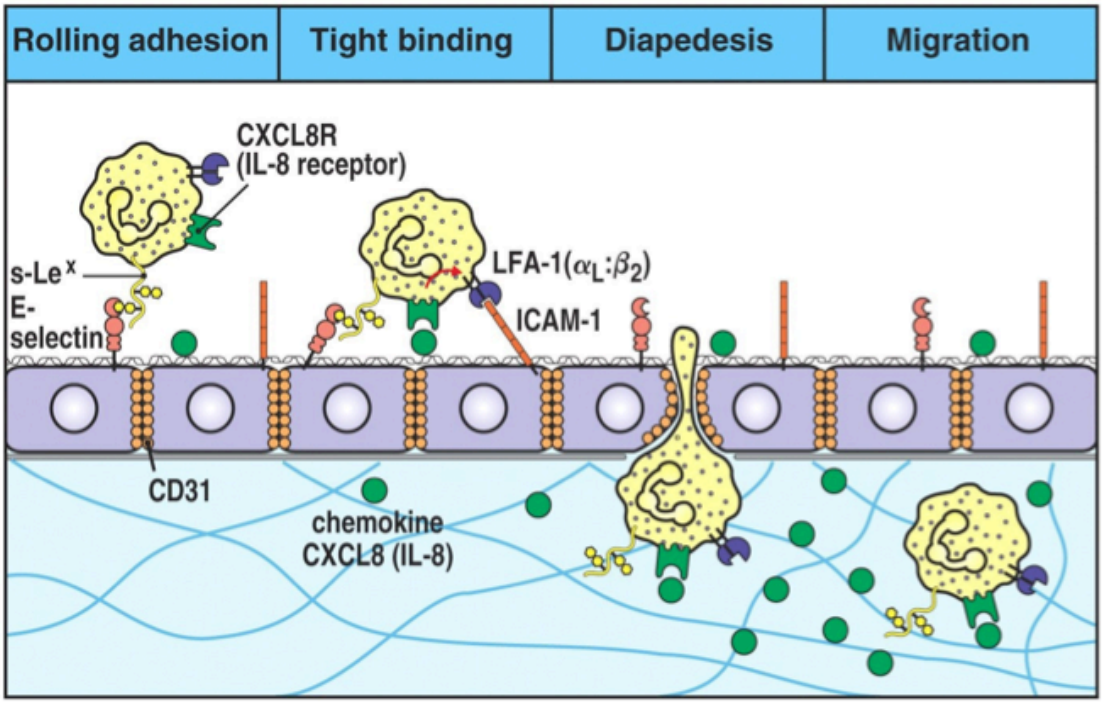

Figure 1.4: The process of cellular extravasation. In the first step, carbohydrates on the blood borne cell surface adhere to carbohydrate-binding proteins on the endothelium thus slowing the cells movement. In the second step, complementary pairs of adhesion molecules to stop cell movement strengthening the interaction established in the first step rolling adhesion. Third, cells squeeze in between endothelial cells in a step known as diapedesis. Finally once on the opposite side of the blood vessel endothelium cells are free to migrate through out the tissue parenchyma. Copyright 2009 from *The Immune System*, 3rd Edition by Parham. Reproduced with permission of Garland Science/Taylor & Francis LLC.

Current State of the Problem

Unfortunately, the majority of studies utilizing hMSCs have been conducted with commercially available human and rat glioma cells lines (e.g. 9L, U87, and U251), which poorly mimic patient tumors *in vivo* (Yong *et al*., 2009; Doucette *et al*., 2011; Shinojima *et al*., 2013). In order to rectify this shortcoming and improve the translational significance of these studies, we used GSCs (see *Therapeutic Limitations* above) intracranially implanted (Lal *et al*., 2000) into athymic nude mice (*nu/nu*) as a clinically relevant model. The GSCs isolated from patient tumors faithfully reflect the genotype and phenotype of the parent tumor *in vivo* (Singh *et al*., 2004; Lee *et al*., 2006). Reproducing previous experiments, hMSCs were transduced with *gfp* using Ad5/F35-CMV-GFP at 50 MOI per 3 mL of serum free medium (Yong *et al*., 2009; Shinojima *et al*., 2013). Cells were trypsinized, harvested, and injected into the right carotid artery of tumor-bearing nude mice (i.e. GSCXs). However, the data indicate that with this more robust model of GBM, hMSCs demonstrate significant variability in their capacity to home to GSCXs (Shinojima *et al*., 2013; **Table 1.1**), which indicates that not all gliomas will support the homing of hMSCs. The fact that some GSCXs attract hMSCs and others do not via the same delivery method suggests that there are key molecular differences that drive or modulate homing and extravasation. The GSC xenografts to which hMSCs home are herein referred to as 'attractors', where as those xenografts that fail to evoke hMSCs homing are referred to as 'non-attractors'.

Attractor	TCGA Cells	TCGA Tumor	Non-Attractor	TCGA Cells	TCGA Tumor
GSCX17	P	M	GSCX11	C	C
GSCX268	C	M	GSCX231	C	C
GSCX274	M	C	GSCX229	P	P

Table 1.1: Glioma stem cell xenografts (**GSCX**) categorized by their phenotype – attractor or non-attractor – and their genomic classification according to TCGA (http://cancergenome.nih.gov/) as stem cells (cells) and patient biopsies (tumor). **P**, proneural; **C**, classical; **M**, mesenchymal.

Overall Significance

It is well documented that hMSCs have an intrinsic tropism towards gliomas that give these cells tremendous clinical potential as therapeutic delivery vehicles. Given the therapeutic potential of hMSCs, it is critically necessary to understand the inherent biological differences between attractors and non-attractors. This project characterizes the molecular differences in proteins, transcripts, N-linked glycans, and lipids, between attractors and non-attractors that may be essential to the homing process. Understanding these differences will be critical in advancing hMSCs as a viable therapeutic strategy in clinical settings or to identify patients most appropriate for hMSC-mediated delivery.

MATERIALS AND METHODS

GENERAL

Chemicals and reagents. LC-MS grade acetonitrile, methanol, and water were from J.T. Baker (Philipsburg, NJ). 2,5 dihydroxybenzoic acid (DHB) xylene, and ammonium acetate were obtained from Sigma-Aldrich (St. Louis, MO). Hematoxylin & eosin was purchased from Amresco (Solon, OH). Conductive indium tin oxide (ITO) coated glass slides were from Delta Technologies (Loveland, CO). LC-MS grade acetonitrile and water were from J.T. Baker (Philipsburg, NJ). Formic acid and RIPA buffer were purchased from Pierce (Rockford, IL). Iodoacetamide (IAA), dithiothreitol (DTT) and ammonium bicarbonate were obtained from Sigma-Aldrich (St. Louis, MO). Sequencing grade trypsin was from Promega (Madison, WI). Sodium fluoride (NaF) was supplied by BDH (West Chester, PA) and PMSF from CalBiochem (Darmstadt, Germany).

Cell culture. GSCs (GSC17, GSC11, GSC274, GSC268, GSC231, and GSC229) were isolated from patient tumors as previously described (Singh *et al.,* 2003; Singh *et al.,* 2004) in accordance with The University of Texas M.D. Anderson Cancer Center IRB. All cell lines were tested for the presence of *Mycoplasma*. GSCs were grown as spheroids and split into separate dishes, one plate received 5 Gy of ionizing radiation and the other remained untreated. Cells were harvested 48 hrs after treatment. Downstream analyses were performed on paired cell cultures from identical batches to reduce the influence of batch variance in the comparative assays.

Animals. Male athymic nude mice (*nu/nu*) were purchased from the Department of Experimental Radiation Oncology, The University of Texas M.D. Anderson Cancer Center (Houston, TX).

Mice were housed n ≤ 5 per cage, on a 12 hr light-dark cycle with food and water *ad libitum*. Mice were allowed to feed until the time of surgery. All animal manipulations were done in accordance with institutional (MDACC) guidelines under Use Committee-approved protocols and in compliance with the USDA Animal Welfare Act and the Guide for the Care and Use of Laboratory Animals.

Glioma Xenograft Model. GSC lines, GSC17, GSC11, GSC229, GSC231, GSC268, and GSC274 were established from patient tumors as previously described (Singh *et al*., 2003; Singh *et al*., 2004). GSCs were harvested, counted, and 1 x 10^6 were resuspended in PBS for intracranial implantation in nude mice via the guide-screw method as previously described (Lal *et al.,* 2000; **Fig. 2.1**). A total of

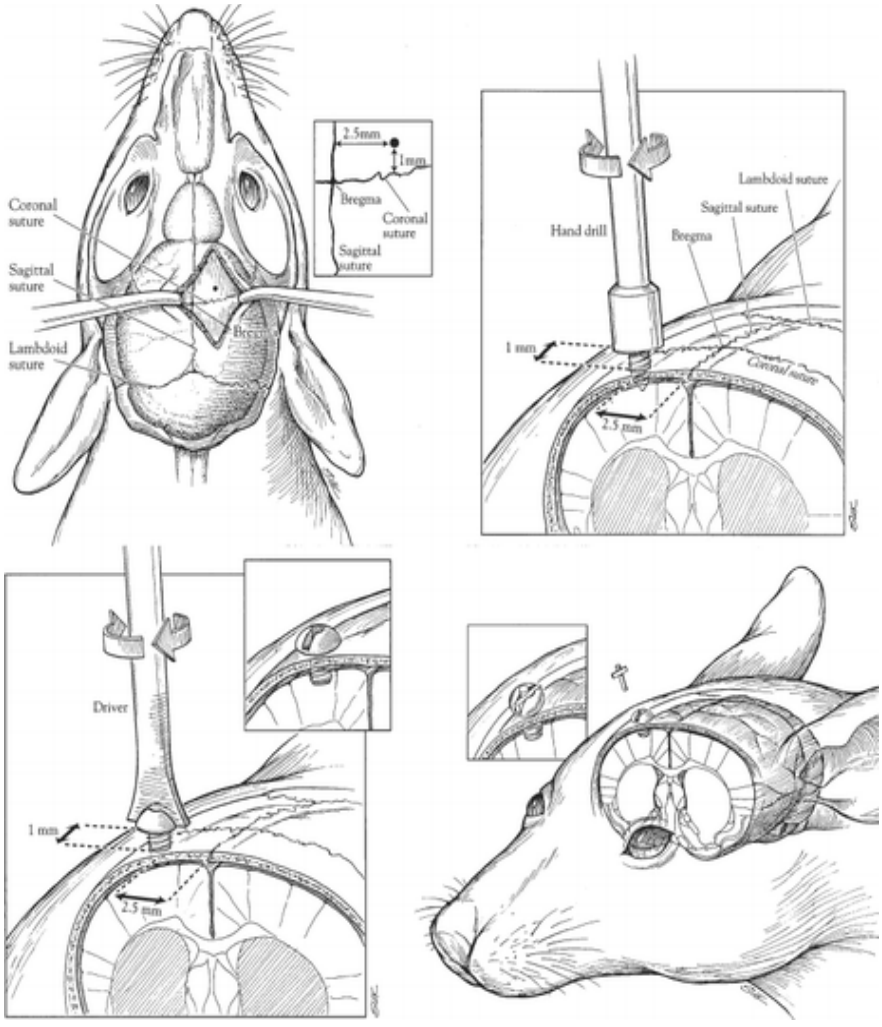

Figure 2.1: Artist's rendition of guide-screw implantation. Adapted from Lal *et al*., J Neurosurg 92: 326-333, pg. 328. Reprinted with permission.

eighteen mice were intracranially injected; each cell line represented by three different animals to produce GSC xenografts (GSCXs). GSCX17, GSCX274, and GSCX268 represent the attractor phenotype and GSCX11, GSCX229, and GSCX231 represent the non-attractor phenotype.

Tissue Dissection, Sampling, and Sectioning. Tumor-bearing mice were anesthetized with a ketamine/xylazine solution (200 mg ketamine and 20 mg xylazine in 17 ml of saline) at a dosage of 0.15mg/10 g body weight delivered by intraperitoneal injection and sacrificed by CO_2 inhalation. Brains were rapidly dissected out of the calvarium and frozen in liquid nitrogen vapor and stored at -80°C (Shavkunov *et al.,* 2013). Using a brain matrix, tumor-containing brain samples were sliced along the coronal plane at 1.5 mm thick ensuring the bolt and injection site were included. From these slices, tissue punches (1.5 mm diameter; Braintree Scientific, Braintree, MA) for proteomics and transcriptomics were taken at the tumor site and flash frozen in liquid nitrogen. The remaining bulk tumor-containing brain samples, were mounted on a cryostat and sectioned at 10 μm along the coronal plane and thaw mounted on ITO glass slides in a block randomized fashion (Oberg & Vitek, 2009). Slides were stored at -80°C until further analysis by MALDI-IMS. In addition to this 15 μm and 20 μm coronal sections were taken at the same time for lipid extraction as previously described (Matyash *et al*., 2008; Wood & Shirley, 2013) with subsequent ESI-MS/MS analysis, and on-tissue glycan release and subsequent LC-MS/MS analysis (Hu *et al*., 2013), respectively.

LIPIDOMICS

Lipid Extraction. Tissue samples were extracted with tert-butyl methyl ether and methanol (Matyash *et al*., 2008; Wood & Shirley, 2013) to which [$^{2}H_{8}$]arachidonic acid, [$^{2}H_{3}$]phytanic acid, [$^{2}H_{4}$]hexacosanoic acid, [$^{2}H_{28}$]hexadecanedioic acid [$^{13}C_{16}$]palmitic acid, [$^{2}H_{7}$]cholesterol sulfate, [$^{2}H_{5}$]MAG 18:1, [$^{2}H_{3}$]Carnitine 18:0, [$^{13}C_{3}$]DAG 36:2, [$^{2}H_{5}$]TAG 48:0, [$^{2}H_{31}$]PtdEtn 34:1, [$^{2}H_{54}$]PtdEtn 28:0, [$^{2}H_{31}$]PtdCh 34:1, [$^{2}H_{54}$]PtdCh 28:0, [$^{2}H_{62}$]PtdCh 32:0, [$^{2}H_{31}$]SM 16:0, [$^{2}H_{31}$]PtdSer 36:1, [$^{2}H_{31}$]PA 34:1, [$^{2}H_{62}$]PG 32:0 were added as internal standards. Glyburide was added as a lock mass. Extracts were dried to completeness *in vacuo* and stored at -80°C until further analysis by ESI-MS/MS.

ESI-MS/MS. Lipid extracts were resuspended in isopropanol:methanol:chloroform (4:2:1) containing 7.5 mM ammonium acetate. Lipid analyses were performed by direct infusion in an Orbitrap mass spectrometer (Thermo Q-Exactive), with successive switching between polarity modes utilizing high-resolution (140,000 at 200 amu) data acquisition, with < 1 ppm mass accuracy. Washes between samples with hexane/ethyl acetate (3:2) were used to minimize ghost effects. In negative and positive ion ESI, the anions and cations, respectively were quantified and lipid identities validated by MS/MS. Precursor ions were selected at unit mass resolution and product ions analyzed at high resolution (140,000) utilizing collision cell energies of 10, 25, and 35. Measured lipid abundances were taken as the ratio of lipid peak area to the peak area of an internal standard corrected for protein concentration. Grubb's test was used to identify and remove outliers in the dataset. Data presented as mean ± SEM with $p \leq 0.05$ considered significant (**Supplemental Table 3.1**).

MALDI-IMS. Slides were dried in a vacuum desiccator for 1 hr, then washed with 50 mM ammonium acetate three times and allowed to dry for 3 hrs *in vacuo*. Matrix 2,5 dihydroxybenzoic acid was applied to slides through sublimation (Hankin, Barkley, and Murphy, 2007). Imaging experiments were acquired in a MALDI TOF/TOF mass spectrometer (Ultraflextreme, Bruker Daltonics, Bremen, Germany) with Flex Control 3.4 and FlexImaging 3.0 (Bruker Daltonics) software. For all analyses, data were collected at 100 µm lateral resolution with a 1 kHz UV laser (smartbeam II) in positive ion mode (500 shots/spot) and in negative ion mode (1,000 shots/spot) over *m/z* 200-1600. Imaging data were subsequently processed and analyzed by FlexImaging™ software. Ion mass-to-charge ratio (*m/z*) and lipid assignments were made through the LIPID Metabolites and Pathways Strategy Database (LipidMaps http://www.lipidmaps.org) (Fahy *et al*., 2007; Fahy *et al*., 2009). Images were normalized to the total ion current (TIC). Collision-induced dissociation (CID) fragmentation was to fragment selected lipids. The DHA lipid standard was spotted on a MALDI plate with DHB (50/50 v/v) and fragmented in negative ion mode using the same parameters described above (**Supplemental Figure S3.1** and **Supplemental Table 3.2**).

H&E STAINING AND OPTICAL IMAGING. After MALDI-IMS experimentation, slides were processed for H&E staining. Slides were washed twice (15 sec each) with 100% ethanol to remove matrix, then successively with 95% ethanol, 70% ethanol, and H_2O (30 sec each). Tissue was stained with hematoxylin for 3 min then washed with H_2O, 70% ethanol, and 95% ethanol (30 sec each). Next tissue was stained with eosin for 1 min followed by washes with 95% and 100% ethanol for 30 sec each and xylene for 2 min. Xenograft tissue were imaged with a Zeiss

Stereomicroscope SteREO Discovery.V20 equipped with an AxioCam MRc5 (Carl Zeiss Microscopy, LLC, Thornwood, NY).

PROTEOMICS

Sample Preparation and Digestion of GSCX Whole Cell Lysate. Tissue punches were suspended in RIPA buffer containing 2 mM NaF, 2X Halt Protease and Phosphatase Inhibitor Cocktail (Thermo-pierce), 25 Units of nuclease, and 1 mM PMSF (final concentrations). Samples were subjected to seven freeze-thaw cycles each consisting of 90 sec in liquid nitrogen and 5 min on ice. Samples were spun for 10 min at 1,000 x g at 4°C. The supernatant was removed and protein concentration measured by BCA (Pierce, Rockford, IL). Whole cell lysates (100 ug) were precipitated with the 2D Clean-Up Kit (GE Healthcare, Piscataway, NJ). Samples were resuspended in 25 mM ammonium bicarbonate (pH 8) with sonication for 5 min. Resuspended lysate was reduced with 10 mM DTT for 1 h at room temperature and alkylated with 5 mM IAA for 1 h at room temperature in the dark. Proteins were digested overnight with trypsin 1:50 (w/w) at 37°C.

nLC-MS/MS of GSCX Whole Cell Lysate Digests. Each individual sample (nine per phenotype) consisting of three biological replicates per cell line were dissolved in 0.1% FA/5% ACN (v/v) and run in a block-randomized fashion (www.random.org) (Oberg & Vitek, 2009). Chromatographic separations were performed with a nano-LC chromatography system (Easy-nLC 1000, Thermo Scientific) online to a hybrid mass spectrometer consisting of a linear quadrupole ion trap and an Orbitrap (LTQ-Orbitrap Elite, Thermo Fisher Scientific) in positive ion mode. Samples were loaded on a C_{18} trap column 100 µm ID x 2 cm (New Objective) for online desalting and eluted from a PicoFrit® (75 µm ID x 15 µm tip) column packed with 10 cm ProteoPep II (5 µm, 300Å, C_{18}, New Objective) with the following gradient at 250 nL/min: 5% solvent B for 5 min; 35% B over 139 min; 95% B over 26 min followed by isocratic at 95% B

for 10 min. Mobile phases were 0.1% formic acid in water (A) and 0.1% formic acid in acetonitrile (B). The instrument was operated in positive ion mode for data-dependent analyses (DDA), automatically switching between survey scans (MS) at *m/z* 350-2000 acquired in the Orbitrap (60,000 at *m/z* 400) in profile mode and MS/MS scans in the Orbitrap in centroid mode (15,000 at *m/z* 400). For each sample, the five most abundant precursor ions above a 10,000 count threshold were selected from each survey scan (MS) for HCD fragmentation (isolation width ±2.0 Da, default charge state of 4, normalized collision energy 30%, activation Q 0.250, and activation time 0.1 s as previously described (Lichti *et al*., 2014; Lichti *et al*., 2015). Ion injection times for the MS and MS/MS scans were 500 ms each. The automatic gain control targets for the Orbitrap were 1×10^6 for the MS scans and 2×10^5 for MS/MS scans. Dynamic exclusion (±10 ppm relative to precursor ion *m/z*) was enabled with a repeat count of 1, maximal exclusion list size of 500, and an exclusion duration of 60 s. Monoisotopic precursor selection (MIPS) was enabled, and unassigned and singly charged ions were rejected. The following ion source parameters were used: capillary temperature 275°C, source voltage 2.2 kV, and S-lens RF level 40%. Spectra were acquired using XCalibur, version 2.0.7 (ThermoFisher).

Data Processing and Analysis of GSCX Whole Cell Lysate. Data files (.raw) were imported into Progenesis LC-MS (version 4.1; Nonlinear Dynamics, Newcastle upon Tyne, U.K) for spectral alignment based on *m/z* and retention time using a proprietary algorithm and manual landmarks using one sample ('Mix Control' an equal protein mixture from each sample) as the reference, as previously described (Hauck *et al*., 2010). The top 5 spectra for each feature were exported as a combined .mgf file and searched with PEAKS (version 6, Bioinformatics Solutions Inc., Waterloo, ON) against a merged UniprotKB/SwissProt HumanMouse database of canonical

sequences (March 2014; 24,541 entries) appended with the Common Repository of Adventitious Proteins (cRAP) contaminant database (February 2012 version, The Global Proteome Machine, www.thegpm.org/cRAP/index.html). The HumanMousecRAP database enabled us to identify peptides belonging to either human or mouse as well as peptides with shared sequences in a single database search. PEAKS automatically generated a decoy-fusion, which appended a decoy sequence to each protein for calculation of FDR (Zhang *et al.*, 2012). All modifications in the Unimod database were considered in the PEAKS search (Han *et al*., 2011; Lichti, *et al*., 2014). PEAKS searches were performed with a precursor ion mass tolerance of 10 ppm and fragment mass tolerance was 0.1 Da. Trypsin was specified as the proteolytic enzyme and a maximum of two missed cleavages were allowed.

Search results with score (-10logP) of 30 or higher, with an estimated FDR value of <1% (at the protein level) as calculated by PEAKS, were exported from PEAKS and re-imported into Progenesis for manual monoisotopic peak correction. Deamidated peptides identified in the PEAKS database search were used to direct manual monoisotopic peak correction, which is done to correct for misassigned monoisotopic *m/z* values not corrected in an automated fashion by Progenesis. After monoisotopic peak correction, the top 5 spectra for each feature were exported as a combined .mgf file and searched with PEAKS and imported into Progenesis for manual conflict resolution. Conflict resolution is the process whereby we ensure that a single peptide sequence is assigned to a single feature, by removing lower scoring peptide assignments to generate a final peptide list with raw abundances as previously described (Wildburger *et al*., 2015). The peptide list was exported as raw abundances to Excel for data analysis. The mass spectrometric data have been deposited in ProteomeXchange (http://proteomecentral.proteomexchange.org) via the PRIDE partner repository (Vizcaíno *et al*.,

2013) with the dataset identifier PXD001778.

All peptides listed as having shared or group accessions, or listed with multiple accessions, were removed – a total of 625 peptides. In this process, peptide sequences belonging to single protein identifications were kept for further statistical analysis while those belonging to more than one (i.e. "shared or group accessions, or listed with multiple accessions") were removed. This criterion (Paris guidelines) increases the confidence of protein quantification (Bradshaw *et al*., 2006; Neilson *et al*., 2011). Next, all post-translational modifications except carbamidomethylation of cysteine and oxidation of methionine were removed. Mouse and human proteins were sorted and separated before data analysis. Proteins identified as exogenous contaminants, such as keratin and trypsin, were eliminated. Finally, all protein identifications required a minimum of two unique peptides. Proteins without at least two peptides were excluded from further analysis. A total of two tables of peptide intensities (human WCL and mouse WCL) were imported into custom scripts for analysis (**Supplemental Tables 4.1 and 4.2**). All calculations were done using SAS PROC MIXED with restricted maximum likelihood estimations (SAS version 9.4, SAS Institute, Cary NC), and type 3 sums of squares (where appropriate). In all cases, the intensity of each peptide ion species was normalized by standardization across all measure of that peptide species. Standardization is a calculation in which the average intensity for all measures of a given peptide is subtracted from each measure, and the resulting difference is then divided by the standard deviation of all measures of the peptide. Missing values, defined as the lack of a reported intensity for a given peptide in a given LC-MS/MS run (i.e. a peptide observed in one replicate but not in another), were assumed to be missing at random and were excluded from the analysis. A random effects model was used to partition variation in the peptide intensities between treatment levels (attractors and non-

attractors), the three biological replicates, and the three analytical replicates. **Supplemental Tables 4.3** and **4.4** contain the results for each protein from each analysis human and mouse, respectively. Next, a hierarchical linear model was used to test for differences in mean intensity between the attractors and non-attractors, while allowing each biological replicate to have its own overall mean. The *p*-values from each analysis were corrected for multiple hypothesis testing with an FDR (*q*) of ≤ 0.05 considered significant (Benjamini & Hochberg, 1995). The same model was run on the $\log_2$ converted raw intensities. The differences in estimated mean between attractor and non-attractor in these tests were taken as an estimate of the overall fold change within the treatment. **Supplemental Tables 4.3** and **4.4** list the test statistics and effect estimates for each protein interrogated within each analysis. The *q*-value reported throughout the text is the instantaneous *q* value (q_inst; **Supplemental Tables 4.3** and **4.4**), which is the FDR if the given protein were taken as the least significant protein differentially expressed. For visualization of data, positive fold change values are indicative of an increase in protein expression in attractors relative to non-attractors and negative fold change values are indicative of a decrease in protein expression in attractors relative to non-attractors. Perseus software (version 1.5.16) was used for visualization the data (Cox & Mann, 2012) and the Database for Annotation, Visualization and Integrated Discovery (DAVID version 6.7) for interrogation of enriched (Huang, Sherman, and Lempicki, 2009a; Huang, Sherman, and Lempicki, 2009b) KEGG pathways (Kanehisa & Goto, 2000; Kanehisa *et al*., 2014) with a false discovery rate (FDR) of < 10% using Benjamini-Hochberg *p*-value correction (*q*-value) (Benjamini & Hochberg, 1995). The relative $\log_2$ protein fold changes were matched to hexadecimal color codes as previously described (Mostovenko, Deelder, and Palmblad, 2011). A fold change of +3 corresponded to #FF0000, 0 to #FFFF00 and -4 to #00FF00 for human proteins. A fold change

of +3 corresponded to #FF0000, 0 to #FFFF00 and -1.9 to #00FF00 for mouse proteins The proteins and their corresponding color codes were then mapped onto metabolic pathways available in KEGG using KEGG Mapper (Kanehisa & Goto, 2000; Kanehisa, *et al*., 2014).

TRANSCRIPTOMICS

A custom targeted microarray chip containing functional human gene sets related to glioma biology was used to examine the relative expression of epigenetics, radiation sensitivity, ion channels, metabolomics, ER stress and unfolded protein response, ubiquitination, all Chromosome 19 and all cloned glycogenes (available at www.cazy.org/) compiled from the NCBI human sequence database as part of the UTMB Cancer Consortium Genechip (Kroes 2007; Kroes 2006; Nilsson 2013; Lichti 2014) – in total 2577 transcripts. Each transcript-specific oligonucleotide was spotted in triplicate on the genechip. A full description of the targeted transcriptomics array dynamic range, accuracy, reproducibility as well as and quality control measures is available in Kroes *et al.* (2006 and 2007).

In this study, the relative quantitation of individual transcript abundance in 18 GSC xenografts or 12 GSC (irradiated and non-irradiated) were compared. Briefly, total RNA from each of the defined sample was extracted and purified for amplification and labeling with fluorescent dye Cy5. RNA from the universal reference (Stratagene, La Jolla, CA) was labeled with Cy3 (Churchill 2002). Individually combined samples and reference RNA was hybridized to microarray chips overnight followed by a series of high-stringency washes (Kroes 2007). Microarray chips were scanned by a high-resolution confocal laser (ScanArray 4000XL; Packard Biochip Technologies, Billerica, MA) at 633 nm and 543 nm at 5 μm resolution. Cy3 and Cy5 fluorescence data was analyzed for quality control parameters including but not limited to spot diameter, uniformity, replicate uniformity, and signal to noise ratio (Kroes 2007) using BlueFuse (Illumina Fulbourn, Cambridge, UK). Spots that did not pass the stringent criteria were flagged. Significance of analysis of microarrays algorithm (SAM, v4.0, Stanford University, Palo Alto, CA) (Tusher 2001) was used with minimum 5000 permutations to determine statistically

significant differentially expressed genes. The significance cutoff in these experiments was set to a FDR of < 10% in order to maximize the number of significant genes for downstream ontological analysis. Positive fold change values are indicative of an increase in protein expression in attractors relative to non-attractors and negative fold change values are indicative of a decrease in protein expression in attractors relative to non-attractors (**Supplemental Table 4.3** and **5.1**).

This dataset was previously published (Wildburger *et al.*, 2015) but was re-analyzed by Gene Set Enrichment Analysis (GSEA) (**Chapter V**) to determine significantly enriched glycomic pathways from a custom-made glycomic pathway database (Crosson *et al*., 2009; Mootha *et al*., 2003; Subramanian *et al*., 2005). Significantly enriched data sets are defined at a $p < 0.05$ and a false discovery rate (FDR) $q < 0.30$. DanteR (version 0.1.1) was used to generate a 3D PCA of all glycogenes from GSCXs.

GLYCOMICS

On-tissue digestion. Coronal sections (20 μm) of all GSCXs were brought to room temperature and spotted with 1 μL of PNGase F (50 Units) on the tumor regions of attractor and non-attractor xenografts. The enzymatic deglycosylation reaction was carried out overnight in a water bath at 37 °C. Released N-glycans were collected, reduced with borane-ammonia followed by solid-phase permethylation (SPP) as previously described (Hu *et al*., 2013).

nanoLiquid Chromatography-Mass Spectrometry. Samples were subjected to nanoLC-MS analysis as previously described, (Hu *et al*., 2013; Desantos-Garcia *et al*., 2011; Hu & Mechref, 2012; Hu, Desantos-Garcia, & Mechref *et al*., 2013; Tsai *et al*., 2014) utilizing an LTQ Orbitrap Velos (Thermo Scientific, San Jose, CA, USA) mass spectrometer and Dionex Ultimate 3000 UHPLC system (Thermo Scientific, Sunnyvale, CA, USA). The flow rate of the nanoLC system was set to 350 nL/min. The mobile phase A consisted of 98% water, 2% acetonitrile and 0.1% formic acid while mobile phase B consisted of 100% acetonitrile and 0.1% formic acid. Permethylated glycans were separated on C_{18} column (Thermo Scientific, Pittsburgh, PA, USA) using the following multi-gradient condition; started with 20% mobile phase B for 10 minutes, then increased to 38% B in one minute, after that the percentage of B increased linearly to 60% in 35 minutes, finally 90% B was applied and keep for 5 minutes in order to ensure all glycans are eluted out of the column. The column oven temperature was set to 55^{o}C. The LC system was coupled to MS using nano electrospray ionization source. The resolution of full MS was set to 15,000, which is adequate to resolve close glycan *m/z* values. MS^2 was conducted in data dependent acquisition (DDA) mode; the 4 most intense peaks were subjected to MS^2 analysis

using both collision-induced dissociation (CID) and higher-energy collisional dissociation (HCD).

Data Processing and Analysis. MultiGlycan (Hu *et al*., 2015; Yu *et al*., 2013) was employed to process the raw data files generated by the mass spectrometer. The peak areas of extracted ion chromatograms were used to represent the abundance of each glycan structure detected in the different samples. Data were filtered based on percent missing values (%NA) with > 50% NA removed. Grubb's test was used to identify and remove outliers in the dataset. Data presented as mean ± SEM with $p \leq 0.05$ considered significant.

Wildburger, N.C., *et al*. (2015). ESI-MS/MS and MALDI-IMS Localization Reveals Alterations in Phosphatidic Acid, Diacylglycerol, and DHA in Glioma Stem Cell Xenografts.

This article contains Supplemental Tables 1-2 and Supplemental Figure S1-2 which can be accessed free of charge via http://pubs.acs.org/

ESI-MS/MS AND MALDI-IMS LOCALIZATION REVEALS ALTERATIONS IN PHOSPHATIDIC ACID, DIACYLGLYCEROL, AND DHA IN GLIOMA STEM CELL XENOGRAFTS

Authors: Norelle C. Wildburger[1-2], Paul L. Wood[4], Joy Gumin[5,6], Cheryl F. Lichti[1,3], Mark R. Emmett[7], Frederick F. Lang[5,6§] and Carol L. Nilsson[1,3§]

Affiliation:
1. Department of Pharmacology & Toxicology, University of Texas Medical Branch, 301 University Blvd, Galveston, Texas, 77555-0617, United States

2. Neuroscience Graduate Program, Graduate School of Biomedical Sciences, University of Texas Medical Branch, 301 University Blvd, Galveston, Texas, 77555-0617, United States

3. UTMB Cancer Center, University of Texas Medical Branch, 301 University Blvd, Galveston, Texas, 77555-1074, United States

4. Department of Physiology and Pharmacology, Lincoln Memorial University, 6965 Cumberland Gap Parkway, Harrogate, TN 37752, United States

5. Department of Neurosurgery, The University of Texas M.D. Anderson Cancer Center, 1515 Holcombe Boulevard, Houston, Texas 77030, United States

6. The Brain Tumor Center, The University of Texas MD Anderson Cancer Center, Box 1004, 1515 Holcombe Boulevard, Houston, Texas 77030, USA

7. Department of Biochemistry and Molecular Biology, University of Texas Medical Branch, 301 University Blvd, Galveston, Texas, 77555-0617, United States

§ To whom correspondence may be addressed: Frederick F. Lang and Carol L. Nilsson

Frederick F. Lang, M.D.
Dept. of Neurosurgery, Box 442
The University of Texas MD Anderson Cancer Center
1515 Holcombe Boulevard
Houston, TX 77030
Tel. +1 (713) 792-2400
Fax. +1 (713) 794-4950
flang@mdanderson.org

Carol L. Nilsson, M.D, Ph.D.
Dept. of Pharmacology & Toxicology
University of Texas Medical Branch
301 University Blvd
Galveston, TX 77555
Tel. +1 (409) 747-1840
Fax. +1 (409) 772-9648
clnilsso@utmb.edu

Keywords: MALDI-Imaging Mass Spectrometry, glioblastoma, xenografts, lipidomics, phosphatidic acid, diacylglycerol, docosahexaenoic acid, bone marrow-derived mesenchymal stem cells

Abstract

Glioblastoma (GBM) is the most common adult primary brain tumor. Despite aggressive multimodal therapy, the survival of patients with GBM remains dismal. However, recent evidence has demonstrated the promise of bone marrow-derived mesenchymal stem cells (BM-hMSCs) as a therapeutic delivery vehicle for anti-glioma agents, due to their ability to migrate or home to human gliomas. While several studies have demonstrated the feasibility of harnessing the homing capacity of BM-hMSCs for targeted delivery of cancer therapeutics, it is now also evident, based on clinically relevant glioma stem cell (GSC) models of GBMs, that BM-hMSCs demonstrate variable tropism towards these tumors. In this study, we compared the lipid environment of GSC xenografts that attract BM-hMSCs (N=9) with those that do not attract (N=9), to identify lipid modalities that are conducive to homing of BM-hMSC to GBMs. We identified lipids directly from tissue by matrix-assisted laser desorption/ionization (MALDI) imaging mass spectrometry (IMS) and electrospray ionization-tandem mass spectrometry (ESI-MS/MS) of lipid extracts. Several species of signaling lipids, including phosphatidic acid (PA 36:2, PA 40:5, PA 42:5, and PA 42:7) and diacylglycerol (DAG 34:0, DAG 34:1, DAG 36:1, DAG 38:4, DAG 38:6, and DAG 40:6) were lower in attracting xenografts. Molecular lipid images showed that PA (36:2), DAG (40:6), and docosahexaenoic acid (DHA) were decreased *within* tumor regions of attracting xenografts. Our results provide the first evidence for lipid signaling pathways and lipid-mediated tumor inflammatory responses in the homing of BM-hMSCs to GSC xenografts. Our studies provide new fundamental knowledge on the molecular correlates of the differential homing capacity of BM-hMSCs toward GSC xenografts.

Introduction

Glioblastoma (GBM, World Health Organization (WHO) grade IV astrocytoma) is the most common (Kleihues & Ohgaki, 1999; Louis *et al*., 2007) adult primary brain tumor, with a median survival rate of 14-15 months (Louis *et al*., 2007; Berens & Giese, 1999; Stupp *et al*., 2005). Despite advances in treatment and an aggressive multimodal therapeutic approach including maximal surgical resection, followed by concurrent chemotherapy, radiotherapy, and adjuvant chemotherapy, the disease is nearly universally fatal. This poor outcome is largely due to poor penetration of therapeutic agents across the blood-tumor barrier (Pardridge, 2003; Kosztowski, Zaidi, and Quiñones-Hinojosa, 2009) and resistance of glioma stem cells (GSCs) to standard treatments. We and others have shown that bone marrow-derived human mesenchymal stem cells (BM-hMSCs) show promise in addressing this deficiency because they selectively migrate or home to gliomas after systemic or intravascular delivery, making them attractive vehicles for targeted therapeutic delivery of anti-glioma agents (Kosztowski, Zaidi, and Quiñones-Hinojosa, 2009; Nakamizo *et al*., 2005; Nakamura *et al*., 2004; Studeny *et al*., 2004; Yong *et al*., 2009; Miletic *et al*., 2007; Doucette *et al*., 2011). In fact, due to their intrinsic tropism towards gliomas, BM-hMSCs have been used to deliver immunotherapy (Kosztowski, Zaidi, and Quiñones-Hinojosa, 2009; Nakamizo *et al*., 2005; Nakamura *et al*., 2004), enzymes for chemotherapeutic pro-drugs (Miletic *et al*., 2007), and oncolytic viruses (Yong *et al*., 2009) to human gliomas in animal models. However, despite the potential clinical application of BM-hMSCs in glioma therapy, the mechanism underlying the ability of BM-hMSCs to home to gliomas remains largely unknown. Deciphering this mechanism is not only of biological interest, but could be exploited also to identify the most appropriate patient groups for BM-hMSC-mediated delivery or to enhance the homing of BM-hMSCs to GBMs.

We have recently shown that in addition to the commonly used "professional" glioma cell lines, BM-hMSCs are also capable of homing to xenografts derived from human GSCs (Shinojima *et al*., 2013). Compared to commercially available rat and human glioma cell lines, which poorly mimic clinical tumors, GSCs faithfully recapitulate the genotype and phenotype of human GBMs *in vivo* (Lee *et al*., 2006) and therefore, offer a more clinically relevant model with high translational significance. Like cancer stem cells from many other tumors, GSCs, which are isolated directly from fresh surgical specimens of patient gliomas, represent a sub-population of cells in GBMs that have stem-like properties, including self-renewal (Singh *et al*., 2004; Singh *et al*., 2004). GSCs grow as spheroids *in vitro* and often express CD133 or CD15 on their surface (Singh *et al*., 2004; Clarke *et al*., 2006). Most importantly, GSCs form tumors that mimic human GBMs when injected in small numbers (100-1000 cells) into the brains of athymic mice and are therefore thought to be the tumor-initiating cells that are often resistant to therapy and responsible for treatment failure (Singh *et al*., 2004; Clarke *et al*., 2006).

Although xenografts formed from GSCs are capable of attracting BM-hMSCs, recent work from our group has indicated that not all GSC xenografts are capable of attracting BM-hMSCs equally (Shinojima *et al*., 2013). In our studies of a large group of GSCs we found that intracranial xenografts of some GSCs were capable of strongly attracting BM-hMSCs after intracarotid injection (GSC17, GSC274, GSC268), whereas others showed a more limited capacity to attract BM-hMSCs (GSC11, GSC229, GSC231). The identification of "attractor" GSCs and "non-attractor" GSCs is not only of therapeutic importance, but provides a unique model for understanding the mechanisms underlying the tropism of BM-hMSCs toward GSCs. Evidence suggests that intravascularly-delivered BM-hMSCs extravasate from the blood vessel endothelium via diapedesis in order to localize to the tumor mass (Yong *et al*., 2009).

Extravasation is a complex multi-step process whereby cells within blood vessels migrate in response to soluble factors released from sites of inflammation and/or tissue damage. Lectins on the endothelial surface recognize and bind carbohydrates on glycolipids or glycoproteins on the opposing cell surface, inducing rolling adhesion of circulating cells. Complementary pairs of adhesion molecules on opposing cell surfaces mediate the strengthening of this interaction. Next, the cells begin the process of squeezing between the endothelial cells (diapedesis) that comprise the blood vasculature and migrate throughout the tumor parenchyma (Yong *et al*., 2009).

Several studies, focused on tumor-derived growth factors and cytokines, such as TGF-β (Shinojima *et al*., 2013), PDGF-BB (Hata *et al*., 2010), and SDF-1 (Son *et al*., 2006), have provided clues about soluble factors that mediate BM-hMSC homing to gliomas. However, knowledge of lipids as molecular correlates of GSC xenograft differential homing of BM-hMSCs is lacking. Lipids are not only crucial to the maintenance of cellular structure, but are also important in signal transduction as second messenger molecules. The main structural components of the biological membranes, different classes of lipids and saturations can significantly modulate membrane fluidity, impacting membrane-dependent cellular functions (Helmreich, 2003; Aureli *et al*., 2015). Lipids as signaling molecules can act independently (e.g. as receptor ligands) or in conjunction with proteins through structural-functional modulation (Fernandis & Wenk, 2007; Berridge, 1987). Alterations in lipids are strongly correlated with cancer and other human diseases (e.g. Alzheimer's disease) (Santos & Schulze, 2012; Wood, 2012). Changes in lipid metabolism may influence biological processes, including growth, proliferation, invasion, and energy homeostasis through lipid signal transduction pathways (Santos & Schulze, 2012). In glioma, this becomes especially relevant because the location of these tumors, the brain, contains the highest lipid content of any organ in the body. Lipids are

critical in cell-to-cell communication in the brain and can act as inflammatory mediators. Given the diverse role of lipids in biological systems, we hypothesized that alterations of lipids between attractor and non-attractor GSCs may provide insight into the elements within the tumor environment that are favorable to or elicit cues for BM-hMSC homing. Consequently, we applied high throughput ESI-MS/MS and MALDI-IMS approaches to identify inherent underlying differences in lipid profiles between those tumors that attract BM-hMSCs (attractors) and those that do not (non-attractors).

We have previously performed lipidomic analysis of GSCs and GBM cells (He *et al*., 2010; He *et al*., 2007). For the first time, we have applied lipidomics and MALDI-IMS to GSC xenografts. We employed quantitative lipidomics and matrix-assisted laser desorption/ionization imaging mass spectrometry (MALDI-IMS) from thin tissue sections. Lipidomic analysis by electrospray ionization-tandem mass spectrometry (ESI-MS/MS) allows for the identification and quantification of lipid species (Matyash *et al*., 2008; Wood & Shirley, 2013), while MALDI-IMS permits localization and identification of lipid biomolecules *within* the GSC xenograft tissue. This technology allows direct detection of ionized analytes by rastering a laser across matrix-coated tissue in an ordered array. Each x-y coordinate contains a spectrum of lipid biomolecular ions. The combination of x-y coordinates with signal intensity produces an image representing an *in situ* molecular-histological map (Norris & Caprioli, 2013). The added advantage to this technology is the minimal sample processing, which preserves the integrity of the tissue and its compatibility with other imaging modalities (Chughtai *et al*., 2013).

Using this approach we now detected both global and tumor-specific differences in signaling lipids phosphatidic acid (PA 36:2, PA 40:5, PA 42:5, and PA 42:7) and diacylglycerol (DAG 34:0, DAG 34:1, DAG 36:1, DAG 38:4, DAG 38:6, and DAG 40:6) in attractor *versus*

non-attractor GSC xenografts. Finally, our data reveals decreased levels of docosahexaenoic acid (DHA) in attractors. Taken together, these results implicate phospholipid signaling and lipid-mediated inflammation in BM-hMSCs homing.

Methods

Methods for glioma xenograft model, tissue dissection, sampling and sectioning, lipid extraction and ESI-MS/MS, MALDI-IMS, H&E staining and optical imaging were outlined previously in this work. A complete description of these techniques is detailed in **Chapter II**. All supplemental tables referenced within this manuscript may be found in the digital repository associated with this dissertation.

Results

General strategy for mass spectrometric analysis and imaging of lipids

We employed the workflow outlined in **Figure 3.1** to investigate lipid species, which were differentially expressed in xenograft tumors in the attractor or non-attractor groups, derived from intracranial implantation of human GSCs (Shinojima *et al*., 2013; Singh *et al*., 2004; Singh *et al*., 2004; Lal *et al*., 2000). Tissue slices were obtained from a total of eighteen xenografts. Slices (15 μm) were extracted and analyzed by ESI-MS/MS (Matyash *et al*., 2008; Wood & Shirley, 2013), or MALDI-IMS (10 μm) as described in *Methods and Materials*). We obtained quantitative measurements of lipid species with high resolution MS/MS confirmation of assignments (**Supplemental Table 3.1**). The MALDI-IMS technology allowed for *in situ* localization of lipid species from the lipidomics analysis as intact molecular ions with confirmation of selected *m/z* assignments by MS/MS.

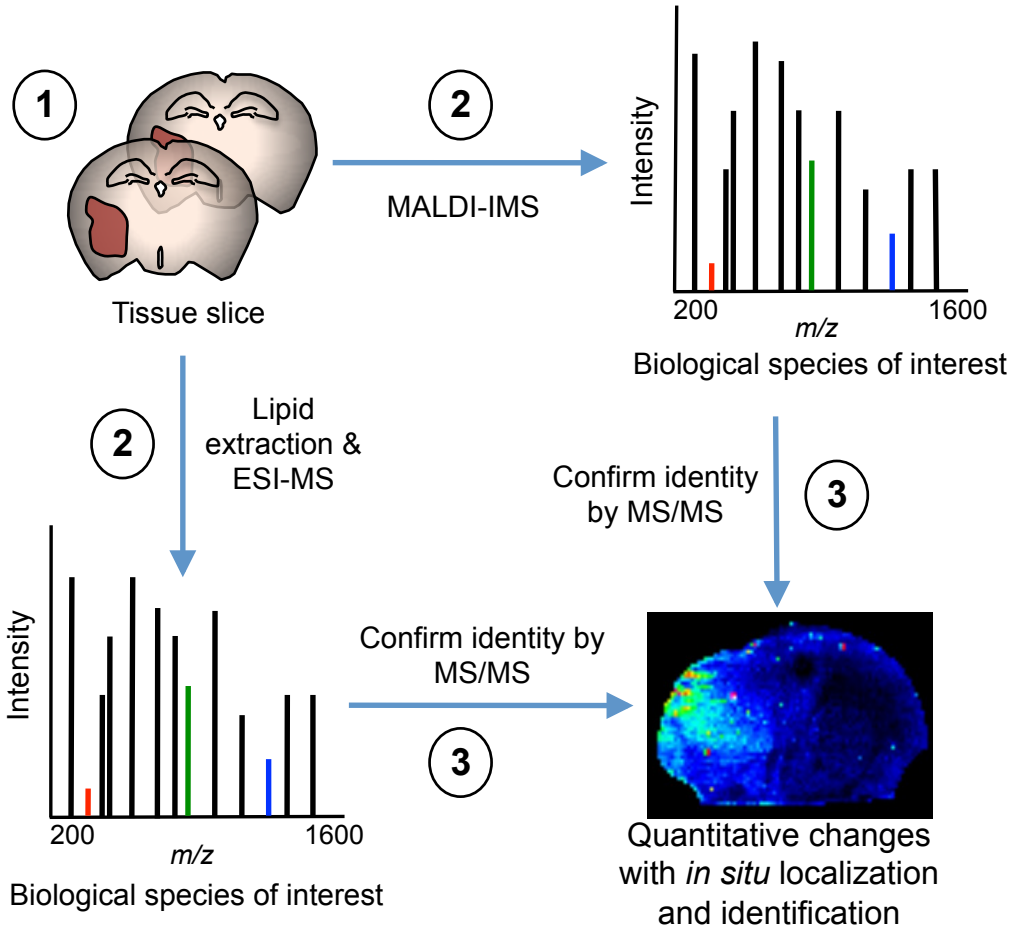

Figure 3.1. Workflow outlining tissue sample preparation for combined lipidomics and MALDI-IMS. (1) Serial coronal sections from GSC xenografts at 10 and 15 µm. (2) MALDI-IMS (10 µm) and lipid extraction ESI-MS/MS (15 µm) experiments were performed in parallel. (3) The identity of biological species of interest was confirmed by MS/MS. Lipid extraction and ESI-MS/MS provide quantitative measures of lipid species at high-resolution with submillimass accuracy and MALDI-IMS provides lipid localization of identified lipids as intact molecular ions

Identification of Phosphatidic Acid Alterations

Analysis of lipid extracts from tissue slices detected multiple species of phosphatidic acid (PA), and quantification of these detected species revealed a subset of PA species PA (36:2), PA (40:5), PA (42:5), and PA (42:7), that were significantly lower in tumors of the attractor phenotype compared with the non-attractor phenotype (**Fig. 3.2A**). This pattern held true even for the PA species that did not reach statistical significance (**Supplemental Table 3.1**). Intriguingly, species of lysophosphatidic acid (LPA), the common precursor of PA via the Kennedy Pathway (Wang *et al*., 2006; Bruntz, Lindsely, and Brown, 2014; Kennedy, 1987), detected and validated by ESI-MS/MS (LPA 16:0, LPA 18:2, and LPA 18:3) were not statistically different between the two tumor phenotypes (**Supplemental Table 3.1**).

Next, we sought to localize the distribution of the significant PA species by MALDI-IMS in negative ion mode through inspection of the intact mass of anions. Of the significant PA species identified by ESI-MS/MS, PA (40:5), PA (42:5), and PA (42:7) did not specifically localize to the tumor region (*data not shown*), suggesting that the elevated levels quantified by ESI-MS/MS represent a global decrease of these species in the attracting xenografts. We did, however, find that PA (36:2) at *m/z* 735.4 $[M+Cl]^-$ was largely depleted in the tumor area of attractors (**Fig. 3.2B**), whereas it was consistently present in the tumor area of non-attractors (**Fig. 3.2D**). Corresponding tissue was stained for hematoxylin-eosin (H&E) to correlate lipid distribution with histological features (**Fig. 3.2C, E**, respectively). To confirm the PA (36:2) finding, we performed MS/MS analysis of *m/z* 735.4 in the MALDI-TOF/TOF directly on the tissue. The tissue-derived MALDI-MS/MS analysis of *m/z* 735.4 yielded product ions consistent with the structure of PA (18:0/18:2) (**Fig. 3.2F** and **Table 3.1**).

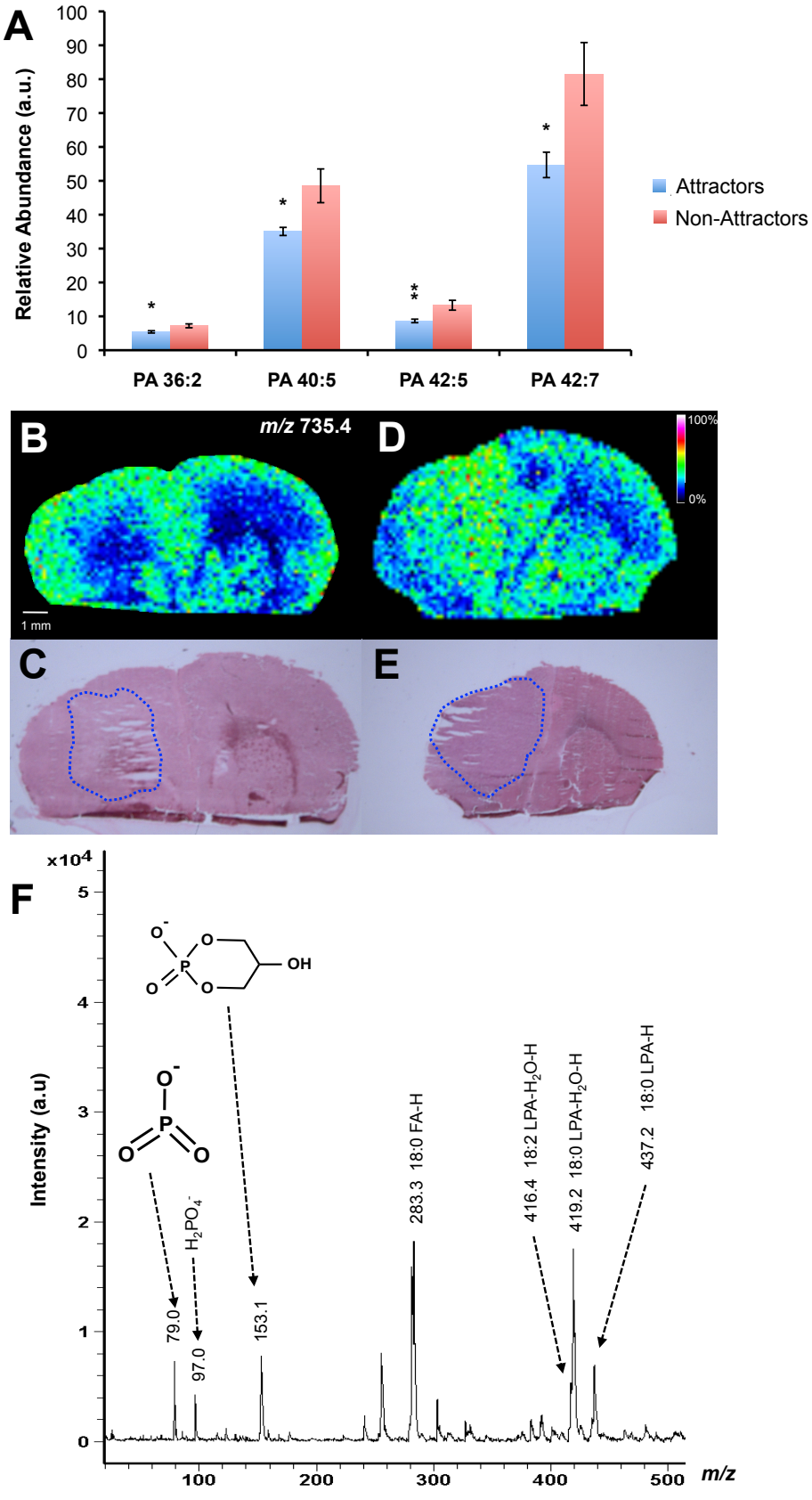
A
Relative Abundance (a.u.)
100
90
80
70
60
50
40
30
20
10
0
PA 36:2
PA 40:5
PA 42:5
PA 42:7
Attractors
Non-Attractors
B
m/z 735.4
D
100%
0%
1 mm
C
E
F
x10^4
Intensity (a.u)
5
4
3
2
1
0
79.0
97.0
153.1
283.3 18:0 FA-H
416.4 18:2 LPA-H2O-H
419.2 18:0 LPA-H2O-H
437.2 18:0 LPA-H
H2PO4-
OH
100
200
300
400
500
m/z

Figure 3.2. Negative ion MALDI-IMS of PA in GSC xenografts. (**A)** Relative abundance of PA (36:2), PA (40:5), PA (42:5), and PA (42:7) as determined by ESI-MS/MS. Values are mean ± SEM (n = 9 for each phenotype) of the lipid abundance as the ratio of lipid peak area to the peak area of an internal standard corrected for protein concentration; * $p < 0.05$ and ** $p < 0.01$ (Student's *t*-test). (**B**) Negative ion image derived from MALDI-IMS experiments of a representative attractor demonstrating the low signal intensity of PA (36:2) (*m/z* 735.4). Color intensity of the ion micrographs corresponds to signal strength. (**C**) H&E staining of corresponding tissue section used in MALDI-IMS experiment. Tumor area is outlined in *blue*. (**D**) Negative ion image derived from MALDI-IMS experiments of a representative non-attractor demonstrating the distribution and signal intensity of *m/z* 735.4. (**E**) H&E staining of corresponding tissue section used in MALDI-IMS experiment. Tumor area is outlined in *blue*. (**F**) Annotated MS/MS spectrum of PA (36:2) suggesting isoform PA (18:0/18:2). MS/MS product ions are shown in **Table 3.1**.

Identification of Diacylglycerol Alterations

ESI-MS/MS of GSC xenograft lipid extracts showed a number of DAG species (DAG 34:0, DAG 34:1, DAG 36:1, DAG 38:4, DAG 38:6, and DAG 40:6) that were significantly and differentially expressed between the two tumor phenotypes. All differentially expressed DAG species were significantly lower in the attractor GSCs compared with non-attractor GSCs (**Fig. 3.3A**). This trend was consistent even for detected DAG species that did not reach significance (**Supplemental Table 3.1**). We analyzed the distribution of the significant DAG species by positive ion mode MALDI-IMS. Of the significant DAG species (**Fig. 3.3A**), DAG (34:0), DAG (34:1), DAG (36:1), DAG (38:4), and DAG (38:6) did not consistently localize to any particular histological region (*data not shown*). This suggests that the lipid levels quantified by ESI-MS/MS represent a global decrease of these species in the attractor brains compared with the non-attractor brains. MALDI-IMS of DAG (40:6), on the other hand, was absent in the tumor area of attractor xenografts (**Fig. 3.3B**) but consistently present at *m/z* 707.1 $[M+K]^+$ in the tumor area of non-attractors (**Fig. 3.3D**). Corresponding tissue was stained to correlate the MALDI-IMS lipid distribution with histopathological features in a representative attractor and non-attractor xenograft (**Fig. 3.3C** and **E**, respectively). Performing MALDI-MS/MS directly from the tissue on the precursor *m/z* 707.1, we were able to obtain some fragmentation (**Supplemental Figure S3.2**) though diacylglycerols are more amenable to ESI-MS/MS than MALDI-MS/MS. The MS/MS spectrum of *m/z* 707.1 $[M+K]^+$ did reveal a product ion at *m/z* 323.6 which is consistent with the potassiated 18:0 FA at the C-1 (*sn*-1) position (Al-Saad *et al*., 2003). This would leave the remaining fatty acyl to consist of C22:6 at either *m/z* 385 (22:6 FA cyclized at the glycerol backbone), an energetically favorable reaction, which forms a six-member ring (Al-Saad *et al*., 2003), or *m/z* 367 $[FA+H+K]^+$ likely at the C-2 (*sn*-2) position. However, these ions

were not observed in our spectrum do to the difficulty of using MALDI to fragment DAG as well as the inherent difficulties of fragmenting DHA or DHA-containing lipids, which ionize better in negative ion mode.

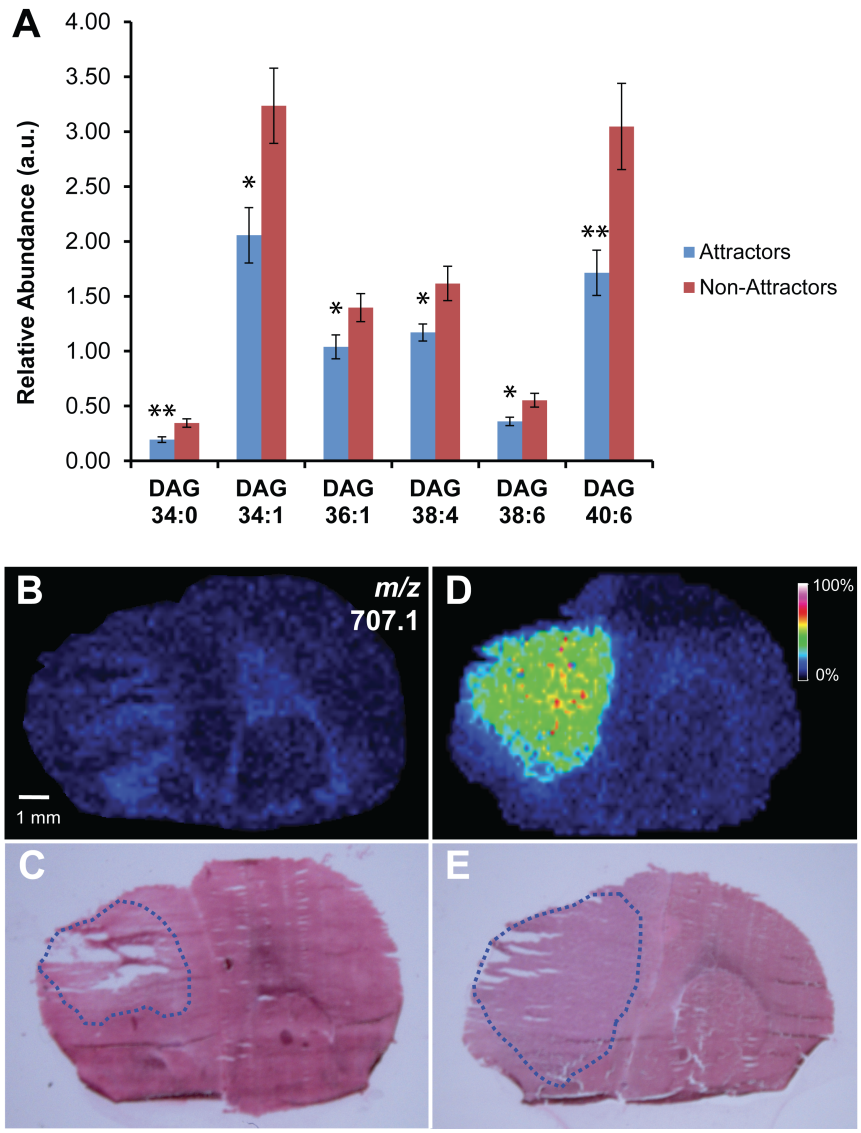

Figure 3.3. Positive ion MALDI-IMS of DAG lipids in GSC xenografts. (**A**) Relative abundance of DAG (34:0), DAG (34:1), DAG (36:1), DAG (38:4), DAG (38:6), and DAG (40:6) as determined by ESI-MS/MS. Values are mean ± SEM (n = 9 for each phenotype) of the lipid abundance as the ratio of lipid peak area to the peak area of an internal standard corrected for protein concentration; * $p < 0.05$ and ** $p < 0.01$ (Student's *t*-test). (**B**) Positive ion image from MALDI-IMS experiments of a representative attractor specimen, demonstrating the localization and signal intensity of DAG (40:6) (*m/z* 707.1). Image color intensity corresponds to signal strength. (**C**) H&E staining of corresponding tissue section analyzed by MALDI-IMS. The tumor area is outlined in *blue*. **(D)** Positive ion image of DAG (40:6), *m/z* 707.1 from MALDI-IMS experiments of a representative non-attractor specimen. (**E**) H&E staining of a corresponding tissue section analyzed by MALDI-IMS. The tumor area is outlined in *blue*.

Docosahexaenoic Acid

Docosahexaenoic Acid (DHA) is one of the most abundant polyunsaturated lipids in the CNS (O'Brien & Sampson, 1965; Svennerholm, 1968) and serves as a precursor for bioactive molecules (Hong *et al*., 2003; Mukherjee *et al*., 2004; Marcheselli *et al*., 2003; Ariel & Serhan, 2007; Schwab *et al*., 2007). Lipid analysis by ESI-MS/MS data identified DHA as significantly decreased in tumors of the attractor phenotype ($p = 0.046$). By MALDI-IMS we found the intact mass of DHA anions, $[M-H]^-$ *m/z* 327.0, to be consistently decreased within the tumor area of attractors compared to non-attractors. Representative negative ion images of an attractor and non-attractor are shown in **Figure 3.4** (**A** and **C**, respectively) with corresponding H&E staining (**Fig. 3.4B** and **D**, respectively) outlining the tumor area (*blue*). Quantified relative abundance of DHA from xenograft tissue using total lipid extract and ESI-MS/MS is shown in **Figure 3.4E**. MALDI-MS/MS fragmentation was performed on the parent anion. The spectrum of *m/z* 327.0 produced product ions that were consistent with its assignment of DHA (**Table 3.1**). The annotated MS/MS spectrum from the MALDI in negative ion mode confirming the identity of DHA can be seen in **Figure 3.4F**. The assignment was also confirmed with the MS/MS spectrum from a standard directly spotted on a MALDI plate with DHB (**Supplemental Figure S3.1**).

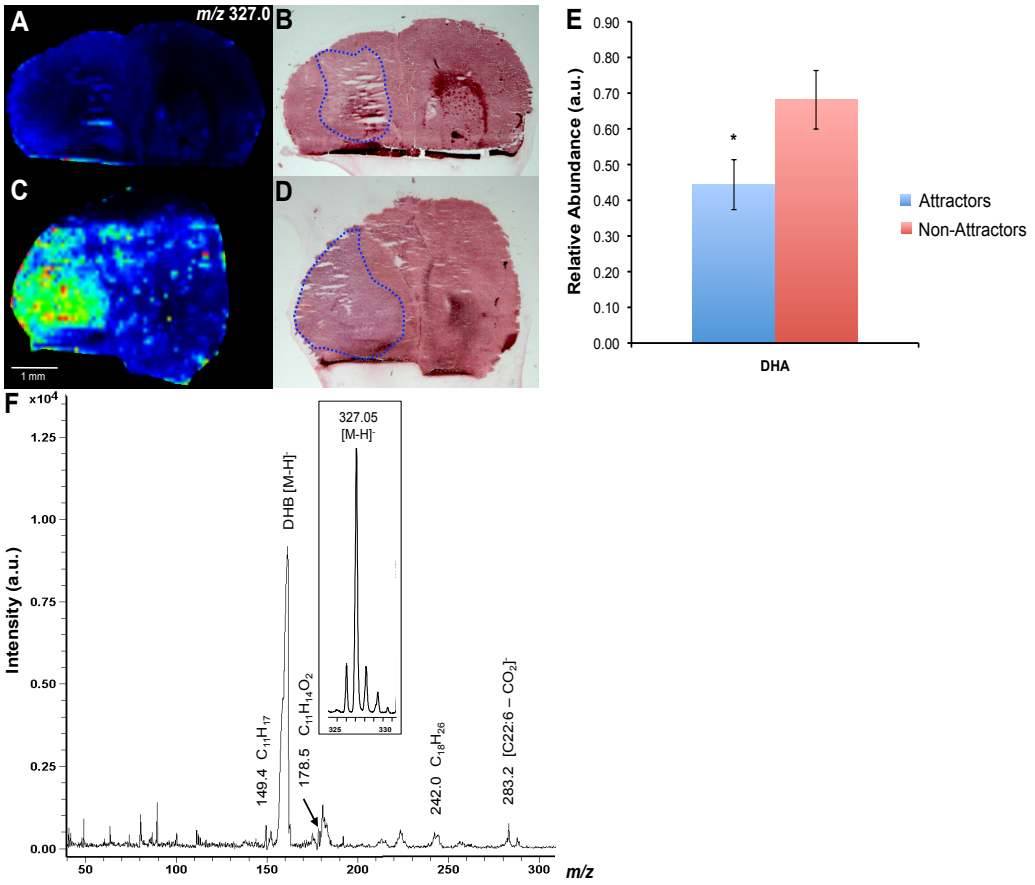

Figure 3.4. Tumor-specific localization of DHA. (**A** and **C**) Negative ion images derived from MALDI-IMS experiments showing the localization and signal intensity of DHA (22:6) *m/z* 327.0 in a representative non-attractor and attractor, respectively. (**B** and **D**) H&E stain of tissue sections used in MALDI-IMS experiments in a non-attractor and attractor, respectively. The tumor area is outlined in *blue*. (**E**) Relative abundance of DHA as determined by ESI-MS/MS (p = 0.046). (**F**) Annotated negative ion MS/MS spectrum of *m/z* 327.0 with precursor ion (*inset*). The most abundant peak, DHB $[M\text{-}H]^-$, represents the matrix. MS/MS product ions are shown in **Table 3.1**.

Table 3.1: Summary of the negative and positive ion MS/MS by CID obtained directly from tumor sections post-MALDI-IMS

Observed (*m/z*)	Product Ions (*m/z*)	Assignment
735.4 [M+Cl]-	79.0, 97.0, 153.1, 283.3, 416.4, 419.2, 437.2	PA (18:0/18:2)
327 [M-H]-	149.4, 178.5, 242.0, 283.2	DHA (22:6)

Discussion

While several studies have demonstrated the feasibility of harnessing the homing capacity of BM-hMSCs for targeted delivery of cancer therapeutics (Kosztowski, Zaidi, and Quiñones-Hinojosa, 2009; Nakamizo *et al*., 2005; Nakamura *et al*., 2004; Studeny *et al*., 2004; Yong *et al*., 2009; Miletic *et al*., 2007; Doucette *et al*., 2011), it is now evident, using a clinically relevant model of glioma, that BM-hMSCs demonstrate variable tropism towards these tumors (Shinojima *et al*., 2013). We demonstrate that specific lipid species including PA, DAG, and DHA species are differentially expressed in GSCs that support BM-hMSC homing, compared with those that do not. To the best of our knowledge, our study is the first to examine lipids in relation to BM-hMSC homing towards glioma. Our approach included ESI-MS/MS based quantitative lipidomics and MALDI-IMS to examine lipid profiles from GSC xenograft tissue. ESI-MS/MS provided high-resolution, high-mass accuracy quantitative data of lipid species (**Supplemental Table 3.1**). MALDI-IMS allowed visualization of the distribution of significant lipid species detected by ESI-MS/MS as molecular ions *within* the tissue; MALDI-MS/MS on tissue-derived molecular ions was provided.

We were intrigued by the results for phosphatidic acid (PA) and diacylglycerol (DAG) due to their capacity to act as signaling lipids and their interconnectivity through the Kennedy Pathway (Kennedy, 1987). Also of interest were docosahexaenoic acid (DHA), an abundant CNS lipid and precursor to many bioactive molecules (O'Brien & Sampson, 1965; Svennerholm, 1968; Hong *et al*., 2003; Mukherjee *et al*., 2004; Marcheselli *et al*., 2003; Ariel & Serhan, 2007; Schwab *et al*., 2007). All were significantly decreased in the attractor phenotype (**Fig. 3.2A** and 3.**3A**, respectively), and this trend remained consistent for the species of PA and DAG that did not achieve significance in our lipid extract analysis (**Supplemental Table 3.1**). MALDI-IMS

analysis demonstrated that of these lipids, PA (36:2) and DAG (40:6) had histopathological relevance, being absent in the tumor regions of attractor xenografts compared with the tumor region of non-attractors, where they were enriched (**Fig. 3.2B-E** and **Fig. 3.3B-E**, respectively). The DAG (40:6) potassiated molecular ion fragmentation spectrum suggests that the particular isoform is DHA containing DAG (22:6/18:0), in which the polyunsaturated fatty acid (PUFA) is located at the *sn*-1 position. Typically, but not invariably the *sn*-1 position will contain a saturated acyl chain and the *sn*-2 position will be occupied by an unsaturated acyl chain (e.g. PUFA) (Cooper, 1970). Several lines of evidence indicate that the *sn*-1 position may be occupied by PUFAs (Beermann *et al*., 2005) including DAG (22:6/18:0) (Quehenberger *et al*., 2010). DHA (22:6) itself was lower in attractors *vs* non-attractors (**Fig. 3.4E**). Further investigation by MALDI-IMS demonstrated that, as with PA (36:2) and DAG (40:6), DHA expression levels correlated histopathologically with the tumor regions. DHA was largely depleted in the tumor region of attractor xenografts, but highly expressed in the tumors of non-attractors (**Fig. 3.4A-D**).

PA and DAG are multifunctional lipids that not only serve as a precursor to other lipids, but as biologically active signaling molecules (Bruntz, Lindsley, and Brown, 2014; Shulga, Topham, and Epand, 2011). Changes in these lipids may affect signaling pathways, nuclear signaling, and membrane ultrastructure in diverse and complex ways (Wang *et al*., 2006; Bruntz, Lindsley, and Brown, 2014; Berridge, 1987; Peddie *et al.,* 2014; Domart *et al*., 2012). In addition, DAGs are non-lamellar lipids that serve critical structural functions in the nuclear envelope, nucleoplasmic reticulum, membrane pore formation, membrane protein fusion, vesicle fusion, and membrane budding (Peddie *et al.,* 2014; Domart *et al*., 2012). All glycerophospholipids are derivatives of PA through DAG (Kennedy, 1987). Glycerophospholipids are important structural lipids as the main component of membranes

(Hermansson *et al*., 2011; van Meer, Voelker, and Feigenson, 2008). However, they may also affect signal transduction because they serve as reservoirs for signaling lipids via lipid remodeling at *sn*-2 (Hermansson *et al*., 2011; van Meer, Voelker, and Feigenson, 2008). The overwhelming majority of glycerophospholipids detected in our dataset were decreased in attractors (**Supplemental Table 3.1**), which is consistent with our measured decreases in the precursors PA and DAG.

Intriguingly, while the detected PA species were consistently lower in the attractors, the lipid precursor to PA – LPA – was not significantly differentially expressed (**Supplemental Table 3.1**). The statistically significant difference in PA levels, but not LPA, suggests that there are underlying biochemical differences governing lipid metabolism between the tumor phenotypes. The acylation of LPA by LPAAT is the most common pathway of PA biosynthesis (Bruntz, Lindsley, and Brown, 2014; Kennedy, 1987), though we do not exclude the possibility of alterations in PA levels due to differences in phospholipase D activity between the two tumor phenotypes (Bruntz, Lindsley, and Brown, 2014). Likewise, PA may serve as a precursor to DAG within the Kennedy Pathway through enzymatic dephosphorylation (Bruntz, Lindsley, and Brown, 2014; Kennedy, 1987; Shulga, Topham, and Epand, 2011), though phospholipase C mediated cleavage of phosphatidylinositol 4,5-bisphosphate (PIP_2) may also contribute to alterations in DAG biosynthesis (Berridge, 1987).

While PA and DAG are effectors for a number of proteins, a point of convergence for both DAG and PA is the activation of protein kinase C (PKC) signaling. The decreased expression of both PA and DAG in attractors may point to a role for PKC signaling as a downstream effector in the BM-hMSC homing (Bruntz, Lindsley, and Brown, 2014; van Meer, Voelker, and Feigenson, 2008). DAG governs the activation of both the classical and novel type

of PKCs (Griner & Kazanietz, 2007), whereas PA has been reported to activate select PKC isoforms representative of all three groups (classical, novel, and atypical) (Bruntz, Lindsley, and Brown, 2014). The role of PKC in tumorigenesis is complex and in glioma poorly understood (Griner & Kazanietz, 2007). This in part stems from past studies using non-selective pharmacological inhibitors of PKC, the relative contribution of each PKC isoform, and the variability of actions (Griner & Kazanietz, 2007). Nonetheless, future studies are needed to dissect the role of PKC in the homing of BM-hMSCs to gliomas.

Lastly, DHA is the major PUFA in the CNS (O'Brien & Sampson, 1965; Svennerholm, 1968; Hong *et al*., 2003) and is a precursor for potent bioactive molecules (Hong *et al*., 2003). As with many other cancers, the balance of fatty acids – arachidonic acid (AA) and DHA – are dysregulated in glioma. A significant decrease in DHA and DHA-containing glycerophospholipids has been previously observed in malignant glioma compared to normal brain tissue (Martin *et al*., 1996; Albert & Anderson, 1977). This decrease was accompanied by unchanged levels of AA (Albert & Anderson, 1977; Elsherbiny, Emara, and Godbout, 2013). The mechanism of this disruption in the homeostatic DHA:AA ratio is unclear. However, one of most important functions of DHA is the resolution of inflammatory processes (Hong *et al*., 2003; Mukherjee *et al*., 2004; Marcheselli *et al*., 2003). The anti-inflammatory actions of DHA are the result of its metabolic products resolvins, neuroprotectins, and maresins (Hong *et al*., 2003; Mukherjee *et al*., 2004; Marcheselli *et al*., 2003; Ariel & Serhan, 2007; Schwab *et al*., 2007). These molecules are transient lipids that are extremely difficult to measure. However, we can surmise that a decrease in DHA in attractor xenografts compared to non-attractors indicates relatively increased lipid-mediated inflammation.

Ultimately, the rationale to use BM-hMSCs for targeted delivery of cancer therapeutics is their unique ability to home and engraft into tissues that have undergone injury or severe stress (Mahmood, Lu, and Chopp, 2004; Li *et al*., 2000; Coussens & Werb, 2002; Orlic *et al*., 2001). Solid tumors are considered "wounds that do not heal" (Dvorak, 1986) and gliomas are no exception. Gliomas not only possess an environment conducive to BM-hMSC engraftment (Nakamizo *et al*., 2005, Studeny *et al*., 2002), but also elicit effective signals for BM-hMSC homing. In relation to the differential homing of BM-hMSCs in attractors *vs* non-attractors, the correlation between decreased DHA and the attractor phenotype may allow a permissive environment for BM-hMSC homing. The elevated levels of DHA in the non-attractor phenotype, on the other hand, may indicate relatively less inflammation correlating to less attraction to intravascularly delivered BM-hMSCs in these tumors. In this context, DHA may serve as a surrogate marker for relatively less inflammation. From a translational standpoint, our observation raises the possibility of DHA as a predictive measure of BM-hMSC homing efficacy. DHA radiotracers (^{11}C) have been used recently to image DHA metabolism in the brain by positron emission tomography (PET) (Basselin, Ramadan, and Rapoport, 2012). More recently, longer-lived ^{18}F-fluoro tracers have been developed to measure DHA content within the brain.

Presently, glioblastoma remains a nearly universally fatal disease despite aggressive treatment. Bone marrow-derived human mesenchymal stem cells show promise as cancer therapeutic delivery vehicles due to their intrinsic tropism for gliomas (Kosztowski, Zaidi, and Quiñones-Hinojosa, 2009; Nakamizo *et al*., 2005; Nakamura *et al*., 2004; Studeny *et al*., 2004; Yong *et al*., 2009; Miletic *et al*., 2007; Doucette *et al*., 2011). In a clinically relevant orthotopic GSC xenograft model, these cells display variable tropism – the molecular basis of which is

poorly understood. In the effort to understand BM-hMSC homing, the focus has been extensively confined to the evaluation of tumor-derived soluble factors (Shinojima *et al*., 2013, Hata *et al*., 2010; Son *et al*., 2006). However, lipids are not only critical to cell membrane properties, but also serve as important signaling molecules and have not been examined in previous homing studies. Our data are the first to suggest that PA and DAG, important lipid signaling hubs, may be involved in the homing process. Furthermore, the elevated levels of DHA in non-attractors compared to attractors may be indicator of relatively lower inflammatory response in these tumors, suggesting that differences in these processes between glioma tumors may regulate BM-hMSC homing efficacy (Albert & Anderson, Elsherbiny, Emara, and Godbout, 2013; Mahmood, Lu, and Chopp, 2004; Li *et al*., 2000; Coussens & Werb, 2002). Taken together, our findings underscore the importance of lipid signaling in gliomas and provide new insights in advancing our understanding of underlying molecular differences that may mediate the differential homing capacity of BM-hMSCs to GSC xenografts and encourage further investigations.

Acknowledgements

The authors gratefully acknowledge the financial support of the Cancer Prevention Research Institute of Texas (CPRIT) and The University of Texas Medical Branch to C.L.N. Grants from the National Cancer Institute CA115729 and 1P50 CA127001, The Broach Foundation for Brain Cancer Research, The Elias Family Fund, The National Brain Tumor Foundation, The Collaborative Ependymoma Research Network (CERN), The Gene Pennebaker Brain Cancer Fund, The Sorenson Foundation, and The Brian McCulloch Fund to F.F.L and Lincoln Memorial University (P.L.W.) are gratefully acknowledged.

Conflict of Interest

The authors do not have any conflicts of interest to disclose.

Author Contributions

N.C.W. conceived of the study, designed, and performed all MALDI-IMS experiments, data analysis and interpretation, and wrote the paper. P.L.W. contributed to the experimental design, performed all lipid extractions, and data acquisition on the Q-Exactive. J.G. grew stem cell lines and performed all animal work. C.F.L. contributed to the experimental design and interpretation of MALDI-TOF/TOF data. M.R.E. conceived the project and contributed critical review of MALDI-TOF/TOF data, technical support, and helpful discussions. C.L.N. and F.F.L conceived the project and supervised the work and critically revised the manuscript. All authors read and approved the final manuscript.

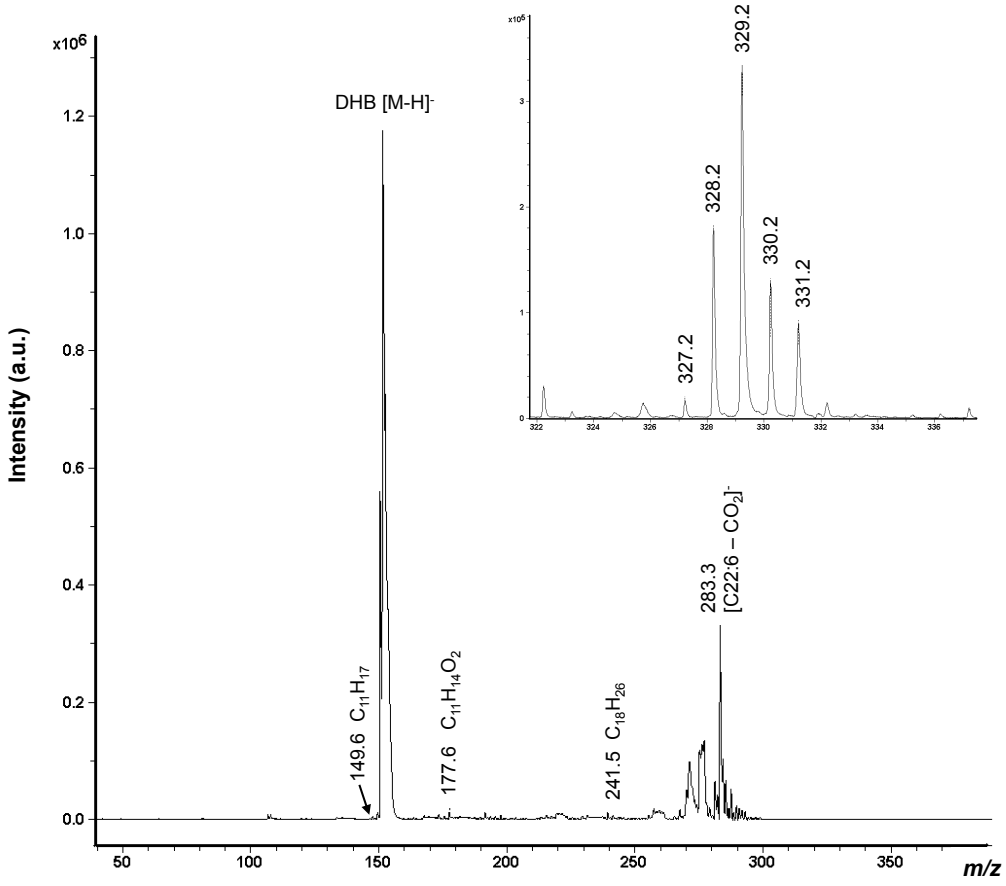

Supplemental Figure S3.1. Annotated MS/MS spectrum of DHA (22:6) standard for comparison to tissue-acquired DHA in **Figure 4F**.

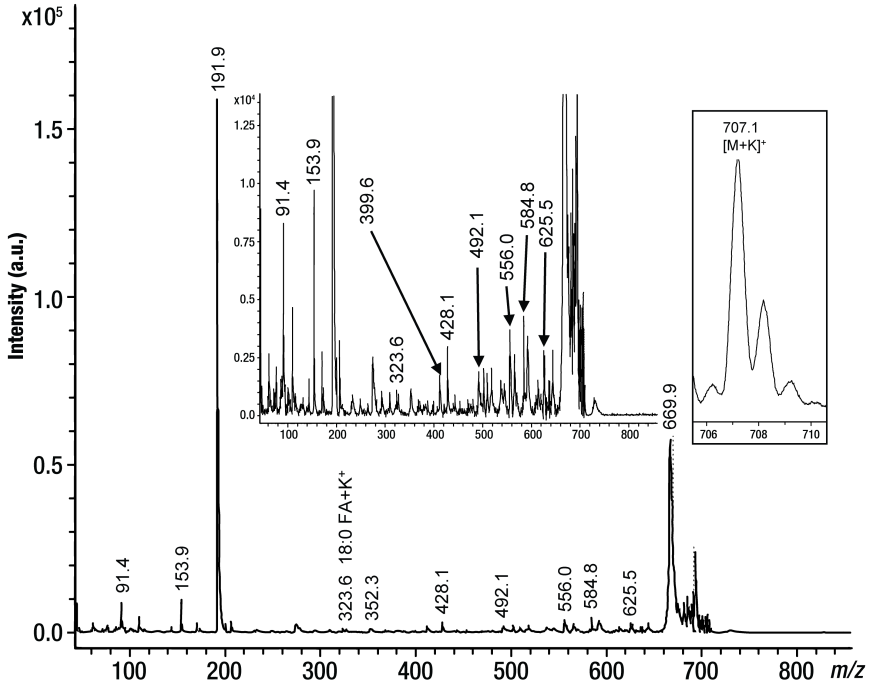

Supplemental Figure S3.2. Annotated MS/MS spectrum of DAG (40:6) suggesting DHA-containing DAG (22:6/18:0). Precursor ion of potassiated DAG (40:6) *m/z* 707.1 is shown (*inset*). Peak at *m/z* 191.9 is DHB matrix ion and the peak at 323.6 represents potassiated 18:0 FA $[FA+K^+]^+$

Tissue DHA

m/z (observed)	*m/z* (theoretical)	s/n	Assignment	Δppm
327.05	327.2	244	$C_{22}H_{31}O_2$	-485.4
149.4	149.1	6	$C_{11}H_{17}$	2012.1
178.5	178.1	4	$C_{11}H_{14}O_2$	2245.9
242.0	242.2	4	$C_{18}H_{26}$	-825.7
283.2	283.2	8	$C_{21}H_{31}$	0

Standard DHA

m/z (observed)	*m/z* (theoretical)	s/n	Assignment	Δppm
327.2	327.2	10	$C_{22}H_{31}O_2$	0
149.6	149.1	4	$C_{11}H_{17}$	3353.4
177.6	178.1	3	$C_{11}H_{14}O_2$	-2807.4
241.5	242.2	2	$C_{18}H_{26}$	-2890.2
283.3	283.2	111	$C_{21}H_{31}$	353.1

Supplemental Table 3.2: Summary of the MS/MS fragmentation of DHA from tissue and standard.

The following chapter was submitted to the EuPa Open Proteomics (February 2015) under the title “Quantitative Proteomics and Transcriptomics Reveals Metabolic Differences in Attracting and Non-Attracting Human-in-Mouse Glioma Stem Cell Xenografts and Stromal Cells”.

QUANTITATIVE PROTEOMICS AND TRANSCRIPTOMICS REVEALS METABOLIC DIFFERENCES IN ATTRACTING AND NON-ATTRACTING HUMAN-IN-MOUSE GLIOMA STEM CELL XENOGRAFTS AND STROMAL CELLS

Authors: Norelle C. Wildburger[1§], Cheryl F. Lichti[2,3], Richard D. LeDuc[4], Mary Schmidt[5], Roger A. Kroes[5], Joseph R. Moskal[5], and Carol L. Nilsson[2,3§]

Affiliation:

1. Neuroscience Graduate Program, Graduate School of Biomedical Sciences, University of Texas Medical Branch, 301 University Blvd, Galveston, Texas, 77555-1074, United States

2. Department of Pharmacology & Toxicology, University of Texas Medical Branch, 301 University Blvd, Galveston, Texas, 77555, United States

3. UTMB Cancer Center, University of Texas Medical Branch, 301 University Blvd, Galveston, Texas, 77555-1074, United States

4. Proteomics Center of Excellence, Northwestern University, 2170 Campus Dr., Evanston, Illinois 60208, United States

5. The Falk Center for Molecular Therapeutics, McCormick School of Engineering and Applied Sciences, Northwestern University, 1801 Maple Street, Evanston, Illinois 60201, United States

§ To whom correspondence may be addressed: Norelle C. Wildburger and Carol L. Nilsson

Norelle C. Wildburger
Dept. of Pharmacology and Toxicology
Dept. of Neuroscience and Cell Biology
University of Texas Medical Branch
301 University Blvd
Galveston, TX 77555-0617
Tel. +1 (409) 772-4965
ncwildbu@utmb.edu

Carol L. Nilsson, M.D, Ph.D.
Dept. of Pharmacology & Toxicology
CPRIT Scholar in Cancer Research
University of Texas Medical Branch
301 University Blvd
Galveston, TX 77555-1074
Tel. +1 (409) 747 1840
Fax. +1 (409) 772 9648
clnilsso@utmb.edu

Keywords: Glioblastoma, bone marrow-derived human mesenchymal stem cells (BM-hMSCs), mass spectrometry, cancer proteomics, transcriptomics, fatty acid metabolism, glycolysis, pentose phosphate pathway, ROS, glycosylation

Highlights

- Compromised fatty acid metabolism reduces the inflammation-resolving lipid DHA
- Glucose-dependent pathways are compromised in BM-hMSC-attracting glioma xenografts
- Down-regulation of PPP in BM-hMSC-attracting glioma xenografts suggests increased ROS
- Glyco-transcriptomics suggests N-glycan signature associated with BM-hMSC-attracting glioma xenografts
- Stroma shows increased glucose metabolism in attracting xenografts

Graphical Abstract

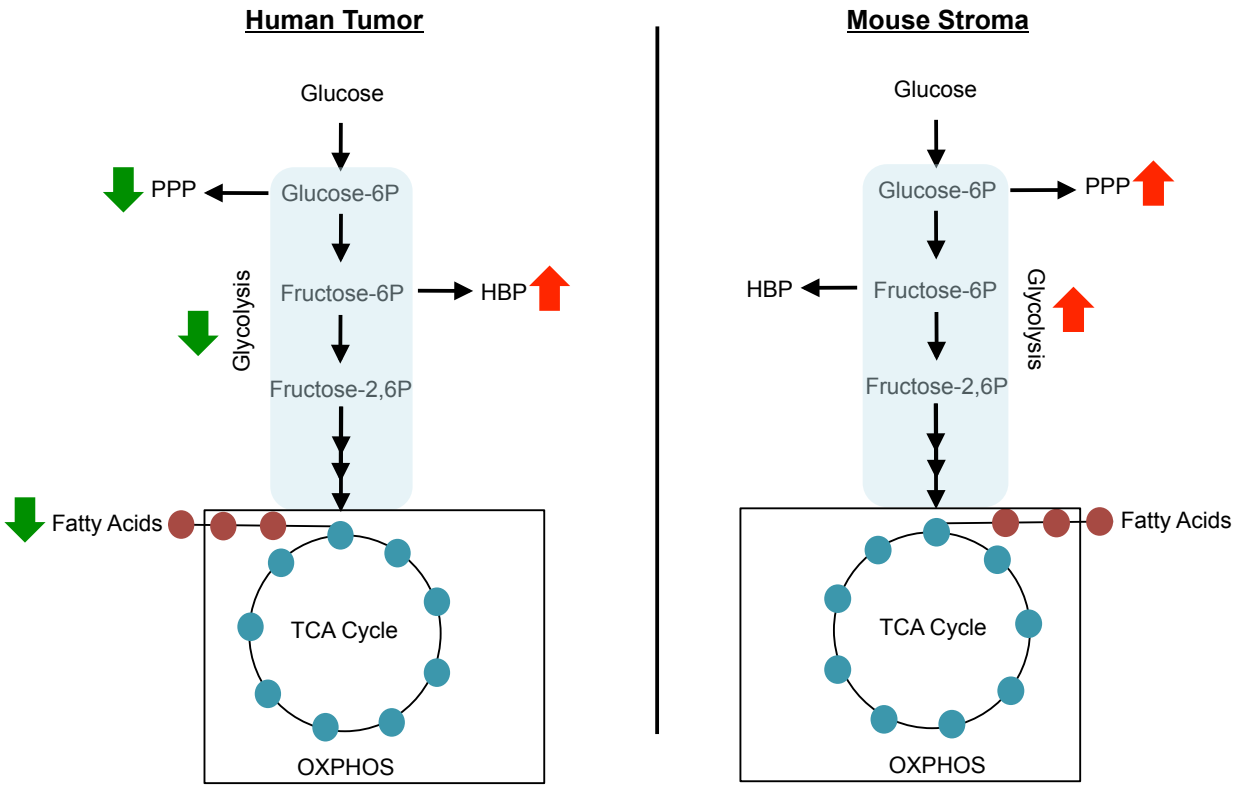

Abstract

Bone marrow-derived human mesenchymal stem cells (BM-hMSCs) show promise as cell-based delivery vehicles for anti-glioma therapeutics, due to innate tropism for gliomas. However, in clinically relevant human-in-mouse glioma stem cell xenograft models, BM-hMSCs tropism is variable. We compared the proteomic profile of cancer and stromal cells in GSCXs that attract BM-hMSCs ("attractors") with those to do not ("non-attractors") to identify pathways that may modulate BM-hMSC homing, followed by targeted transcriptomics. The results provide the first link between fatty acid metabolism, glucose metabolism, ROS, and N-glycosylation patterns in attractors. Reciprocal expression of these pathways in the stromal cells suggests microenvironmental cross-talk.

Introduction

Glioblastoma (GBM) is the most common adult primary brain tumor (Kleihues & Ohgaki, 1999; Louis *et al*., 2007). Despite an aggressive multimodal therapeutic approach, the median survival rate is approximately one year (Berens & Giese, 1999; Louis, *et al.*, 2007; Stupp *et al*., 2005). One of the major factors contributing to the poor outcome of GBM is the lack of therapeutics that can penetrate the blood-tumor barrier to effectively deliver anti-glioma agents (Doucette *et al*., 2011; Groothuis, 2000; Pardridge, 2003; Yong *et al*., 2009). To circumvent this obstacle, we and others have utilized bone-marrow human mesenchymal stem cells (BM-hMSCs) for targeted delivery of anti-glioma agents, due to their intrinsic tropism for gliomas following intra-arterial delivery (Doucette *et al*., 2011; Kosztowski, Zaidi, and Quiñones-Hinojosa, 2009; Nakamizo *et al*., 2005; Yong *et al*., 2009). Though the mechanisms underlying BM-hMSC homing to gliomas remain largely unknown, BM-hMSCs are capable of homing to xenografts derived from commercially available "professional" glioma cell lines (Nakamizo *et al*., 2005; Yong *et al*., 2009), syngenic glioma models (Doucette *et al*., 2011), and glioma stem cells (GSCs) (Shinojima *et al*., 2013).

GCSs are isolated directly from fresh tumor surgical resections and grown as spheroids *in vitro,* often expressing CD133 or CD15 cell surface markers (Clarke *et al*., 2006; Singh *et al*., 2004). These small subpopulations of cells have stem-like properties (Singh *et al*., 2003; Singh, *et al*., 2004). GSCs are hypothesized to be tumor-initiating cells, responsible for treatment failure due to their stem-like properties, particularly unlimited self-renewal, and their resistance to treatment (Singh *et al*., 2003; Singh *et al*., 2004). GSC-derived xenografts (GSCXs), compared to xenografts from commercial rat and human cell lines, offer the highest translational significance as a clinical model of glioma. GSCs faithfully mimic both the genotype and

phenotype of the parent tumor *in vivo* (Lee *et al*., 2006). Though GSCXs are translationally significant (Lee *et al*., 2006) and are capable of eliciting BM-hMSC homing, recent work from our group has demonstrated that not all GSCXs elicit BM-hMSCs homing equally (Shinojima *et al*., 2013). In that study, some GSCXs were able to strongly attract BM-hMSCs after intra-arterial injection, whereas others were unable to attract BM-hMSCs. Those GSCXs that elicited BM-hMSC homing are herein termed 'attractors' while those that do not are termed 'non-attractors'. The attractor and non-attractor phenotypes provide a unique opportunity to understand the mechanisms underlying BM-hMSC homing. That understanding could eventually help identify patients most appropriate for BM-hMSC-mediated delivery.

Previous studies have focused on soluble tumor-derived factors such as PDGF-BB (Hata *et al*., 2010), SDF-1 (Son *et al*., 2006), and TGF-β (Shinojima, *et al*., 2013) as inflammation-related cues for BM-hMSC homing. These studies have yielded some insight into the mediators of BM-hMSC homing. However, to the best of our knowledge, a mass spectrometry-based proteomic approach has not been applied to decipher the molecular correlates of BM-hMSC homing to GSCXs. Proteins have functions integral to cell-cell signaling, cell structure, and metabolic pathways. Alterations in the proteomic profiles of cells result in the phenotypic characteristics of cancers, such as uncontrolled growth and proliferation, invasion, and metabolic changes to support these features (Lunt & Vander Heiden, 2011; Vander Heiden, Cantley, and Thompson, 2009). In addition, proteomic alterations in the tumor microenvironment may support malignancies via cross-talk between cancer and stromal cells (Nieman *et al*., 2011; Pavlides *et al*., 2009; W. Zhang *et al*., 2012). In principle, high-resolution nLC-MS/MS should allow the distinction between human and mouse proteins on a large scale; identified human proteins would be derived from malignant tumor cells, while identified mouse proteins would represent the

stromal component. Therefore, we hypothesized that alteration of the proteomic profile of cancer and stromal cell populations between attractor and non-attractor GSC xenografts may provide insights into key biochemical pathways involved in the attraction of BM-hMSCs to gliomas. We have previously performed label-free quantitative proteomic and targeted transcriptomic studies on GSCs and GBM cells (He *et al*., 2010; Kroes *et al*., 2010; Lichti *et al*., 2014; Puchades *et al*., 2007). For the first time, we extend these methodologies to attractor and non-attractor GSCXs.

Methods

Methods for glioma xenograft model, tissue dissection, sampling and sectioning, protein extraction, nLC-MS/MS, transcriptomics, and data analysis were outlined previously in this work. A complete description of these techniques is detailed in **Chapter II**. All supplemental tables referenced within this manuscript may be found in the digital repository associated with this dissertation.

Results and Discussion

Mouse tumor xenografts provide a valuable tool as a preclinical model of GBM. GSC-derived xenografts (GSCXs) have a higher translational significance compared to xenografts derived from commonly used commercial glioma cell lines (Lee *et al*., 2006). However, GSCXs exhibiting differential attraction of for BM-hMSCs have not been systematically studied at either the proteomic or transcriptomic level. We utilized label-free quantitative proteomics as a reliable technique previously employed by our lab (Lichti *et al*., 2014; Wildburger *et al*., 2015) that is cost effective, yields high proteome coverage, and does not suffer from dynamic range limitations (Neilson *et al*., 2011; Schulze & Usadel, 2010). We also utilized a targeted transcriptomic platform (Kroes *et al*., 2007; Kroes *et al*., 2006; Nilsson *et al*., 2013), which

contains genesets related to GBM biology, in parallel to label-free proteomics (**Fig. 4.2**). The targeted microarray was used to overcome the limitations of mass spectrometric detection of low abundance proteins (e.g. glycosylation-related enzymes) by measuring gene expression. For statistical rigor of biological significance, nine biological replicates were analyzed per phenotype.

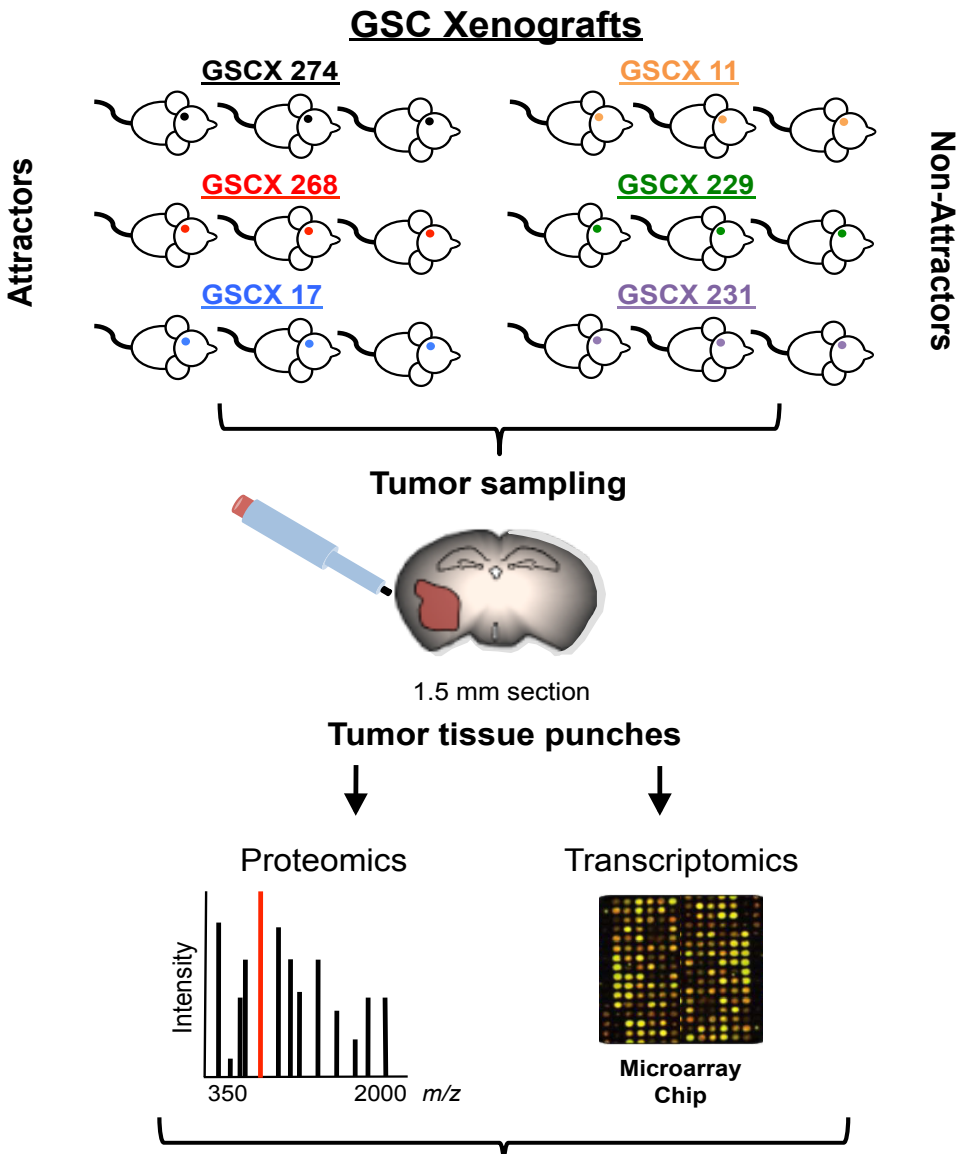

Figure 4.2. Workflow for proteomic and transcriptomic analysis of GSC xenografts. Glioma stem cells (GSCs) derived from patient tumors were intracranially implanted into athymic mice. Three of these cell lines represent BM-hMSC homing GSC xenografts (GSCX) (i.e. attractors; GSCX274, GSCX268, and GSCX17) and three represent non-homing GSCXs (i.e. non-attractors; GSCX11, GSCX229, and GSCX231). Nine biological replicates per phenotype were analyzed for statistical inference of biological significance. Brains were removed from tumor-bearing mice and processed for tumor tissue sampling as described in *Materials and Methods*. Individual tumor tissue punches were processed in parallel for label-free quantitative proteomics and targeted transcriptomic microarray. Quantitative proteomic and transcriptomic data were used to decipher underlying biological differences between the two phenotypes (phenome).

Employing a hierarchical linear model, 552 and 299 human and mouse proteins, respectively were significantly differentially expressed between attractors and non-attractors (**Fig. 4.3**). A hierarchical linear model allows us to correctly support the known variance structure within the data with the advantage of being able to detect events of a small magnitude compared to simpler approaches, thus, increasing the number of statistically differentially expressed proteins. Fold changes of small magnitude may have a significant impact on a biological system in reactions with catalytic effect such as metabolism, examined here, particularly if the change occurs at a rate-limiting step. Small magnitude changes in proteins may be critically relevant differences between the two phenotypes.

Within the human tumor protein dataset, 46 proteins were increased in the attractor phenotype and 506 were decreased relative to non-attractors. The mouse protein dataset, which represents the stromal (brain parenchyma) component, 206 proteins are increased in the attractor phenotype and 93 were decreased relative to non-attractors (**Fig. 4.3)**. We interrogated the KEGG biological pathways using DAVID (Huang, Sherman, and Lempicki 2009a; Huang, Sherman, and Lempicki 2009b; Kanehisa & Goto, 2000; Kanehisa *et al*., 2014) for the 552 differentially expressed human tumor proteins in the heatmap generated by Perseus (**Fig. 4.4A**). The top 12 KEGG pathways associated with differential protein expression using a false discovery rate (FDR) of < 10% (Benjamini-Hochberg *q*-value) are displayed with corresponding protein counts (**Fig. 4.4B**). Among the top-ranked KEGG pathways were fatty acid metabolism, glycolysis/gluconeogenesis, and the pentose phosphate pathway (PPP). Next we examined the differentially expressed mouse proteins (**Fig. 4.5A**) representing the stromal (brain parenchyma) component. DAVID analysis of KEGG biological pathways (Huang, Sherman, and Lempicki 2009a; Huang, Sherman, and Lempicki 2009b; Kanehisa & Goto, 2000; Kanehisa *et al*., 2014)

revealed glycolysis/gluconeogenesis and the PPP among the top-ranked KEGG pathways (**Fig. 4.5B**).

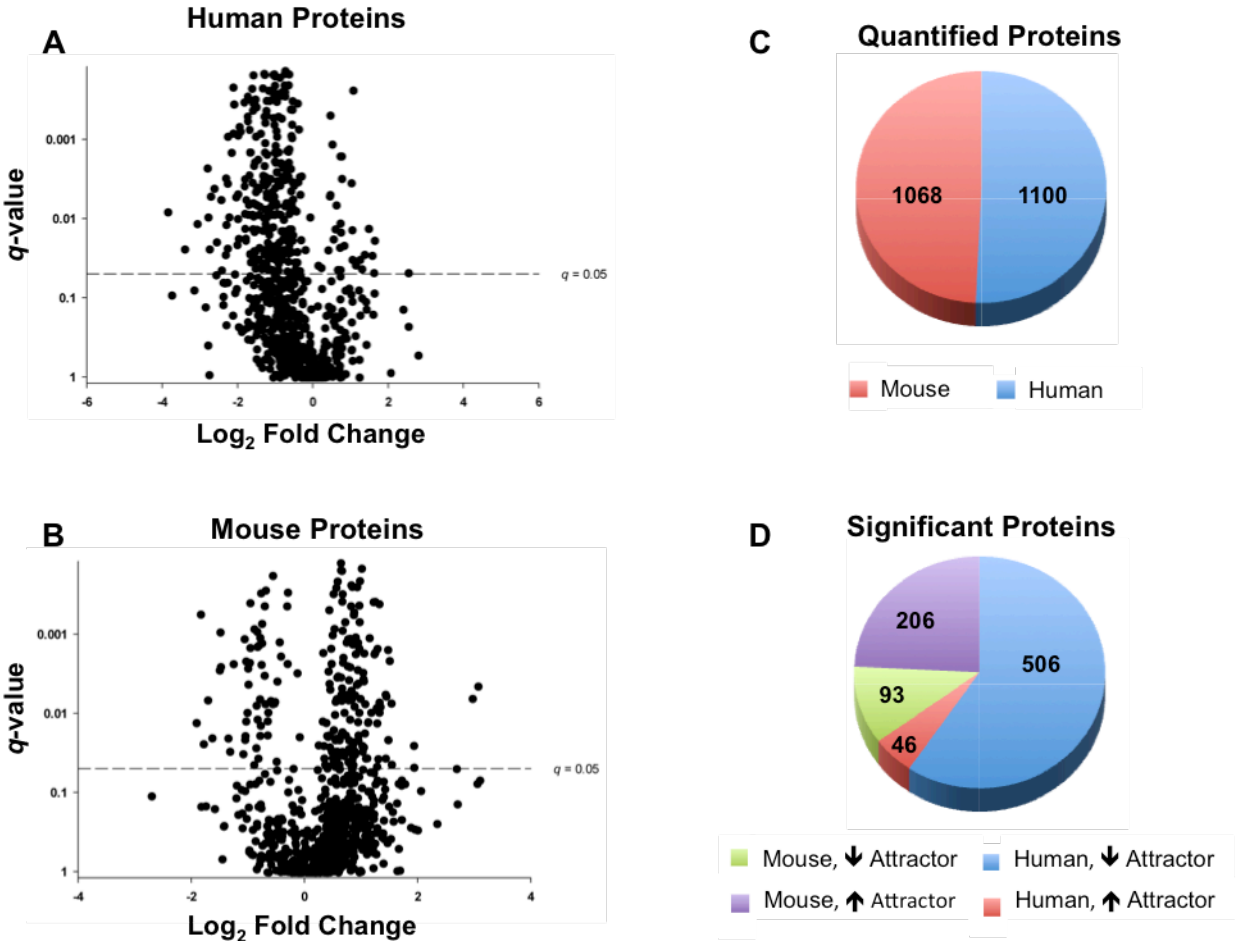

Figure 4.3. Volcano plots (*q*-value *vs* $\log_2$ fold change) for human tumor and mouse stromal proteins. (*A*) Logarithmic ratios of attractor (N=9) *vs* non-attractor (N=9) human tumor proteins plotted against the *q*-value (where $q \leq 0.5$ is considered significant; horizontal line) of the hierarchical linear model. Positive fold change values are indicative of an increase in protein expression and a negative fold change value a decrease in protein expression in attractors relative to non-attractors. (*B*) Logarithmic ratios of attractor (N=9) *vs* non-attractor (N=9) mouse stroma proteins plotted against the *q*-value (where $q \leq 0.5$ is considered significant; horizontal line) of the hierarchical linear model. Positive fold change values are indicative of an increase in protein expression and a negative fold change value a decrease in protein expression in attractors relative to non-attractors. (*C*) Number of quantified human and mouse proteins. (*D*) Employing a hierarchical linear model (see *Materials and Methods*) 552 human and 299 mouse proteins were significantly differentially expressed between the attractor and non-attractor phenotype. All proteins are listed in **Supplemental Table 3** and **4** with their respective *q*-values and $\log_2$ fold change.

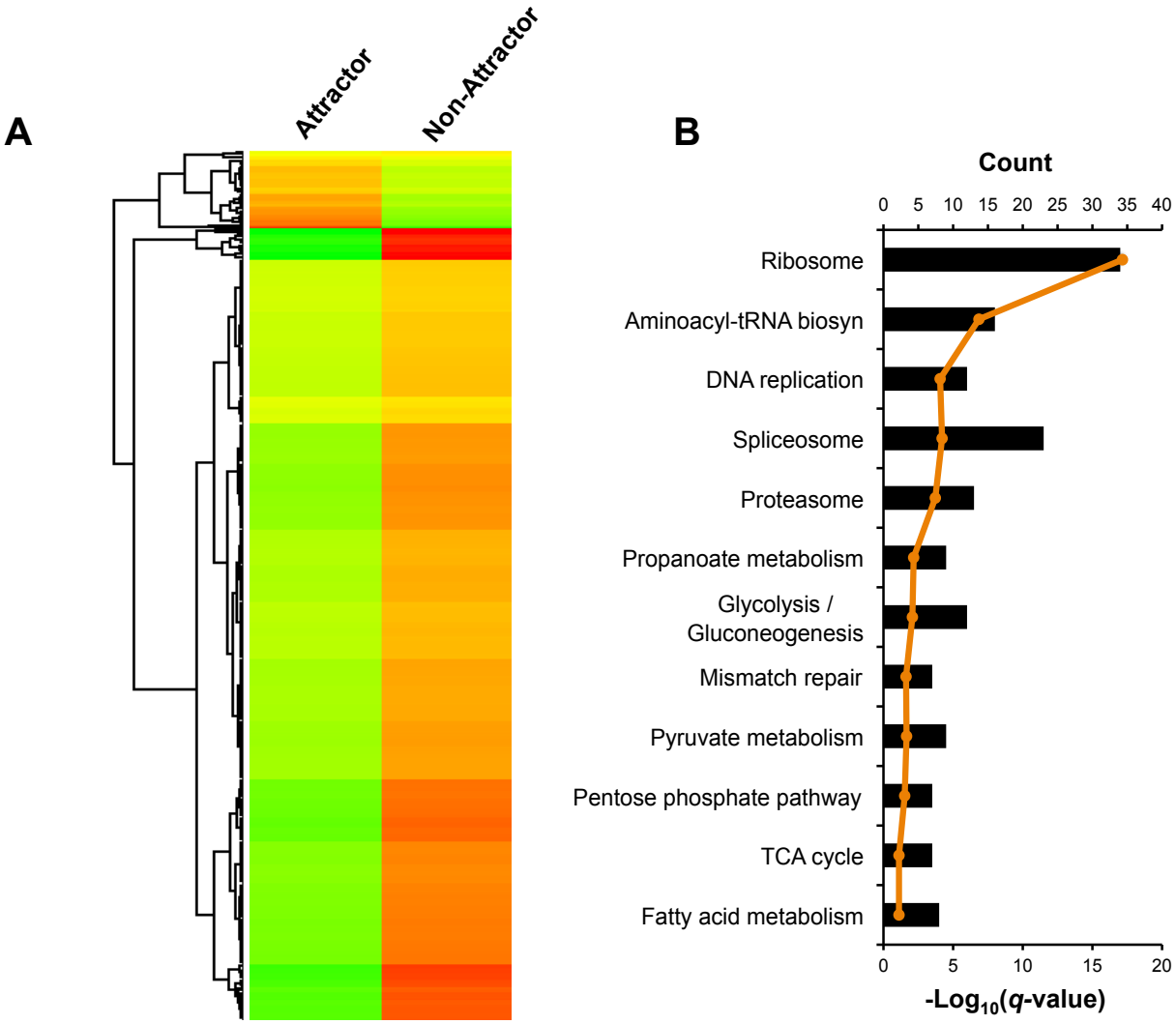

Figure 4.4. Analysis of significant human GSC xenograft proteins (*A*) Unsupervised hierarchical clustering of all significant human xenograft proteins using $\log_2$ fold change values. (*B*) Bioinformatic analysis of enriched KEGG pathways using DAVID functional analysis. The top 12 KEGG pathways associated with significantly differentially expressed human proteins are shown. KEGG terms are ranked by the $-\log_{10}(q\text{-value})$ after Benjamini-Hochberg *p*-value correction (*orange line*). The black bars show the number of proteins that is common between KEGG term's set and the respective human protein set.

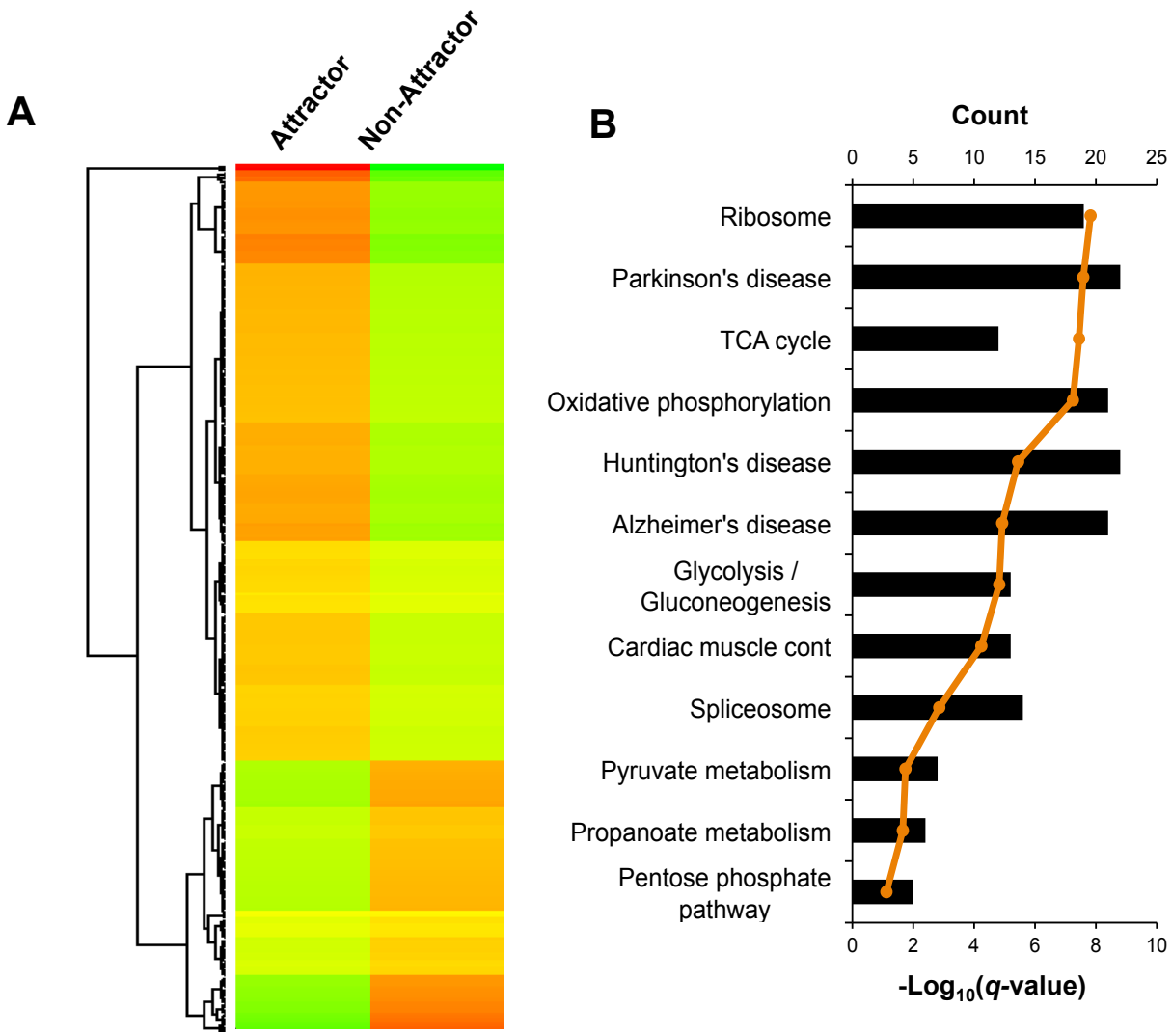

Figure 4.5 Analysis of significant xenograft mouse stromal proteins. (*A*) Unsupervised hierarchical clustering of all significant xenograft mouse stromal compartment proteins using $\log_2$ fold change values. (*B*) Bioinformatic analysis of enriched KEGG pathways using DAVID functional analysis. The top 12 KEGG pathways associated with significantly differentially expressed mouse proteins are shown. KEGG terms are ranked by the $-\log_{10}$(*q*-value) after Benjamini-Hochberg *p*-value correction (*orange line*). The black bars show the number of proteins that is common between KEGG term's set and the respective mouse protein set.

Fatty Acid Metabolism

In order to determine how fatty acid metabolism differs between attractors and non-attractors, the $\log_2$ protein fold change values were converted to hexadecimal color codes and mapped onto the KEGG pathway (Mostovenko *et al*., 2011). The mapped protein expression data showed an overall decrease in the KEGG fatty acid metabolism pathway in the attractors relative to the non-attractors (**Fig. S4.1**). Docosahexaenoic acid (DHA), one of the most abundant fatty acids in the CNS (O'Brien & Sampson, 1965; Svennerholm, 1968), is a member of this pathway. As seen in **Figure S4.1,** there is a decrease in relative expression of proteins involved in DHA synthesis in attractors (e.g trifunctional enzyme subunit alpha and very-long-chain enoyl-CoA reductase), as well as many upstream enzymes indirectly involved in DHA synthesis including: acetyl-CoA acetyltransferase, hydroxyacyl-coenzyme A dehydrogenase, enoyl-CoA hydratase, and fatty acid synthase.

DHA is a precursor to many bioactive molecules with anti-inflammatory effects (Ariel & Serhan, 2007; Hong *et al*., 2003; Marcheselli *et al*., 2003; Mukherjee *et al*., 2004; Schwab *et al*., 2007). Our lab has previously shown, using ESI-MS/MS and MALDI-IMS followed by MALDI-MS/MS, that DHA, the precursor to inflammatory-resolving molecules, is decreased in the attractor phenotype . The fact that the proteomic data from our xenografts is congruent with our previous lipidomic analysis on these samples adds a level of confidence to our dataset, providing orthogonal validation to the lower expression levels of the DHA observed in attractors. The decreased levels of DHA and the proteins responsible for its synthesis may be a key component to the homing permissive environment of attractors .

Glycolysis and the Pentose Phosphate Pathway

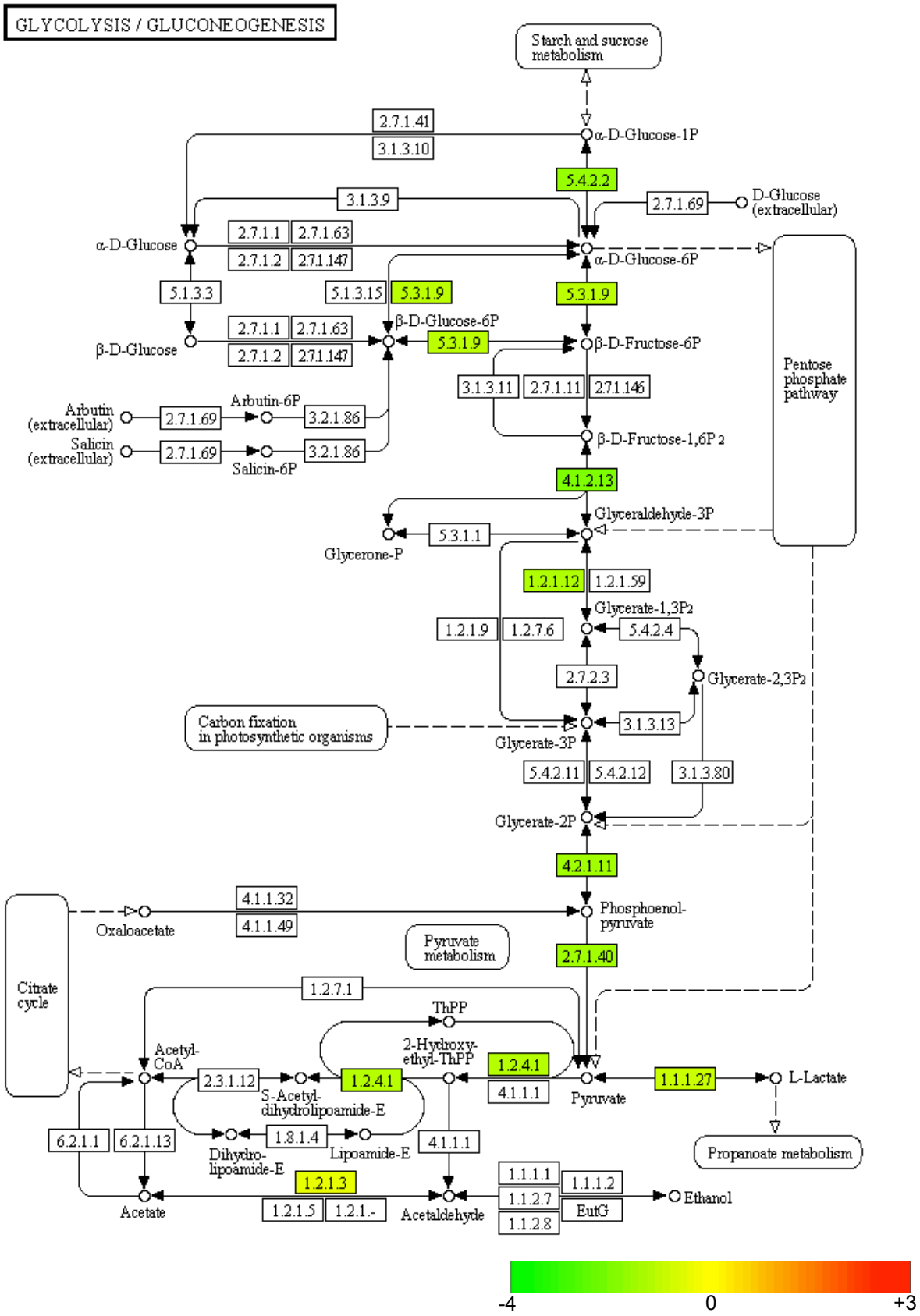
GLYCOLYSIS / GLUCONEOGENESIS
Starch and sucrose metabolism
2.7.1.41
3.1.3.10
α-D-Glucose-1P
5.4.2.2
3.1.3.9
2.7.1.69
D-Glucose (extracellular)
α-D-Glucose
2.7.1.1
2.7.1.63
2.7.1.2
2.7.1.147
α-D-Glucose-6P
5.1.3.3
5.1.3.15
5.3.1.9
5.3.1.9
β-D-Glucose-6P
β-D-Glucose
2.7.1.1
2.7.1.63
2.7.1.2
2.7.1.147
5.3.1.9
β-D-Fructose-6P
Pentose phosphate pathway
3.1.3.11
2.7.1.11
2.7.1.146
Arbutin (extracellular)
2.7.1.69
Arbutin-6P
3.2.1.86
Salicin (extracellular)
2.7.1.69
Salicin-6P
3.2.1.86
β-D-Fructose-1,6P 2
4.1.2.13
Glyceraldehyde-3P
5.3.1.1
Glycerone-P
1.2.1.12
1.2.1.59
Glycerate-1,3P2
1.2.1.9
1.2.7.6
5.4.2.4
2.7.2.3
Glycerate-2,3P2
Carbon fixation in photosynthetic organisms
3.1.3.13
Glycerate-3P
5.4.2.11
5.4.2.12
3.1.3.80
Glycerate-2P
4.2.1.11
4.1.1.32
4.1.1.49
Oxaloacetate
Phosphoenol-pyruvate
Pyruvate metabolism
2.7.1.40
Citrate cycle
1.2.7.1
ThPP
Acetyl-CoA
2-Hydroxy-ethyl-ThPP
1.2.4.1
2.3.1.12
1.2.4.1
4.1.1.1
Pyruvate
1.1.1.27
L-Lactate
S-Acetyl-dihydrolipoamide-E
6.2.1.1
6.2.1.13
1.8.1.4
Dihydro-lipoamide-E
Lipoamide-E
4.1.1.1
Propanoate metabolism
1.2.1.3
1.1.1.1
1.1.1.2
1.1.1.27
EutG
1.1.2.8
Ethanol
Acetate
1.2.1.5
1.2.1.-
Acetaldehyde
-4
0
+3

Figure 4.6. Human GSC xenograft protein expression values mapped onto the Glycolysis/Gluconeogenesis KEGG pathway. The human protein expression profiles from GSCXs mapped onto the Fatty Acid Metabolism pathway highlights protein fold changes in attractors relative to non-attractors. The measured protein fold changes were converted to color and mapped onto KEGG pathways. Proteins up-regulated in attractors relative to non-attractors are marked in red, down-regulated proteins in attractors relative to non-attractors are marked in green.

Glycolysis is a cancer-related pathway (Lunt & Vander Heiden, 2011; Vander Heiden *et al*., 2009), and its enrichment in our bioinformatic analysis via DAVID is a validating measure in our xenograft tumor samples. A characteristic feature of transformed or malignant cells is a metabolic shift towards glycolysis, first described by Otto Warburg (Warburg, 1925; Warburg, 1956). The glycolytic shift in tumor cells is independent of defects in mitochondrial respiration and oxygen availability (Lunt & Vander Heiden, 2011; Vander Heiden *et al*., 2009); gliomas are no exception to this phenomenon. GBM cells have been observed to convert 90% of glucose to lactate and alanine via glycolysis *in vitro* (DeBerardinis *et al*., 2007). To understand the regulated changes in glycolysis between attractors and non-attractors, we mapped the $\log_2$ protein fold change values of human tumor proteins to the KEGG glycolysis pathway. We found that in the attractors, the glycolytic pathway was down-regulated relative to non-attractors (**Fig. 4.6**). The attractor stromal microenvironment, on the other hand, had reciprocal expression of glycolysis. Glycolysis was up-regulated in attractors relative to non-attractors (**Fig. S4.3A**).

The down-regulation of glycolysis in attractors prompted us to consider the status of other glucose-dependent pathways. Glucose, upon entering the cell through glucose transporters and phosphorylated by hexokinases, may also be consumed by glucose-6-phosphate dehydrogenase (G6PDH) and converted to 6-phosphogluconolactone, thus entering the PPP (Berg, Tymoczko, and Stryer, 2002). The PPP is a biochemical pathway that metabolizes glucose to produce NADPH for fatty acid metabolism, redox reactions, and ribose 5-phosphate for nucleotide synthesis. Up-regulation of the PPP has been posited to provide a selective advantage to cancer cells (Gillies & Gatenby, 2007; Langbein *et al*., 2006). We examined the protein expression profile of GSCXs in the PPP, which notably was also a KEGG pathway enriched in our analysis (**Fig. 4.4B**). Mapping the $\log_2$ protein fold change values of human tumor proteins to

the KEGG pentose phosphate pathway, we observed that the PPP was also down-regulated in attractors relative to non-attractors (**Fig. S4.2**). Notably, G6PDH, which catalyzes the first and rate-limiting step in the PPP, and 6-phosphogluconolactonase, another key enzyme in the oxidative branch, were decreased in attractors (**Supplemental Table 4.3**). Transketolase, a component of the non-oxidative branch in the PPP, was also decreased in attractors (**Fig. S4.2**) (Berg, Tymoczko, and Stryer, 2002; Vander Heiden *et al*., 2009). The down-regulation of the PPP would suggest compromised defense against reactive oxygen species (ROS) in attractors compared to non-attractors. Consistent with this, we found a down-regulation of glutathione S-transferase and superoxide dismutase in attractors relative to non-attractors. In addition, the down-regulation of the PPP in attractors would reduce the NADPH production necessary for fatty acid synthesis (Kang, Lee, and Lee, 2015). Congruent with this, the fatty acid metabolism pathway, as described above, is concomitantly decreased in attractors relative to non-attractors.

Similar to glycolysis, the attractor stromal microenvironment had reciprocal expression of glucose-dependent metabolic pathway, PPP (**Fig. S4.3B**). Taken together, our findings suggest microenvironmental cross-talk between the tumor and the stroma. This is supported by several reports of the microenvironment supporting tumor growth, survival, and metastasis (Nieman *et al*., 2011; Pavlides *et al*., 2009; Zhang *et al*., 2012). The possibility of stromal cell support via reciprocal expression of glucose metabolism may point to a role for the stroma as an important component in BM-hMSC homing.

Glycosylation Targeted Transcriptomics

Glucose is the primary carbon source for fatty acid metabolism, glycolysis, and the PPP (Vander Heiden *et al*., 2009). With the down-regulation of all three of these pathways in

attractors, it is possible, though not mutually exclusive, that either attractors have decreased glucose transport across the cell membrane, or attractors are shunting glucose towards the hexosamine biosynthesis pathway, which is responsible for generating activated sugars for glycosylation (Aebi & Hennet, 2001; Marshall, Bacote, and Traxinger, 1991; Wellen & Thompson, 2012). To gain insight into the latter possibility, that glucose metabolism may be shifted towards the hexosamine pathway, we used a custom microarray platform containing 2,577 transcripts (Kroes *et al*., 2007; Kroes *et al*., 2006).

Microarray analysis revealed 254 genes that were significantly differentially expressed at < 10% FDR. Of the 254 differentially expressed transcripts, 121 had increased expression in attractors relative to non-attractors and 133 had decreased expression in attractors relative to non-attractors (**Supplemental Table 4.5**). Glutamine fructose-6-phosphate amidotransferase 1 (*Gfpt1*), which controls the flux of glucose into the hexosamine biosynthesis pathway along with (*Gfpt2*), was down-regulated (-1.28-fold) in attractors. Yet, enzymes involved in the N-linked glycosylation pathway synthesis, dolichol-phosphate mannosyltransferase subunit 1 (*DPM1*) and dol-P-Man:Man(7)GlcNAc(2)-PP-Dol alpha-1,6-mannosyltransferase (*ALG12*), had increased expression in attractors relative to non-attractors (**Supplemental Table 4.5**) (Aebi & Hennet, 2001). Dolichyl-diphosphooligosaccharide-protein glycosyltransferase (*STT3B*), which catalyzes the transfer of the high mannose lipid-linked oligosaccharide to nascent polypeptides, was up-regulated 1.33 fold in attractors (Aebi & Hennet, 2001). Enzymes involved in the biosynthesis of complex-type N-glycans beta-1,4-galactosyltransferase 5 (*B4GALT5*) and the commitment step of complex N-glycans, alpha-mannosidase 2x (*MAN2A2*) were 1.27 and 1.21 fold up-regulated, respectively. The transcript *NGLY1* encoding the enzyme commonly known as PNGase F, which

removes N-linked glycans, was down-regulated (-1.35 fold) in attractors relative to non-attractors.

The expression of these significant human glycogenes found in our targeted transcriptomic dataset provide evidence that N-linked glycosylation is increased in attractors relative to non-attractors based key enzymes responsible for N-glycan processing, the commitment step towards complex-type N-glycans, and the transfer to nascent proteins. Additionally, the enzyme responsible for N-glycan hydrolysis (*NGLY1*) was down-regulated. The relevance of cell-surface glycosylation in brain tumors (Moskal, Kroes, and Dawson, 2009) warrants further glycomics-based investigation of the tumor cell surface.

Conclusion

We showed a decrease in the human proteins responsible for fatty acid metabolism in attractors compared to non-attractors. The predicted outcome of this would be a decrease in the biosynthesis of DHA in attractors, which supports our previous lipidomic study (59). We also show an overall down-regulation in glucose-dependent metabolic pathways – glycolysis and the PPP – in attractors relative to non-attractors. A consequence of such regulation is decreased NAPDH for fatty acid metabolism and homeostasis of ROS. Despite the decrease in glucose-dependent metabolic pathways, we found an increase in glyco-transcripts involved in glucose-dependent N-linked glycosylation in attractors relative to non-attractors. Finally, our data reveals an up-regulation of glucose-dependent metabolic pathways in the mouse stromal component in attractors relative to non-attractors, in contrast to the human tumor proteins. Taken together, these results implicate lipids and ROS in glioma-induced BM-hMSC homing and suggest a role for tumor microenvironmental cross-talk.

Acknowledgements

The authors gratefully acknowledge the financial support of the Cancer Prevention Research Institute of Texas (CPRIT) and The University of Texas Medical Branch to C.L.N. as well as the Dr. Ralph and Marian Falk Medical Research Trust to J.R.M, are gratefully acknowledged. The authors would like to thank Dr. Ekaterina Mostovenko for the R script for visualizing log_2-transformed expression values as hexadecimal color codes. The authors gratefully acknowledge Dr. Frederick F. Lang and Joy Gumin for the glioma stem cell xenografts (GSCXs) at MD Anderson Cancer Center for this study.

Conflict of Interest

The authors do not have any conflicts of interest to disclose.

Author Contributions

N.C.W. conceived of the study, designed, and performed all proteomics and transcriptomics experiments, data analysis and interpretation, and wrote the paper. C.F.L. contributed to the experimental design, interpretation of data, provided tools for data analysis and contributed to writing the manuscript. R.D.L. performed statistical analysis on proteomic data. M.S. assisted in transcriptomics experiments and data analysis. R.A.K. and J.R.M. contributed transcriptomics data analysis tools and provided helpful discussion. C.L.N. conceived the project and supervised the work and critically revised the manuscript. All authors read and approved the final manuscript.

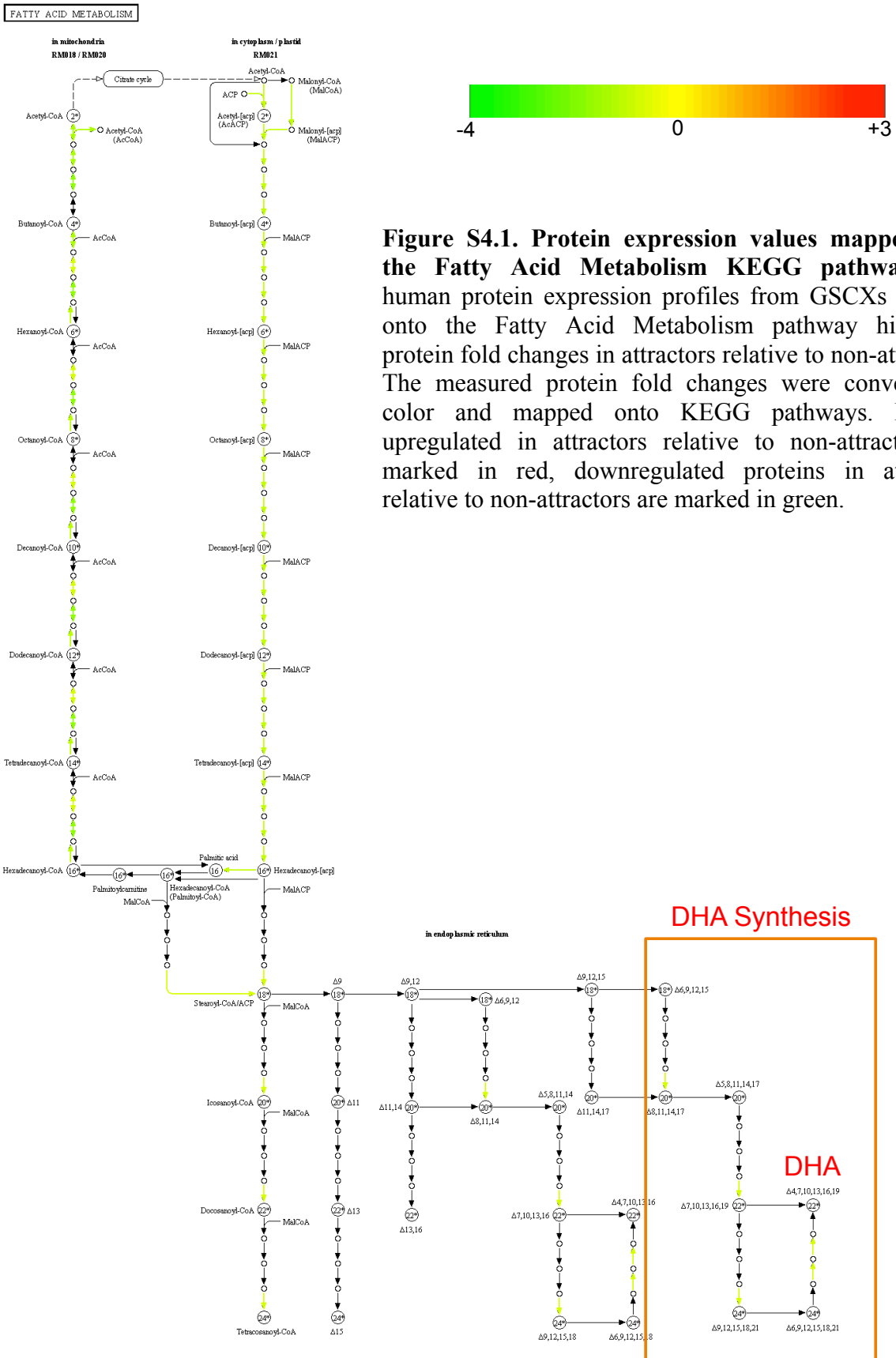

Figure S4.1. Protein expression values mapped onto the Fatty Acid Metabolism KEGG pathway. The human protein expression profiles from GSCXs mapped onto the Fatty Acid Metabolism pathway highlights protein fold changes in attractors relative to non-attractors. The measured protein fold changes were converted to color and mapped onto KEGG pathways. Proteins upregulated in attractors relative to non-attractors are marked in red, downregulated proteins in attractors relative to non-attractors are marked in green.

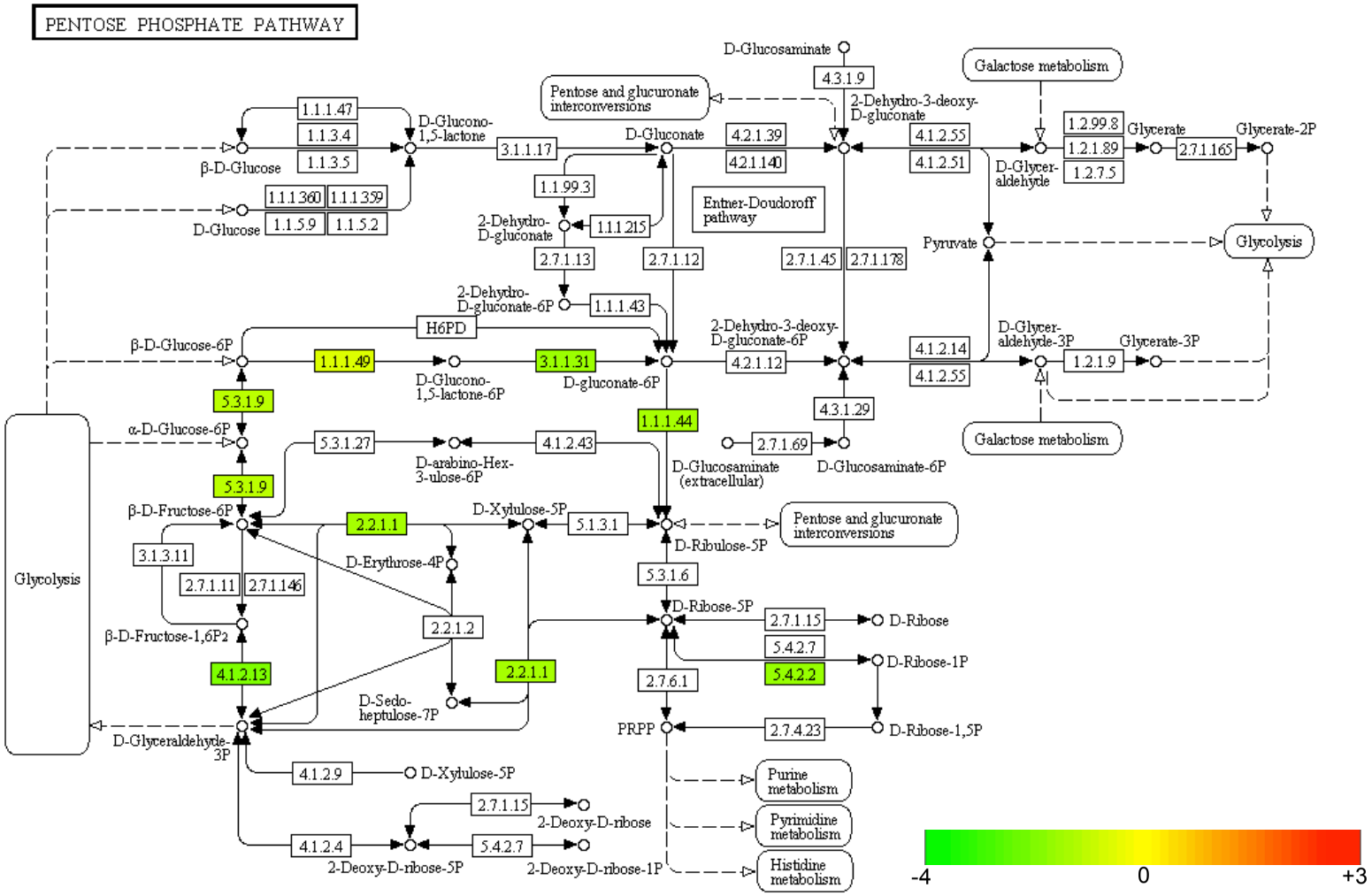

Figure S4.2. Protein expression values mapped onto the Pentose phosphate KEGG pathway. The human protein expression profiles from GSCXs mapped onto the Pentose phosphate pathway highlights protein fold changes in attractors relative to non-attractors. The measured protein fold changes were converted to color and mapped onto KEGG pathways. Proteins upregulated in attractors relative to non-attractors are marked in red, downregulated proteins in attractors relative to non-attractors are marked in green.

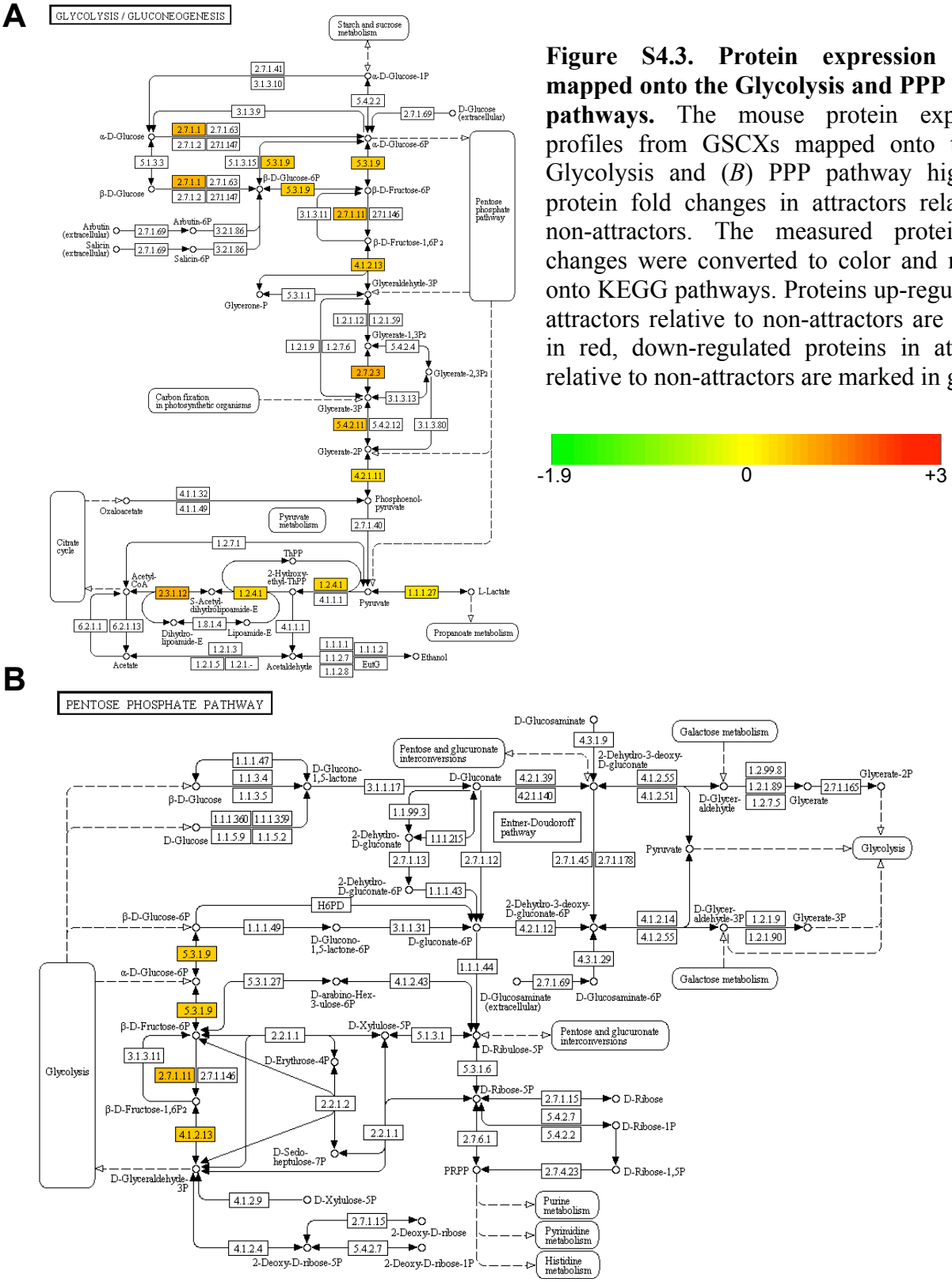

Figure S4.3. Protein expression values mapped onto the Glycolysis and PPP KEGG pathways. The mouse protein expression profiles from GSCXs mapped onto the (*A*) Glycolysis and (*B*) PPP pathway highlights protein fold changes in attractors relative to non-attractors. The measured protein fold changes were converted to color and mapped onto KEGG pathways. Proteins up-regulated in attractors relative to non-attractors are marked in red, down-regulated proteins in attractors relative to non-attractors are marked in green.

The following chapter was submitted to the Journal of Proteome Research (May 2015) under the title “Integrated Transcriptomic and Glycomic Profiling of Glioma Stem Cell Xenografts”.

INTEGRATED TRANSCRIPTOMIC AND GLYCOMIC PROFILING OF GLIOMA STEM CELL XENOGRAFTS

Authors: Norelle C. Wildburger[1*], Shiyue Zhou[2*], Lauren G. Zacharias[2], Roger A. Kroes[3], Joseph R. Moskal[3], Mary Schmidt[3], Parvin Mirzaei[2], Joy Gumin[4,5], Frederick F. Lang[4,5], Yehia Mechref[2§] and Carol L. Nilsson[6,7§]

Affiliation:

1. Neuroscience Graduate Program, Graduate School of Biomedical Sciences, University of Texas Medical Branch, 301 University Blvd, Galveston, Texas, 77555-1074, United States

2. Department of Chemistry and Biochemistry, Texas Tech University, 2500 Broadway, Lubbock, TX 79409, United States

3. The Falk Center for Molecular Therapeutics, McCormick School of Engineering and Applied Sciences, Northwestern University, 1801 Maple Street, Evanston, Illinois 60201, United States

4. Department of Neurosurgery, The University of Texas M.D. Anderson Cancer Center, 1515 Holcombe Boulevard, Houston, Texas 77030, United States

5. The Brain Tumor Center, The University of Texas MD Anderson Cancer Center, Box 1004, 1515 Holcombe Boulevard, Houston, Texas 77030, USA

6. Department of Pharmacology & Toxicology, University of Texas Medical Branch, 301 University Blvd, Galveston, Texas, 77555, United States

7. UTMB Cancer Center, University of Texas Medical Branch, 301 University Blvd, Galveston, Texas, 77555-1074, United States

§ To whom correspondence may be addressed: Yehia Mechref and Carol L. Nilsson
* These authors contributed equally

Yehia Mechref, Ph.D.
Dept. of Chemistry & Biochemistry
Texas Tech University
Memorial Circle & Boston
Lubbock, TX 79409-1061
Tel +1 (806) 834 8246
Fax +1 (806) 742 1289
yehia.mechref@ttu.edu

Carol L. Nilsson, M.D, Ph.D.
Dept. of Pharmacology & Toxicology
CPRIT Scholar in Cancer Research
University of Texas Medical Branch
301 University Blvd
Galveston, TX 77555-1074
Tel. +1 (409) 747 1840
Fax. +1 (409) 772 9648
clnilsso@utmb.edu

Keywords: Glioblastoma, bone marrow-derived human mesenchymal stem cells, transcriptomics, glycomics, N-linked glycosylation, high mannose, sialic acid

Abstract

Bone marrow-derived human mesenchymal stem cells (BM-hMSCs) have the innate ability to home to and engraft in tumors such as glioblastoma (GBM). Due to this unique property of BM-hMSCs we and others have explored their use for cell-mediated therapeutic delivery for the advancement of GBM treatment. Extravasation, the process by which blood-borne cells – such as BM-hMSCs – enter tissue is a highly complex process but is heavily dependent upon glycosylation for glycan-glycan and glycan-protein adhesion between the cell and endothelium. However, in a translationally significant pre-clinical glioma stem cell xenograft (GSCX) model of GBM, BM-hMSCs demonstrate unequal tropism towards these tumors. We hypothesized that there may be differences in the glycan compositions between the GSCXs that elicit homing ("attractors") and those that do not ("non-attractors") that facilitate or impede the engraftment of BM-hMSCs to the tumor. In this study, the glycotranscriptomic analysis revealed significant heterogeneity within the attractor phenotype and the enrichment of high mannose type N-glycan biosynthesis in the non-attractor phenotype. Orthogonal validation with topical PNGase F deglycosylation on the tumor regions of xenograft tissue, followed by nLC-ESI-MS, confirmed the presence of increased high mannose type N-glycans in the non-attractors. Additional evidence provided by our glycomic study revealed the prevalence of terminal sialic acid containing N-glycans in non-attractors and terminal galactose and N-acetyl-glucosamine N-glycans in attractors. Our results provide the first evidence for differential glycomic profiles in GSCXs based on the capacity to attract or home BM-hMSCs and extend the scope of molecular determinates in BM-hMSC homing to glioma.

Introduction

Glycosylation is the most common protein post-translational modification (PTM). It is estimated that 50% of all proteins within the human proteome are glycosylated though only 10% of proteins have evidence supporting the presence of this PTM (Apweiler, Hermjakob, and Sharon, 1999; Lichti *et al*., 2014). The glycan moieties on membrane and secreted proteins are important modulators of protein folding, stability, and trafficking (Dwek, 1996; Lichti *et al*., 2014). Glycosylation also mediates biological functions such as cell-cell or cell-matrix adhesion (Lichti *et al*., 2014; Ohtsubo & Marth, 2006; Varki, 1993; Varki, 2009), host-pathogen interactions (Baum *et al*., 2014; Lichti *et al*., 2014; Ohtsubo & Marth, 2006), and receptor-ligand interactions (Ferluga *et al*., 2013; Ohtsubo & Marth, 2006). One important cell-cell adhesion process critically reliant on and predominantly mediated by glycan moieties is extravasation.

Extravasation is the process whereby cells within blood vessels home to sites of inflammation or damaged tissue (Scott & Patel, 2013; Varki, 2009). In the first step, rolling adhesion, carbohydrate-carbohydrate interactions are critical (Scott & Patel, 2013; Wright & Cooper, 2014). Carbohydrate binding proteins (e.g. P- and E-selectin) on the endothelial surface recognize and bind carbohydrates (e.g. Sialyl Lewis^{X}) on glycolipids or glycoproteins on the opposing cell surface. The next step, tight binding, predominantly relies on complementary pairs of adhesion molecules on the opposing cell surfaces to strengthen of the initial interaction established by rolling adhesion. Many adhesion proteins such as integrins and ICAMs are themselves heavily glycosylated (Scott & Patel, 2013; Wright & Cooper, 2014). The importance of glycosylation in extravasation is highlighted by the consequences of genetic deletion of enzymes related to O- and N-linked glycan processing (Wright & Cooper, 2014). For instance, mice lacking polypeptide N-acetylgalactosamine transferase-1 (*Galnt1*$^{-/-}$), which initiates O-

linked glycosylation, demonstrate significantly reduced extravasation at every critical step (Block, Ley, and Zarbock, 2012). Genetic ablation of sialyltransferase ST3Gal-IV in mice reduced CXCR2-mediated firm adhesion (Frommhold *et al*., 2008).

Recent observations of intra-arterially delivered bone marrow-derived human mesenchymal stem cells (BM-hMSCs), for cell-based therapeutic delivery of anti-glioma agents (Kosztowski, Zaidi, and Quiñones-Hinojosa, 2009; Nakamizo *et al.*, 2005; Nakamura *et al*., 2004; Shinojima *et al*., 2013; Studeny *et al*., 2002; Studeny *et al.,* 2004; Yong *et al*., 2009), suggest that these cells extravasate from the blood vessel endothelium via diapedesis after intravascular injection to engraft into the tumor mass (Yong *et al.*, 2009). GFP-labeled BM-hMSCs injected into the internal carotid artery of tumor-bearing mice were found in linear arrangements co-localized with endothelial marker CD31 up until two days post-treatment (Yong *et al*., 2009). By the third day, BM-hMSCs were seen dispersed throughout the tumor parenchyma supporting the hypothesis of extravasation-mediated localization (Yong *et al*., 2009). However, the fact that some GSCXs attract BM-hMSCs (‘attractors’) and others do not (‘non-attractors’) suggests that there are differences in the tumor expressed glycans (Shinojima *et al*., 2013), which may make attractors conducive to BM-hMSC engraftment.

We have previously found alterations in the lipid compositions (Wildburger *et al.*, 2015) and proteins comprising cell-signaling pathways (Wildburger *et al.*, 2015) of the attractor and non-attractor GSCXs, which have shed light on the different phenotypes. We have analyzed the glycomic profiles of U373MG xenografts (Kroes *et al*., 2010) and glioma stem cells (He *et al*., 2010), but the differential glycan profile of attractor and non-attractor GSCXs remains unexamined. Thus, we set out to uncover the glycan profile of these tumors to expand our understanding of the variable BM-hMSC tropism. We first used glycogene-targeted

transcriptomics of to generate an informed data-driven glycomics approach. Data derived from targeted glyco-microarrays prompted an N-linked glycan specific approach using on-tissue digestion of N-glycans from the tumor areas of the attractor and non-attractor xenografts followed by nLC-ESI-MS analysis (Hu *et al*., 2013).

Methods

Methods for glioma xenograft model, tissue dissection, sampling and sectioning, transcriptomics, on-tissue PNGase F digestion and nLC-MS/MS for glycomics, and data analysis were outlined previously in this work. A complete description of these techniques is detailed in **Chapter II**. All supplemental tables referenced within this manuscript may be found in the digital repository associated with this dissertation.

Results

The glycomics of GSCXs exhibiting differential homing for BM-hMSCs – attractors and non-attractors – have not been systematically studied. Because glycans are essential to the extravasation process (Lichti *et al*., 2014; Wright & Cooper, 2014), it is critical to gain a better understanding of the differential glycan profiles of the attractor and non-attractor phenotypes. We employed the workflow outlined in **Figure 5.1** to investigate glycotranscripts and N-glycans, differentially expressed in GSCXs exhibiting attractor and non-attractor phenotypes.

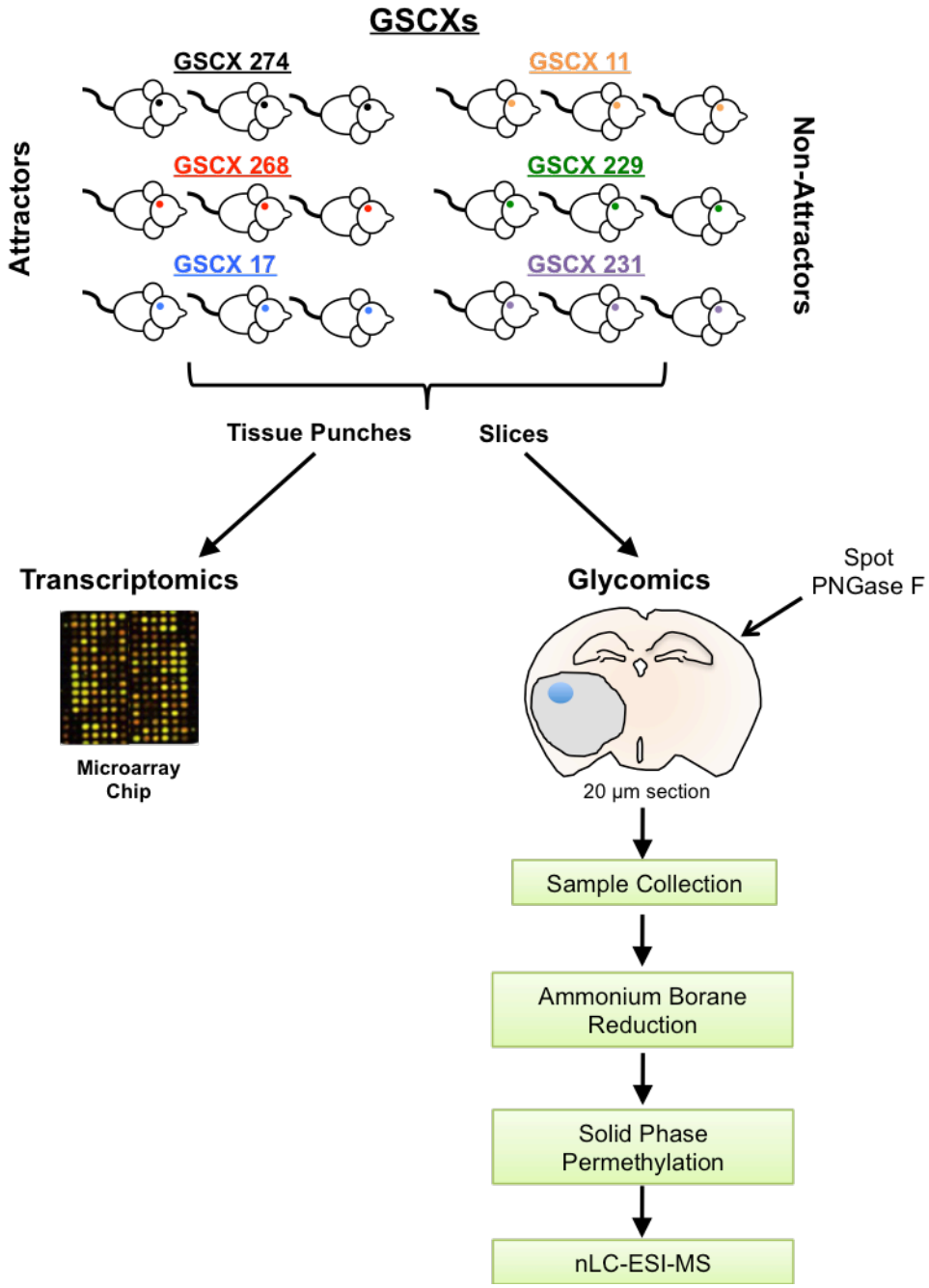

Figure 5.1. Workflow outlining tissue sample preparation for combined transcriptomics and glycomics. Tissue punches (*left*) take from GSC xenografts (1.5 mm thick x 1.5 mm diameter) were taken for targeted transcriptomics (as described in *Materials and Methods*). Serial coronal sections from GSC xenografts at 20 µm (*right*) were made after the tissue punches were taken and thaw mounted on glass microscope slides. PNGase F (1 µL) was spotted on the tumors of each GSCX for N-glycan release overnight. Release N-glycans were collected, reduced, permethylated, and analyzed by nLC-ESI-MS.

Targeted Transcriptomics Reveals Enrichment of High Mannose Type N-Glycans in Non-Attractor Phenotype.

Previously published data from a targeted microarray platform containing 2,577 total transcripts related to glioma biology was re-analyzed, focusing on all the cloned human glycogenes contained on the chip (Wildburger *et al*., 2015) (**Supplemental Table 5.1**). PCA analysis of all glycotranscripts from attractors and non-attractors (**Fig. 5.2A**) demonstrated clear separation between the two phenotypes (PC1). The clustering of biological replicates (individual animals with the same cells line) for attractors (PC3, 8.09%) and non-attractors (PC2, 8.96%) was similar. Yet, from the overall clustering of both individual cells lines (e.g. GSC17) and biological replicates within a given phenotype, the attractors demonstrated greater glycotranscript heterogeneity compared to non-attractors. GSEA analysis of the transcripts using a custom-made glycogene database revealed high mannose type N-glycan biosynthesis (nominal *p*-value = 0.0383; FDR *q*-value = 0.2962) to be significantly enriched in the non-attractor phenotype (**Fig. 2B**). However, no glycan synthesis or degradation pathway met our threshold requirements in GSEA for attractors (*data not shown*).

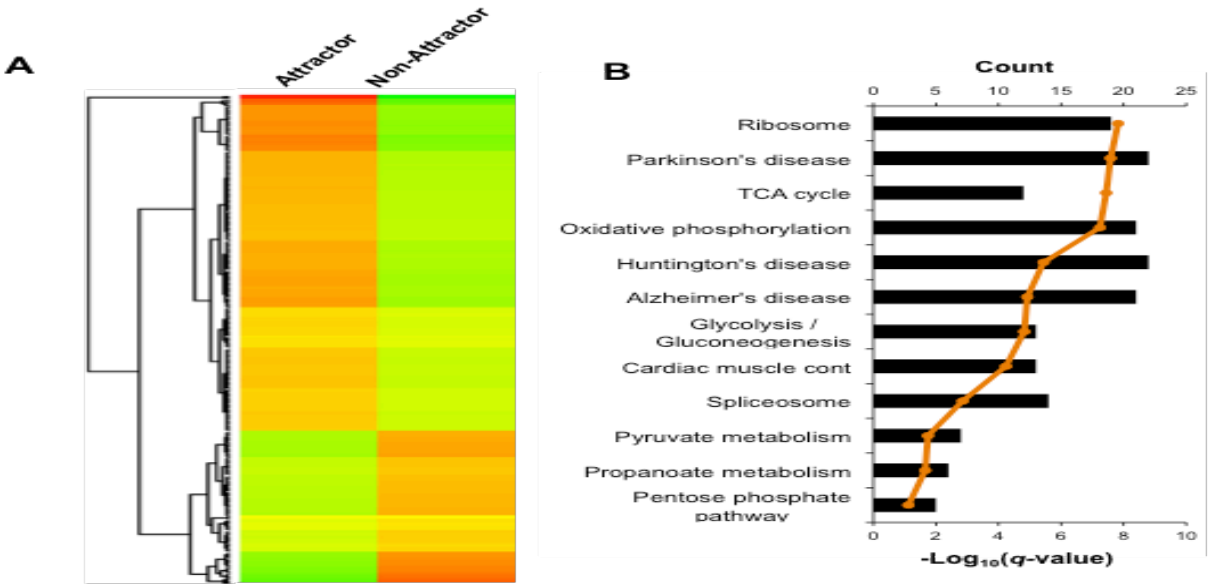

Figure 5.2. Targeted transcriptomic analysis. (**A**) Principal component analysis of all human glycogenes from targeted microarray. Attractors are in blue while non-attractors are shown in red. GSC followed by a number designates the glioma stem cell line used for the xenograft and the number following the hyphen indicates the biological replicate. (**B**) GSEA enrichment plots for statistically significant genes. The high mannose N-glycan type glycogene set enriched in the non-attractor phenotype is depicted. Black bars illustrate the position of the probe sets in the context of all of the glycoprobes on the array. The running enrichment score plotted as a function of the position of the ranked list of array probes is shown in green. The rank list metric shown in gray illustrates the correlation between the signal-to-noise values of all individually ranked genes according to the class labels (attractor *vs* non-attractor). The genes overrepresented on the leftmost side of the enrichment plots are those that correlate to differential expression in the non-attractor phenotype. Significantly enriched data sets are defined at a $p < 0.05$ and a false discovery rate (FDR) < 0.30.

Quantitative Glycomics of Attractor *vs* Non-Attractor GSCXs.

To corroborate the glycotranscriptomic findings and obtain tumor specific N-glycan information we performed nLC-ESI-MS glycomic experiments from on-site PNGase F deglycosylation of 20 μm coronal sections from the GSC xenografts. Of the detectible species passing our filters (*Materials and Methods*) we identified 18 glycan compositions, 9 of which were significantly differentially expressed between the two phenotypes (**Figure 5.3**). Consistent with our previous work (Wildburger *et al.*, 2015) there were more significant complex N-glycan compositions in the attractors compared to non-attractors. The high mannose glycans were significantly less abundant in the attractor phenotype, in accordance with the GSEA biosynthesis pathway enrichment from the transcriptomic data (**Figure 5.2**). Further, the transcript *MAN1C1*, coding for the protein mannosyl-oligosaccharide 1,2-alpha-mannosidase IC was decreased in attractors relative to non-attractors (**Supplemental Table 5.1**). The *MAN1C1* enzyme produces $Man_8GlcNAc_2$ then $Man_6GlcNAc_2$ from $Man_9GlcNAc_2$, the nascent N-linked glycan emerging from the Golgi. Notably, $Man_6GlcNAc_2$ was one of the significant high mannose N-glycans found to be decreased in attractors compared to non-attractors.

Terminal mono- or disialylation of N-glycans ($GlcNAc_4Man_3Gal_2Sia_1$, $GlcNAc_4Man_4Gal_2Sia_2$, and $GlcNAc_4Man_4Gal_2Fuc_1Sia_1$) was significantly decreased in the attractors compared to the non-attractors; the presence of sialic acid on galactose could be either α2-3 or α2-6 linked (Varki, 2009). This trend was consistent for those N-glycan compositions ($GlcNAc_4Man_3Gal_2Sia_1$, $GlcNAc_4Man_4Gal_2Sia_2$, and $GlcNAc_4Man_4Gal_2Fuc_1Sia_1$) that did not reach significance (**Figure 5.3**). We note that the exception to this is N-glycan composition $GlcNAc_6Man_3Gal_4Fuc_2Sia_3$ (tetrantennary), which was increased in attractors and possess three terminal sialic acids. Interestingly, $GlcNAc_6Man_3Gal_4Fuc_2Sia_3$ has a fucose on the antennae in

addition to the core fucose, which must be α1-6 linked, as PNGase F cannot cleave N-glycans containing core α1-3 fucose. The fucose present on the N-glycan antenna is linked to the N-acetylglucosamine, which typically occurs as a α1-3 or α1-4 linkage. The transcript *FUT5* that

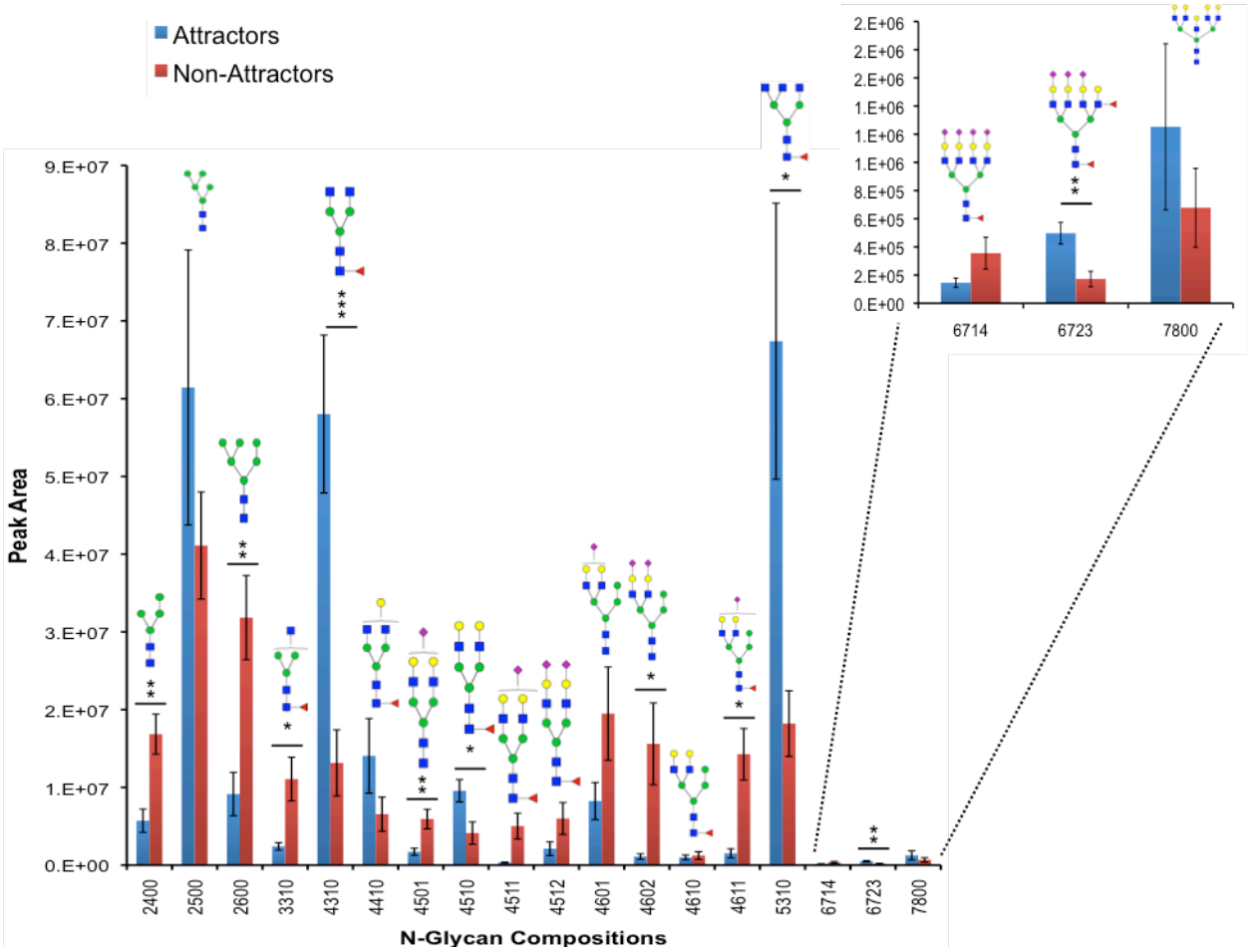

Figure 5.3. N-glycan Compositions in Attractors and Non-Attractors. Bar graphs of the permethylated N-glycan peak from attractor (*blue*) and non-attractor (*red*) GSCXs through on-tissue (tumor) digestions. The y-axis represents peak area and the x-axis represents glycan compositions (GlcNAc, Man, Gal, Fuc, NeuNAc). Symbols; GlcNAc, blue squares; Man, green circles, Gal, yellow circles, NeuNAc, magenta diamonds, and Fuc red triangles. Values are mean ± SEM; * $p < 0.05$, ** $p < 0.01$, and *** $p < 0.001$ (Student's *t*-test).

codes for the enzyme alpha-(1,3)-fucosyltransferase 5 was increased in attractors relative to non-attractors (**Supplemental Table 5.1**). This enzyme is responsible for the placement of a α1-4 linked fucose to N-acetyl-glucosamine (GlcNAc) and thus offers support for the N-glycan

composition seen in $GlcNAc_6Man_3Gal_4Fuc_2Sia_3$.

In contrast, the N-glycan compositions increased in attractors compared to non-attractors are of the complex type possessing either a terminal galactose or GlcNAc. Composition $GlcNAc_4Man_3Gal_2Fuc_1$ (p = 0.016) terminating in galactose was increased in attractors and compositions $GlcNAc_4Man_3Gal_1Fuc_1$ and $GlcNAc_7Man_3Gal_5$, while not significant follow the same trend. Complex N-glycans $GlcNAc_4Man_3Fuc_1$ (p = 0.0005) and $GlcNAc_5Man_3Fuc_1$ (p = 0.022) are the two most abundant N-glycans in attractors and terminate with two or more GlcNAcs ($GlcNAc_4Man_3Fuc_1$, fold change = 4.4 & $GlcNAc_5Man_3Fuc_1$, fold change = 3.7) in a N-acetyllactosamine (LacNAc) formation (Varki, 2009). Composition $GlcNAc_3Man_3Fuc_1$ is an exception to this though, ending with one GlcNAc monosaccharide at the reducing end unlike compositions $GlcNAc_4Man_3Fuc_1$ and $GlcNAc_5Man_3Fuc_1$.

Discussion

BM-hMSCs demonstrate significant promise as cell-based delivery vehicles for anti-glioma therapeutics (Doucette *et al*., 2011; Kosztowski *et al*., 2009; Miletic *et al*., 2007; Nakamizo *et al*., 2005; Nakamura *et al*., 2004; Studeny *et al*., 2004; Yong *et al*., 2009). However, evidence suggests that in GSCXs, the 'gold standard' of glioma models, these cells do not home or extravasate equally (Shinojima *et al*., 2013). Given the importance of glycosylation in the extravasation process, (Scott & Patel, 2013; Varki, 2009; Wright & Cooper, 2014) we examined the glycomic profile of attractors and non-attractors. The transcriptomic platform contains all human glycogenes, enabling analysis of all glycosylation pathways including, but not limited to, N-linked and O-linked glycosylation, gangliosides, and glycosaminoglycans. By utilizing this targeted transcriptomic approach, we were able to focus further glycomic studies on protein N-glycosylation in a data-driven approach for tumor-specific glycomic profiles. The value of this workflow is that the high-throughput targeted transcriptomic platform yields informative data about genes related to all types of glycosylation, which then serves to inform orthogonal glycomics experiments (**Fig. 5.1**).

The transcriptomic data revealed no significantly enriched glyco-synthetic or degradative pathways in attractors by use of GSEA analysis. This may be attributed to glycan heterogeneity in the attractor phenotype, which can clearly be seen in the PCA analysis (**Fig. 5.2A**). However, high mannose biosynthesis was a significantly enriched N-linked glycosylation pathway in the non-attractor phenotype (**Fig. 5.2B**) prompting us to examine the N-glycan profile of the GSCXs using the previously developed, highly efficient method for N-glycan profiling of tissue sections (Hu *et al*., 2013). The utility of this approach is that information relevant to histopathology is obtained from small samples derived from xenografts (Hu *et al.*, 2013).

Orthogonal glycomic experiments confirmed the presence of high mannose N-glycans in the non-attractors (**Fig. 5.3**), which could be an indicator of an embryonic, undifferentiated phenotype (An *et al*., 2012). Increased expression of high mannose type N-glycans also have been observed in colorectal cancer cell lines of varying malignancy (Balog *et al*., 2012; Holst, Wuhrer, & Rombouts, 2015; Sethi *et al*., 2014) and in breast cancer cell lines and tissue (de Leoz *et al*., 2011; Hua *et al*., 2014; Liu *et al*., 2013). The biological significance of this glycomic alteration in cancer is not clear, yet the presence of high (truncated) mannose indicates some level of incomplete N-linked glycosylation processing (Hakomori, 1985). To what extent and whether or not the truncated high mannose is protein specific is unknown, as levels of terminal sialic acid (complex and hybrid) N-glycans, which represent uncompromised N-glycan processing were increased in the non-attractors (**Fig. 5.3**).

Sialic acids carry a strong electronegative charge and have dual biological functions (Varki, 2009). They can either act as ligands for sialic acid binding proteins or they may serve to "mask" sites like galactose from galactose-binding receptors (Schultz, Swindall, and Bellis, 2012; Varki, 2009). It has been observed that the increase in sialic acid content of tumor cells results in decreased attachment of the cell to the basement membrane via electrostatic repulsion, promoting metastasis (Schultz *et al*., 2012; Varki, 2009). While GBM is confined within the cranium and does not metastasize, it is possible that via the same phenomenon, the non-attractors repel BM-hMSCs preventing extravasation and dispersion into the tumor parenchyma. Concomitantly, the sialic acid residues may be "masking" cell surface ligands that BM-hMSCs utilize for extravasation and dissemination throughout the tumor paraenchyma. For instance, sialic acid is known to inhibit galectin binding, which binds to either galactose or GlcNAc depending on the galectin isoform (Hirabayashi *et al*., 2002; Zhuo & Bellis, 2011). The

structures increased in the attractors terminate in either GlcNAc or galactose, in contrast to their sialylated counterparts, which were increased in the non-attractors (**Fig. 5.3**). At present, only galectin-1 has been identified on the cell surface of BM-hMSCs (Siegel *et al*., 2013). The functional cell surface expression of other galectin isoforms on BM-hMSCs remains unresolved.

Interestingly, recent evidence suggests that sialic acids may scavenge free radicals, providing an antioxidant effect (Gavella *et al*., 2010; Gavella & Lipovac, 2013; Iijima, Ichikawa, & Yamazaki, 2009; Iijima *et al*., 2004; Ogasawara *et al*., 2007; Varki, 2009). Sialic acids on glycosphingolipids have been reported to provide protection against ROS (Gavella *et al*., 2010; Gavella & Lipovac, 2013). Free N-acetylneuraminic acid (Neu5Ac, sialic acid) in solution was able to reduce the concentration of organic peroxides, lipid hydroperoxides and, the arachidonic acid derivative HpETE as well as attenuate cytotoxicity in culture with these agents (Iijima *et al*., 2009; Iijima *et al*., 2004). Pharmacologically, the hypersialylated analogue of human erythropoietin (r-HuEPO), was able to attenuated TNF-α-induced ROS and activation of JNK and MSK1, kinases upstream NFkB. However, upon desialylation, r-HuEPO lost its ability to inhibit JNK and MSK1 and reduce TNF-α-induced ROS.

We have previously demonstrated that the pentose phosphate pathway (PPP) was down-regulated in attractors relative to non-attractors (Wildburger *et al*., 2015). Supporting this was the down-regulation of glutathione S-transferase and superoxide dismutase in attractors relative to non-attractors and compromised fatty acid metabolism – heavily dependent on NADPH generated from the PPP (Wildburger *et al*., 2015). These data suggest that reactive oxidative species (ROS), which incite pro-inflammatory reactions, would be more prevalent in attractors than non-attractors. In fact, ROS species have been documented to decrease the sialic acid content of mammalian cell surface oligosaccharides (Eguchi *et al*., 2005; Yasuda *et al*., 2006),

which offers a possible explanation for the overall decreased levels of sialic acid containing N-glycans in the attractors (**Fig. 5.3**). The role of sialic acid containing N-glycans as free radical scavengers (Gavella *et al*., 2010; Gavella & Lipovac, 2013; Iijima *et al*., 2009; Ogasawara *et al*., 2007; Varki, 2009) and its consistent up-regulation in non-attractors in our glycomic study would presumably lead to lower levels of ROS and ROS-mediated inflammation in non-attractors. We note that our previous lipidomic study demonstrated DHA, an inflammatory-resolving lipid, to be increased in the tumor regions of non-attractors (Wildburger *et al*., 2015). DHA is a fatty acid dependent upon NADPH generated by the PPP for its biosynthesis (Kang, Lee, and Lee, 2015). The PPP and the proteins directly and indirectly involved in DHA metabolism were up-regulated in the non-attractor phenotype relative to the attractor phenotype, supporting decreased inflammation including ROS-generated inflammation (Wildburger *et al*., 2015). The increase in terminal sialic acid N-glycans in the non-attractor phenotype generates a new layer of complexity adding new valuable information and supporting our previous work (Wildburger *et al.*, 2015; Wildburger *et al*., 2015).

Our study of the N-glycan profile of attractor and non-attractor GSCXs yielded highly informative N-glycan compositions from the tumor regions of glioma xenograft tissue. Because we applied the on-tissue PNGase F deglycosylation protocol (Hu *et al*., 2013), we are confident that the N-glycan compositions we observed come from the cell surface in contrast to membrane fractionation, which invariably yields membrane contamination from the endoplasmic reticulum and Golgi apparatus (An *et al*., 2012). However, we acknowledge that a limitation to this study is that the N-glycans and subsequent mass spectrometric measurements are derived from a thin slice of tissue, limiting the analytical depth of the tumor microenvironment and any N-glycan micro-heterogeneity associated with differential intratumoral microenvironments. Nonetheless,

the results of this study motivate future investigations into the identity of proteins modified by N-glycans and their sites of attachment and linkage, along with mechanistic studies on their biological significance and functional relevance, including N-glycan expression by BM-hMSCs.

Acknowledgements

The authors gratefully acknowledge the financial support of the Cancer Prevention Research Institute of Texas (CPRIT) and The University of Texas Medical Branch to C.L.N. CPRIT (RP130624) and Texas Tech University to Y.M. Grants from the National Cancer Institute CA115729 and 1P50 CA127001, The Dr. Ralph and Marian Falk Medical Research Trust, Chicago IL (to JRM), The Broach Foundation for Brain Cancer Research, The Elias Family Fund, The National Brain Tumor Foundation, The Collaborative Ependymoma Research network (CERN), The Gene Pennebaker Brain Cancer Fund, the Sorenson Foundation, and the Brian McCulloch Fund to F.F.L are gratefully acknowledged.

Conflict of Interest

The authors do not have any conflicts of interest to disclose.

Author Contributions

N.C.W. conceived the study, performed experiments, data analysis and interpretation, wrote the manuscript. S.Z. performed experiments, conducted data analysis and interpretation, and assisted in writing in the manuscript. L.G.Z. performed glycan extractions, data acquisition, and data analysis. R.A.K. and J.R.M. contributed transcriptomics data analysis tools and provided helpful discussion. M.S. assisted in transcriptomics experiments and data analysis. P.M. assisted with glycan extractions. J.G. grew stem cell lines and performed all animal work. F.F.L., Y.M. and C.L.N. conceived the project, supervised the work, and critically revised the manuscript. All authors read and approved the final manuscript.

CONCLUSIONS

The concept of utilizing stem cells for active transport of therapeutics for the treatment of gliomas only emerged in the last 15 years, when Aboody *et al*., (2000) and Nakamura *et al.,* (2004) demonstrated that NSCs and hMSCs, respectively, migrated from distal sites to the tumor after intracranial implantation, to deliver therapeutically relevant molecules. Additionally, these cells were capable of migrating across the blood-brain and blood-tumor barriers after intra-arterial injection (Aboody *et al*., 2000; Nakamizo *et al*., 2005), which provided a solution to the long sought-after transvascular route of drug delivery. The excitement generated by these landmark studies has driven researchers to find the optimal therapeutic for these cells to carry and deliver to tumors in an effort to effectively cure GBM. However, there remains a fundamental lack of understanding of how hMSCs home to gliomas. Much of our understanding has come from studies using commercially available human glioma cell lines in xenografts or syngenic models. While these studies have generated valuable insights into hMSC homing, these studies are limited in their translational significance. Commercially available human glioma cell lines and syngenic models imprecisely reflect human gliomas *in vivo*. GSCs, on the other hand, form tumors that mimic human gliomas, thus offering a significantly translatable model (Singh *et al*., 2003; Singh 2004; Lee *et al*., 2006), though not all GSCXs home hMSCs equally (Shinojima *et al*., 2013). In our studies, the identification of "attractor" and "non-attractor" GSCXs provides a unique opportunity to resolve the factors required for successful hMSC homing and engraftment in tumors. Insights derived from comparison of the attractor and non-attractor phenotypes are not only of biological interest, but could inform our efforts to enhance hMSC homing to gliomas or to identify patients with maximum likelihood for successful hMSC-mediated therapeutic delivery. The experiments, results, and discussions reported in **Chapters**

III-V of this dissertation describe the first extensive studies of attractor and non-attractor GSCXs. In particular, this dissertation utilized high-throughput transcriptomics and high-resolution, high-mass accuracy mass spectrometry for the lipidomic, proteomic, and glycomic characterization of attracting and non-attracting GSCXs in a comprehensive manner.

Investigations into the homing of hMSCs to gliomas have typically used single target approaches with biochemical and cell biology methodologies. While significant advances have been made, assessing features or targets individually is an arduous task and lacks the high-throughput capacity critically needed to expand our understanding of hMSC tropism for advancing clinical therapeutics. Therefore, we chose an 'omics' approach in order to i) analyze multiple features simultaneously and ii) broaden our scope to include lipidomics, glycomics, as well as transcriptomics in addition to standard proteomic experimentation using GSCXs as a clinically relevant brain tumor model.

The brain has the highest content of lipids compared to any other organ in the body; 50-60% of the brain's [dry] weight is attributed to lipids. In a biological system, lipids are crucial to the maintenance of the cell membrane structure and serve as important signaling molecules (Helmreich, 2003; Aureli *et al*., 2015; Fernandis & Wenk, 2007). Given the location of GBM, the brain, there is a surprising lack of studies investigating the lipid composition of GBM tumors and how lipid modalities may correlate to hMSC homing. Examination of the lipid compositions (**Chapter III**) by ESI-MS/MS revealed 38 lipid species to be significantly differentially expressed between attractors and non-attractors. We focused further examinations on two classes of lipids diacyglycerol (DAG) and phosphatidic acid (PA) due to their dual functions as both cell membrane structural components and signaling molecules, and further their biochemical linkage to each other via the Kennedy pathway (Kennedy, 1987) (**Figures 3.2** and **3.3**). DAG and PA

were consistently decreased in attractors, with PA 36:2 and DAG 40:6 bearing histopathological relevance. Adding confidence to these findings was that fact that of nearly all glycerophospholipids, of which DAG and PA are the precursors to (Kennedy, 1987), were down-regulation in the attractors. DAG and PA are major signaling hubs in cells exerting their effects on both lipids and proteins. Their effects are numerous and vast, but their common convergence on proteins, such as PKC, warrants further examination (**Chapter III**).

Another significant finding in our ESI-MS/MS analysis was docosahexaenoic acid (DHA) (**Figure 3.4**), which was depleted in the attractor tumor regions but significantly elevated in the non-attractor tumor regions, as seen by MALDI-IMS. We argue that since DHA is a major inflammatory-resolving lipid in the brain, DHA may serve as a surrogate marker for decreased levels on inflammation in non-attractor GSCXs. We speculate that as a result of this, the elevated levels of DHA may be hampering pro-inflammatory cues that would otherwise promote hMSC homing to GSCXs. One noteworthy limitation to this study is our lack of quantitative data on the levels of arachidonic acid (AA), the pro-inflammatory counterpart to DHA. By being able to quantify the relative levels of AA in the GSCXs we could make a comparison to levels of DHA. Unfortunately, no reliable measurements of AA with low signal-to-noise were obtained in our ESI-MS/MS or MALDI-IMS analysis, which can be attributed to the low molecular weight of AA, 304.2402 g/mol (exact mass) or as $[M-H]^-$ at 303.2330 *m/z*. Analytes within this low mass range tend to be difficult to reliably measure as they metabolize quickly and are near the lower limit of detection.

Existing literature demonstrates that in glioma, the levels of AA are unchanged while levels of DHA are markedly decreased (Martin *et al*., 1996; Albert & Anderson, 1977; Elsherbiny, Emara, and Godbout, 2013). This observation of decreased levels of DHA in

attractors is supported by these observations, yet the elevated DHA in non-attractors runs contrary to these findings. However, we are confident in our lipid assessment of DHA for the following reasons i) DAG 40:6 (**Figure 3.3**) was determined to be a likely DHA-containing glyceride was also decreased in the non-attractors compared to the attractors consistent with the observations that DHA and DHA-containing lipid are decreased in glioma (Martin *et al*., 1996; Albert & Anderson, 1977). ii) We observed and measured this change using two independent mass spectrometry techniques, ESI-MS/MS and MALDI-IMS followed by CID fragmentation, which makes these results orthogonal to each other. iii) It is noteworthy in our proteomics study (**Chapter IV**) that amongst the top 12 KEGG pathways differentially expressed between the two phenotypes was fatty acid metabolism (**Figure 4.4**). DHA is a fatty acid and is synthesized via this pathway. The proteins both directly and indirectly (i.e. upstream to DHA) were decreased in the attractors relative to the non-attractors (**Figure S4.1**).

In **Chapter IV**, we attributed the down-regulation of the fatty acid metabolism pathway to the down-regulation of the pentose phosphate pathway (PPP) in attractors relative to non-attractors (**Figure S4.2**). NADPH, produced by the PPP is utilized by the fatty acid pathway for the synthesis of fatty acids such as DHA. Another consequence of reduce PPP activity in cells would be the inability to control the production of ROS, as NADPH is essential to the maintenance of ROS homeostasis. We reasoned that it might be possible that in addition to decreased levels of DHA, ROS may be more abundant in attractors; ROS are known to act as inflammatory mediators (Schreck, Rieber, and Baeuerle, 1991; Hensley *et al*., 2000). Granted the evidence only indirectly implicates ROS in the differential homing of hMSCs to gliomas. Yet, if our hypothesis holds, this would be the first implication, to the best of our knowledge, that ROS are critical players in hMSC homing.

Other significant metabolic alterations observed between the two phenotypes were the down-regulation of glycolysis in attractors relative to non-attractors (**Figure 4.5**) and the reciprocal expression of glycolysis and other glucose-dependent pathways in the mouse stroma. The significance of these metabolic differences is not fully understood (**Chapter IV**). But, given the down-regulation of other glucose-dependent pathways in the human tumors, such as the PPP, there could be a difference in glucose transport between attractors and non-attractors. This may manifest as decreased expression of glucose transporters, of which there are 13 isoforms (Joost & Thorens, 2001) or decreased glucose intake via the existing transporters. Unfortunately, we were unable to examine glucose transporters in these samples due to vast size of the transporter family and that in a Western blot analysis, antibody may not be able to properly distinguish between mouse and human protein. Active glucose uptake could also not be examined as these GSCX samples were *ex vivo*.

Of note, however, our transcriptomic analysis, appeared to indicate that N-linked glycosylation – also glucose dependent – was increased in attractors compared to non-attractors. This might offer a possible explanation for the decrease in other glucose pathways, namely PPP and glycolysis, though we do not exclude compromise glucose transport as described above. In pursuit of more evidence and the noted role of glycans in the extravasation process (Wright & Cooper, 2014), which is likely how the hMSCs exit the blood vasculature and enter the tumor parenchyma (Yong *et al*., 2009), we carried out a glycomics study on the attractor and non-attractor GSCXs (**Chapter V**). From these studies, the high mannose type N-glycans were shown to be prevalent in non-attractors compared to attractors, but there were more significant complex type N-glycans in attractors (**Figure 5.3**), which recapitulated the transcriptomics evidence in **Chapter IV**. Intriguingly, sialic acid containing N-glycans were consistently

decreased in attractors, while increased in non-attractors. It is notable that recent studies have defined sialic acid as a ROS scavenger (Gavella *et al*., 2010; Gavella *et al*., 2013; Iijima *et al*., 2009; Yang *et al*., 2011; Ogasawara *et al*., 2007; Iijima *et al*., 2004). Based on the data in **Chapter IV**, we reasoned that ROS might be elevated in attractors. Given our findings in **Chapter IV** and the newly defined biological function of sialic acid, the decreased levels of sialic acid N-glycans in attractors (**Chapter V**) offers additional support for the "attractor ROS hypothesis". Additionally, we speculate that sialic acid may be "masking" critical hMSC binding sites for extravasation and engraftment in non-attractors.

In all, the differential homing of hMSCs to attractor and non-attractor GSCXs provides an excellent model to examine and discern the factors critical to homing. The studies herein have provided a wealth of intriguing observations, which will serve as the foundation for many new and exciting avenues of research for the scientific community as we aim to bring meaningful hMSC-mediated therapeutics to the clinic. Some potential future studies derived from the data obtained in these multifaceted studies are described in the following section.

FUTURE DIRECTIONS

The *long-term* goal of this project is to understand the key factors that drive hMSCs to home to gliomas. The rationale is to harness hMSCs for successful cell-based therapeutics in the clinic or to identify patients amenable to this approach through the discovery and elucidation of these key factors. The results presented in this body of work provide novel, hypothesis-generating data for future studies. Potential future studies derived from the results of each major study on this project are described below.

Pro-inflammatory signals released from injured or stressed tissue elicit the homing of mature leukocytes (see *Homing* above). Tumors have the same phenotypic characteristics of injured or stressed tissue and thus have been described as "wounds that do not heal" as they (Dvorak, 1986). Several factors known to mediate hMSC homing to gliomas have reported roles as pro-inflammatory stimulators (Hata *et al*., 2010; Shinojima *et al*., 2013; Son *et al*., 2006; Ponte *et al*., 2007). In the lipidomic study (**Chapter III**), ESI-MS/MS determined that DHA was increased globally in the non-attractors. MALDI-IMS demonstrated that DHA was increased exclusively in the tumor regions of non-attractors. DHA mediates the resolution of inflammatory processes through its metabolic products (Hong *et al*., 2003; Marcheselli *et al*., 2003; Mukherjee *et al*., 2004; Ariel & Serhan, 2007; Schwab *et al*., 2007). If we assume the high levels of DHA to be surrogate marker for decreased inflammation and as a consequence inefficient homing of hMSCs to non-attractors, DHA could be employed as a predicative measure of phenotype (i.e., attractor *vs* non-attractor).

Within this context, only six GSC lines to-date are phenotypically defined as attractor or non-attractor (**Table 1.1**). A component of the *long-term* goal is to test the remaining GSC lines to determine their phenotype. As a potential future experiment, radiotracers (^{11}C) or ^{18}F-

fluorotracers (Basselin, Ramadan, and Rapoport, 2012) could be used to measure DHA metabolism in the brains of phenotypically unknown GSCXs. Quantified levels of DHA in GSCX brain tissue could then be used to predict which GSCs fall into either the attractor or non-attractor phenotype. In parallel, using the same GSCs, independent double-blind studies can be conducted using intra-artial injection of GFP-labeled hMSCs followed by fluorescence microscopy, as previously described (Yong *et al*., 2009; Shinojima *et al*., 2013), to determine phenotype. The two independent datasets can then be compared to determine congruency between DHA metabolism measured in imaging studies and phenotype as determined in previous work (Yong *et al*., 2009; Shinojima *et al*., 2013). If a positive correlation from these double-blind experiments results, one potential application to patients with GBM (in keeping with the *long-term* goals) would be to employ imaging of DHA metabolism to determine those most appropriate for hMSC-mediated delivery of anti-glioma therapeutics.

In the quantitative proteomic study (**Chapter IV**), the pentose phosphate pathway was decreased in attractors relative to non-attractors. The reduction of this pathway would lead to increased ROS as a consequence of decreased NADPH production. Supporting this data, the fatty acid metabolism pathway, which requires NADPH, was also decreased in attractors relative to non-attractors. Congruent with this, DHA, a major fatty acid in the CNS, was markedly decreased in attractors (lipidomics study, **Chapter III**). Given the known role of ROS in the activation of pro-inflammatory pathways (see **Chapter IV**), ROS-mediated inflammation may be a key component to hMSC homing to glioma. However, the role of ROS in glioma and specifically in hMSC homing to glioma remains largely unexplored. Given the possible link to ROS-mediated inflammation in the attractor phenotype, future studies should explore the role of ROS in eliciting hMSC homing. For instance, would the chronic administration of ROS

scavangers to attractor GSCXs compromise partially or in full their ability to elicit hMSC homing? Further studies should ascertain the impact of different ROS, hydroxyl radicals ($OH^{\bullet}$), superoxide ($O_2^{\bullet-}$), and hydrogen peroxide (H_2O_2), on hMSC homing.

In the last study (**Chapter V**), glycomic analysis of GSCXs further reinforced the notion of ROS in hMSC homing to glioma. Sialic acid, a known ROS scavenger (Gavella *et al*., 2010; Gavella *et al*., 2013; Iijima *et al*., 2009; Yang *et al*., 2011; Ogasawara *et al*., 2007; Iijima *et al*., 2004), was decrease in the attractors. Sialic acid may also be "masking" non-attractor cell surface ligands required for hMSC extravasation and engraftment. While it is yet unclear if the sialic acids are α2-3 or α2-6 linked, a reasonable strategy to enhance hMSCs homing to GSCXs would be to transfect and stably express sialic acid binding lectins on the cell surface of hMSCs.

Overall, the results presented in the series of studies contained in this dissertation should provide a framework for future studies to advance our understanding of hMSC differential homing to glioma stem cell xenografts, and ways to capitalize on this new knowledge to improve treatment for GBM. The experiments proposed above provide the next logical steps in understanding and enhancing hMSC homing to gliomas. However, while feasible, these types of experiments will require well-designed experimental paradigms with excellent positive and negative controls in place.

BIBLIOGRAPHY

Aboody, K. S., Brown, A., Rainov, N. G., Bower, K. A., Liu, S., Yang, W., et al. (2000). Neural stem cells display extensive tropism for pathology in adult brain: evidence from intracranial gliomas. Proc Natl Acad Sci U S A, 97(23), 12846-12851.

Aebi, M., & Hennet, T. (2001). Congenital disorders of glycosylation: genetic model systems lead the way. Trends Cell Biol, 11(3), 136-141.

Aggarwal, S., & Pittenger, M. F. (2005). Human mesenchymal stem cells modulate allogeneic immune cell responses. Blood, 105(4), 1815-1822.

Al-Saad, K. A., Siems, W. F., Hill, H. H., Zabrouskov, V., & Knowles, N. R. (2003). Structural analysis of phosphatidylcholines by post-source decay matrix-assisted laser desorption/ionization time-of-flight mass spectrometry. J Am Soc Mass Spectrom, 14(4), 373-382.

Albert, D. H., & Anderson, C. E. (1977). Fatty acid composition at the 2-position of ether-linked and diacyl ethanolamine and choline phosphoglycerides of human brain tumors. Lipids, 12(9), 722-728.

An, H. J., Gip, P., Kim, J., Wu, S., Park, K. W., McVaugh, C. T., et al. (2012). Extensive determination of glycan heterogeneity reveals an unusual abundance of high mannose glycans in enriched plasma membranes of human embryonic stem cells. Mol Cell Proteomics, 11(4), M111.010660.

Apweiler, R., Hermjakob, H., & Sharon, N. (1999). On the frequency of protein glycosylation, as deduced from analysis of the SWISS-PROT database. Biochim Biophys Acta, 1473(1), 4-8.

Ariel, A., & Serhan, C. N. (2007). Resolvins and protectins in the termination program of acute inflammation. Trends Immunol, 28(4), 176-183.

Auffinger, B., Tobias, A. L., Han, Y., Lee, G., Guo, D., Dey, M., et al. (2014). Conversion of differentiated cancer cells into cancer stem-like cells in a glioblastoma model after primary chemotherapy. Cell Death Differ, 21(7), 1119-1131.

Aureli, M., Grassi, S., Prioni, S., Sonnino, S., & Prinetti, A. (2015). Lipid membrane domains in the brain. Biochim Biophys Acta.

Balog, C. I., Stavenhagen, K., Fung, W. L., Koeleman, C. A., McDonnell, L. A., Verhoeven, A., et al. (2012). N-glycosylation of colorectal cancer tissues: a liquid chromatography and mass spectrometry-based investigation. Mol Cell Proteomics, 11(9), 571-585.

Bao, S., Wu, Q., McLendon, R. E., Hao, Y., Shi, Q., Hjelmeland, A. B., et al. (2006). Glioma stem cells promote radioresistance by preferential activation of the DNA damage response. Nature, 444(7120), 756-760.

Basselin, M., Ramadan, E., & Rapoport, S. I. (2012). Imaging brain signal transduction and metabolism via arachidonic and docosahexaenoic acid in animals and humans. Brain Res Bull, 87(2-3), 154-171.

Baum, L. G., Garner, O. B., Schaefer, K., & Lee, B. (2014). Microbe-Host Interactions are Positively and Negatively Regulated by Galectin-Glycan Interactions. Front Immunol, 5, 284.

Beermann, C., Möbius, M., Winterling, N., Schmitt, J. J., & Boehm, G. (2005). sn-position determination of phospholipid-linked fatty acids derived from erythrocytes by liquid chromatography electrospray ionization ion-trap mass spectrometry. Lipids, 40(2), 211-218.

Bellail, A. C., Hunter, S. B., Brat, D. J., Tan, C., & Van Meir, E. G. (2004). Microregional extracellular matrix heterogeneity in brain modulates glioma cell invasion. Int J Biochem Cell Biol, 36(6), 1046-1069.

Benjamini, Y., & Hochberg, Y. (1995). Controlling the false discovery rate: a practical and powerful approach to multiple testing. Journal of the Royal Statistical Society Series B (Methodological), 57, 289-300.

Berens, M. E., & Giese, A. (1999). "...those left behind." Biology and oncology of invasive glioma cells. Neoplasia, 1(3), 208-219.

Berg, J. M., Tymoczko, J. L., & Stryer, L. (2002). Biochemistry (5th ed.). New York: W.H. Freeman.

Bernstein, J. J., Laws, E. R., Levine, K. V., Wood, L. R., Tadvalkar, G., & Goldberg, W. J. (1991). C6 glioma-astrocytoma cell and fetal astrocyte migration into artificial basement membrane: a permissive substrate for neural tumors but not fetal astrocytes. Neurosurgery, 28(5), 652-658.

Bernstein, J. J., & Woodard, C. A. (1995). Glioblastoma cells do not intravasate into blood vessels. Neurosurgery, 36(1), 124-132; discussion 132.

Berridge, M. J. (1987). Inositol trisphosphate and diacylglycerol: two interacting second messengers. Annu Rev Biochem, 56, 159-193.

Bianco, P., Riminucci, M., Gronthos, S., & Robey, P. G. (2001). Bone marrow stromal stem cells: nature, biology, and potential applications. Stem Cells, 19(3), 180-192.

Bieback, K., Kern, S., Klüter, H., & Eichler, H. (2004). Critical parameters for the isolation of mesenchymal stem cells from umbilical cord blood. Stem Cells, 22(4), 625-634.

Bittira, B., Shum-Tim, D., Al-Khaldi, A., & Chiu, R. C. (2003). Mobilization and homing of bone marrow stromal cells in myocardial infarction. Eur J Cardiothorac Surg, 24(3), 393-398.

Blasberg, R. G. (1977). Methotrexate, cytosine arabinoside, and BCNU concentration in brain after ventriculocisternal perfusion. Cancer Treat Rep, 61(4), 625-631.

Blasberg, R. G., Patlak, C. S., & Shapiro, W. R. (1977). Distribution of methotrexate in the cerebrospinal fluid and brain after intraventricular administration. Cancer Treat Rep, 61(4), 633-641.

Block, H., Ley, K., & Zarbock, A. (2012). Severe impairment of leukocyte recruitment in ppGalNAcT-1-deficient mice. J Immunol, 188(11), 5674-5681.

Brandes, A. A., Franceschi, E., Tosoni, A., Bartolini, S., Bacci, A., Agati, R., et al. (2010). O(6)-methylguanine DNA-methyltransferase methylation status can change between first surgery for newly diagnosed glioblastoma and second surgery for recurrence: clinical implications. Neuro Oncol, 12(3), 283-288.

Brat, D. J., & Van Meir, E. G. (2001). Glomeruloid microvascular proliferation orchestrated by VPF/VEGF: a new world of angiogenesis research. Am J Pathol, 158(3), 789-796.

Brat, D. J., & Van Meir, E. G. (2004). Vaso-occlusive and prothrombotic mechanisms associated with tumor hypoxia, necrosis, and accelerated growth in glioblastoma. Lab Invest, 84(4), 397-405.

Brennan, C. W., Verhaak, R. G., McKenna, A., Campos, B., Noushmehr, H., Salama, S. R., et al. (2013). The somatic genomic landscape of glioblastoma. Cell, 155(2), 462-477.

Bruntz, R. C., Lindsley, C. W., & Brown, H. A. (2014). Phospholipase D Signaling Pathways and Phosphatidic Acid as Therapeutic Targets in Cancer. Pharmacol Rev, 66(4), 1033-1079.

Bryan, P. (1974). CSF seeding of intra-cranial tumours: a study of 96 cases. Clin Radiol, 25(3), 355-360.

Burger, P. C., Heinz, E. R., Shibata, T., & Kleihues, P. (1988). Topographic anatomy and CT correlations in the untreated glioblastoma multiforme. J Neurosurg, 68(5), 698-704.

Caplan, A. I., & Bruder, S. P. (2001). Mesenchymal stem cells: building blocks for molecular medicine in the 21st century. Trends Mol Med, 7(6), 259-264.

Chakravarti, A., Erkkinen, M. G., Nestler, U., Stupp, R., Mehta, M., Aldape, K., et al. (2006). Temozolomide-mediated radiation enhancement in glioblastoma: a report on underlying mechanisms. Clin Cancer Res, 12(15), 4738-4746.

Charles, N., & Holland, E. C. (2009). Brain tumor treatment increases the number of cancer stem-like cells. Expert Rev Neurother, 9(10), 1447-1449.

Chughtai, K., Jiang, L., Greenwood, T. R., Glunde, K., & Heeren, R. M. (2013). Mass spectrometry images acylcarnitines, phosphatidylcholines, and sphingomyelin in MDA-MB-231 breast tumor models. J Lipid Res, 54(2), 333-344.

Churchill, G. A. (2002). Fundamentals of experimental design for cDNA microarrays. Nat Genet, 32 Suppl, 490-495.

Clarke, M. F., Dick, J. E., Dirks, P. B., Eaves, C. J., Jamieson, C. H., Jones, D. L., et al. (2006). Cancer stem cells--perspectives on current status and future directions: AACR Workshop on cancer stem cells. Cancer Res, 66(19), 9339-9344.

Cooper, R. A. (1970). Lipids of human red cell membrane: normal composition and variability in disease. Semin Hematol, 7(3), 296-322.

Costello, J. F., Futscher, B. W., Tano, K., Graunke, D. M., & Pieper, R. O. (1994). Graded methylation in the promoter and body of the O6-methylguanine DNA methyltransferase (MGMT) gene correlates with MGMT expression in human glioma cells. J Biol Chem, 269(25), 17228-17237.

Costello, J. F., Plass, C., Arap, W., Chapman, V. M., Held, W. A., Berger, M. S., et al. (1997). Cyclin-dependent kinase 6 (CDK6) amplification in human gliomas identified using two-dimensional separation of genomic DNA. Cancer Res, 57(7), 1250-1254.

Coussens, L. M., & Werb, Z. (2002). Inflammation and cancer. Nature, 420(6917), 860-867.

Cox, J., & Mann, M. (2012). 1D and 2D annotation enrichment: a statistical method integrating quantitative proteomics with complementary high-throughput data. BMC Bioinformatics, 13 Suppl 16, S12.

Crosson, L. A., Kroes, R. A., Moskal, J. R., & Linsenmeier, R. A. (2009). Gene expression patterns in hypoxic and post-hypoxic adult rat retina with special reference to the NMDA receptor and its interactome. Mol Vis, 15, 296-311.

Curtin, N. J., Wang, L. Z., Yiakouvaki, A., Kyle, S., Arris, C. A., Canan-Koch, S., et al. (2004). Novel poly(ADP-ribose) polymerase-1 inhibitor, AG14361, restores sensitivity to temozolomide in mismatch repair-deficient cells. Clin Cancer Res, 10(3), 881-889.

Dahan, P., Martinez Gala, J., Delmas, C., Monferran, S., Malric, L., Zentkowski, D., et al. (2014). Ionizing radiations sustain glioblastoma cell dedifferentiation to a stem-like phenotype through survivin: possible involvement in radioresistance. Cell Death Dis, 5, e1543.

Dandy, W. E. (1928). Removal of right cerebral hemisphere for certain tumors with hemiplegia preliminary report (Vol. 90): The Journal of the American Medical Association.

de Leoz, M. L., Young, L. J., An, H. J., Kronewitter, S. R., Kim, J., Miyamoto, S., et al. (2011). High-mannose glycans are elevated during breast cancer progression. Mol Cell Proteomics, 10(1), M110.002717.

DeAngelis, L. M. (2001). Brain tumors. N Engl J Med, 344(2), 114-123.

DeBerardinis, R. J., Lum, J. J., Hatzivassiliou, G., & Thompson, C. B. (2008). The biology of cancer: metabolic reprogramming fuels cell growth and proliferation. Cell Metab, 7(1), 11-20.

DeBerardinis, R. J., Mancuso, A., Daikhin, E., Nissim, I., Yudkoff, M., Wehrli, S., et al. (2007). Beyond aerobic glycolysis: transformed cells can engage in glutamine metabolism that exceeds the requirement for protein and nucleotide synthesis. Proc Natl Acad Sci U S A, 104(49), 19345-19350.

Desantos-Garcia, J. L., Khalil, S. I., Hussein, A., Hu, Y., & Mechref, Y. (2011). Enhanced sensitivity of LC-MS analysis of permethylated N-glycans through online purification. Electrophoresis, 32(24), 3516-3525.

Dirks, P., Bernstein, M., Muller, P. J., & Tucker, W. S. (1993). The value of reoperation for recurrent glioblastoma. Can J Surg, 36(3), 271-275.

Dmitriev, I., Krasnykh, V., Miller, C. R., Wang, M., Kashentseva, E., Mikheeva, G., et al. (1998). An adenovirus vector with genetically modified fibers demonstrates expanded tropism via utilization of a coxsackievirus and adenovirus receptor-independent cell entry mechanism. J Virol, 72(12), 9706-9713.

Domart, M. C., Hobday, T. M., Peddie, C. J., Chung, G. H., Wang, A., Yeh, K., et al. (2012). Acute manipulation of diacylglycerol reveals roles in nuclear envelope assembly & endoplasmic reticulum morphology. PLoS One, 7(12), e51150.

Dominici, M., Le Blanc, K., Mueller, I., Slaper-Cortenbach, I., Marini, F., Krause, D., et al. (2006). Minimal criteria for defining multipotent mesenchymal stromal cells. The International Society for Cellular Therapy position statement. Cytotherapy, 8(4), 315-317.

Doucette, T., Rao, G., Yang, Y., Gumin, J., Shinojima, N., Bekele, B. N., et al. (2011). Mesenchymal stem cells display tumor-specific tropism in an RCAS/Ntv-a glioma model. Neoplasia, 13(8), 716-725.

Dunn, G. P., Rinne, M. L., Wykosky, J., Genovese, G., Quayle, S. N., Dunn, I. F., et al. (2012). Emerging insights into the molecular and cellular basis of glioblastoma. Genes Dev, 26(8), 756-784.

Dvorak, H. F. (1986). Tumors: wounds that do not heal. Similarities between tumor stroma generation and wound healing. N Engl J Med, 315(26), 1650-1659.

Dwek, R. A. (1996). Glycobiology: Toward Understanding the Function of Sugars. Chem Rev, 96(2), 683-720.

Eguchi, H., Ikeda, Y., Ookawara, T., Koyota, S., Fujiwara, N., Honke, K., et al. (2005). Modification of oligosaccharides by reactive oxygen species decreases sialyl lewis x-mediated cell adhesion. Glycobiology, 15(11), 1094-1101.

Elsherbiny, M. E., Emara, M., & Godbout, R. (2013). Interaction of brain fatty acid-binding protein with the polyunsaturated fatty acid environment as a potential determinant of poor prognosis in malignant glioma. Prog Lipid Res, 52(4), 562-570.

Erices, A., Conget, P., & Minguell, J. J. (2000). Mesenchymal progenitor cells in human umbilical cord blood. Br J Haematol, 109(1), 235-242.

Esteller, M., Hamilton, S. R., Burger, P. C., Baylin, S. B., & Herman, J. G. (1999). Inactivation of the DNA repair gene O6-methylguanine-DNA methyltransferase by promoter hypermethylation is a common event in primary human neoplasia. Cancer Res, 59(4), 793-797.

Facchino, S., Abdouh, M., Chatoo, W., & Bernier, G. (2010). BMI1 confers radioresistance to normal and cancerous neural stem cells through recruitment of the DNA damage response machinery. J Neurosci, 30(30), 10096-10111.

Fahy, E., Subramaniam, S., Murphy, R. C., Nishijima, M., Raetz, C. R., Shimizu, T., et al. (2009). Update of the LIPID MAPS comprehensive classification system for lipids. J Lipid Res, 50 Suppl, S9-14.

Fahy, E., Sud, M., Cotter, D., & Subramaniam, S. (2007). LIPID MAPS online tools for lipid research. Nucleic Acids Res, 35(Web Server issue), W606-612.

Fearon, K. C., & Moses, A. G. (2002). Cancer cachexia. Int J Cardiol, 85(1), 73-81.

Feigin, I., Allen, L. B., Lipkin, L., & Gross, S. W. (1958). The endothelial hyperplasia of the cerebral blood vessels with brain tumors, and its sarcomatous transformation. Cancer, 11(2), 264-277.

Felsberg, J., Thon, N., Eigenbrod, S., Hentschel, B., Sabel, M. C., Westphal, M., et al. (2011). Promoter methylation and expression of MGMT and the DNA mismatch repair genes MLH1, MSH2, MSH6 and PMS2 in paired primary and recurrent glioblastomas. Int J Cancer, 129(3), 659-670.

Ferluga, S., Hantgan, R., Goldgur, Y., Himanen, J. P., Nikolov, D. B., & Debinski, W. (2013). Biological and structural characterization of glycosylation on ephrin-A1, a preferred ligand for EphA2 receptor tyrosine kinase. J Biol Chem, 288(25), 18448-18457.

Fernandis, A. Z., & Wenk, M. R. (2007). Membrane lipids as signaling molecules. Curr Opin Lipidol, 18(2), 121-128.

Friedenstein, A. J., Gorskaja, J. F., & Kulagina, N. N. (1976). Fibroblast precursors in normal and irradiated mouse hematopoietic organs. Exp Hematol, 4(5), 267-274.

Frolov, M. V., & Dyson, N. J. (2004). Molecular mechanisms of E2F-dependent activation and pRB-mediated repression. J Cell Sci, 117(Pt 11), 2173-2181.

Frommhold, D., Ludwig, A., Bixel, M. G., Zarbock, A., Babushkina, I., Weissinger, M., et al. (2008). Sialyltransferase ST3Gal-IV controls CXCR2-mediated firm leukocyte arrest during inflammation. J Exp Med, 205(6), 1435-1446.

Fueyo, J., Alemany, R., Gomez-Manzano, C., Fuller, G. N., Khan, A., Conrad, C. A., et al. (2003). Preclinical characterization of the antiglioma activity of a tropism-enhanced adenovirus targeted to the retinoblastoma pathway. J Natl Cancer Inst, 95(9), 652-660.

Fueyo, J., Gomez-Manzano, C., Alemany, R., Lee, P. S., McDonnell, T. J., Mitlianga, P., et al. (2000). A mutant oncolytic adenovirus targeting the Rb pathway produces anti-glioma effect in vivo. Oncogene, 19(1), 2-12.

Furnari, F. B., Fenton, T., Bachoo, R. M., Mukasa, A., Stommel, J. M., Stegh, A., et al. (2007). Malignant astrocytic glioma: genetics, biology, and paths to treatment. Genes Dev, 21(21), 2683-2710.

Gage, F. H. (2000). Mammalian neural stem cells. Science, 287(5457), 1433-1438.

Galli, R., Binda, E., Orfanelli, U., Cipelletti, B., Gritti, A., De Vitis, S., et al. (2004). Isolation and characterization of tumorigenic, stem-like neural precursors from human glioblastoma. Cancer Res, 64(19), 7011-7021.

Gaspar, L. E., Fisher, B. J., Macdonald, D. R., LeBer, D. V., Halperin, E. C., Schold, S. C., et al. (1992). Supratentorial malignant glioma: patterns of recurrence and implications for external beam local treatment. Int J Radiat Oncol Biol Phys, 24(1), 55-57.

Gatenby, R. A., & Gillies, R. J. (2004). Why do cancers have high aerobic glycolysis? Nat Rev Cancer, 4(11), 891-899.

Gavella, M., Garaj-Vrhovac, V., Lipovac, V., Antica, M., Gajski, G., & Car, N. (2010). Ganglioside GT1b protects human spermatozoa from hydrogen peroxide-induced DNA and membrane damage. Int J Androl, 33(3), 536-544.

Gavella, M., & Lipovac, V. (2013). Protective effects of exogenous gangliosides on ROS-induced changes in human spermatozoa. Asian J Androl, 15(3), 375-381.

Giese, A., Bjerkvig, R., Berens, M. E., & Westphal, M. (2003). Cost of migration: invasion of malignant gliomas and implications for treatment. J Clin Oncol, 21(8), 1624-1636.

Giese, A., Rief, M. D., Loo, M. A., & Berens, M. E. (1994). Determinants of human astrocytoma migration. Cancer Res, 54(14), 3897-3904.

Gillies, R. J., & Gatenby, R. A. (2007). Adaptive landscapes and emergent phenotypes: why do cancers have high glycolysis? J Bioenerg Biomembr, 39(3), 251-257.

Griner, E. M., & Kazanietz, M. G. (2007). Protein kinase C and other diacylglycerol effectors in cancer. Nat Rev Cancer, 7(4), 281-294.

Grobben, B., De Deyn, P. P., & Slegers, H. (2002). Rat C6 glioma as experimental model system for the study of glioblastoma growth and invasion. Cell Tissue Res, 310(3), 257-270.

Groothuis, D. R. (2000). The blood-brain and blood-tumor barriers: a review of strategies for increasing drug delivery. Neuro Oncol, 2(1), 45-59.

Hadjipanayis, C. G., & Van Meir, E. G. (2009). Tumor initiating cells in malignant gliomas: biology and implications for therapy. J Mol Med (Berl), 87(4), 363-374.

Hakomori, S. (1985). Aberrant glycosylation in cancer cell membranes as focused on glycolipids: overview and perspectives. Cancer Res, 45(6), 2405-2414.

Hankin, J. A., Barkley, R. M., & Murphy, R. C. (2007). Sublimation as a method of matrix application for mass spectrometric imaging. J Am Soc Mass Spectrom, 18(9), 1646-1652.

Happold, C., Roth, P., Wick, W., Schmidt, N., Florea, A. M., Silginer, M., et al. (2012). Distinct molecular mechanisms of acquired resistance to temozolomide in glioblastoma cells. J Neurochem, 122(2), 444-455.

Harris, L. C., Potter, P. M., Tano, K., Shiota, S., Mitra, S., & Brent, T. P. (1991). Characterization of the promoter region of the human O6-methylguanine-DNA methyltransferase gene. Nucleic Acids Res, 19(22), 6163-6167.

Hata, N., Shinojima, N., Gumin, J., Yong, R., Marini, F., Andreeff, M., et al. (2010). Platelet-derived growth factor BB mediates the tropism of human mesenchymal stem cells for malignant gliomas. Neurosurgery, 66(1), 144-156; discussion 156-147.

Hattori, R., Hamilton, K. K., Fugate, R. D., McEver, R. P., & Sims, P. J. (1989). Stimulated secretion of endothelial von Willebrand factor is accompanied by rapid redistribution to the cell surface of the intracellular granule membrane protein GMP-140. J Biol Chem, 264(14), 7768-7771.

Hauck, S. M., Dietter, J., Kramer, R. L., Hofmaier, F., Zipplies, J. K., Amann, B., et al. (2010). Deciphering membrane-associated molecular processes in target tissue of autoimmune uveitis by label-free quantitative mass spectrometry. Mol Cell Proteomics, 9(10), 2292-2305.

He, H., Conrad, C. A., Nilsson, C. L., Ji, Y., Schaub, T. M., Marshall, A. G., et al. (2007). Method for lipidomic analysis: p53 expression modulation of sulfatide, ganglioside, and phospholipid composition of U87 MG glioblastoma cells. Anal Chem, 79(22), 8423-8430.

He, H., Nilsson, C. L., Emmett, M. R., Ji, Y., Marshall, A. G., Kroes, R. A., et al. (2010). Polar lipid remodeling and increased sulfatide expression are associated with the glioma therapeutic candidates, wild type p53 elevation and the topoisomerase-1 inhibitor, irinotecan. Glycoconj J, 27(1), 27-38.

He, H., Nilsson, C. L., Emmett, M. R., Marshall, A. G., Kroes, R. A., Moskal, J. R., et al. (2010). Glycomic and transcriptomic response of GSC11 glioblastoma stem cells to STAT3 phosphorylation inhibition and serum-induced differentiation. J Proteome Res, 9(5), 2098-2108.

Hegi, M. E., Diserens, A. C., Gorlia, T., Hamou, M. F., de Tribolet, N., Weller, M., et al. (2005). MGMT gene silencing and benefit from temozolomide in glioblastoma. N Engl J Med, 352(10), 997-1003.

Helmreich, E. J. (2003). Environmental influences on signal transduction through membranes: a retrospective mini-review. Biophys Chem, 100(1-3), 519-534.

Hensley, K., Robinson, K. A., Gabbita, S. P., Salsman, S., & Floyd, R. A. (2000). Reactive oxygen species, cell signaling, and cell injury. Free Radic Biol Med, 28(10), 1456-1462.

Hermansson, M., Hokynar, K., & Somerharju, P. (2011). Mechanisms of glycerophospholipid homeostasis in mammalian cells. Prog Lipid Res, 50(3), 240-257.

Hirabayashi, J., Hashidate, T., Arata, Y., Nishi, N., Nakamura, T., Hirashima, M., et al. (2002). Oligosaccharide specificity of galectins: a search by frontal affinity chromatography. Biochim Biophys Acta, 1572(2-3), 232-254.

Hochberg, F. H., & Pruitt, A. (1980). Assumptions in the radiotherapy of glioblastoma. Neurology, 30(9), 907-911.

Holst, S., Wuhrer, M., & Rombouts, Y. (2015). Glycosylation characteristics of colorectal cancer. Adv Cancer Res, 126, 203-256.

Honczarenko, M., Le, Y., Swierkowski, M., Ghiran, I., Glodek, A. M., & Silberstein, L. E. (2006). Human bone marrow stromal cells express a distinct set of biologically functional chemokine receptors. Stem Cells, 24(4), 1030-1041.

Hong, S., Gronert, K., Devchand, P. R., Moussignac, R. L., & Serhan, C. N. (2003). Novel docosatrienes and 17S-resolvins generated from docosahexaenoic acid in murine brain, human blood, and glial cells. Autacoids in anti-inflammation. J Biol Chem, 278(17), 14677-14687.

Hu, Y., Desantos-Garcia, J. L., & Mechref, Y. (2013). Comparative glycomic profiling of isotopically permethylated N-glycans by liquid chromatography/electrospray ionization mass spectrometry. Rapid Commun Mass Spectrom, 27(8), 865-877.

Hu, Y., & Mechref, Y. (2012). Comparing MALDI-MS, RP-LC-MALDI-MS and RP-LC-ESI-MS glycomic profiles of permethylated N-glycans derived from model glycoproteins and human blood serum. Electrophoresis, 33(12), 1768-1777.

Hu, Y., Zhou, S., Khalil, S.I., Renteria, C.L., & Mechref, Y. (2013). Glycomic profiling of tissue sections by LC-MS. Anal Chem, 85(8), 4074-4079.

Hu, Y., Zhou, S., Yu, C. Y., Tang, H., & Mechref, Y. (2015). Automated annotation and quantitation of glycans by liquid chromatography/electrospray ionization mass spectrometric analysis using the MultiGlycan-ESI computational tool. Rapid Commun Mass Spectrom, 29(1), 135-142.

Hua, S., Saunders, M., Dimapasoc, L. M., Jeong, S. H., Kim, B. J., Kim, S., et al. (2014). Differentiation of cancer cell origin and molecular subtype by plasma membrane N-glycan profiling. J Proteome Res, 13(2), 961-968.

Huang, D. W., Sherman, B. T., & Lempicki, R. A. (2009a). Bioinformatics enrichment tools: paths toward the comprehensive functional analysis of large gene lists. Nucleic Acids Res, 37(1), 1-13.

Huang, D. W., Sherman, B. T., & Lempicki, R. A. (2009b). Systematic and integrative analysis of large gene lists using DAVID bioinformatics resources. Nat Protoc, 4(1), 44-57.

Ignatova, T. N., Kukekov, V. G., Laywell, E. D., Suslov, O. N., Vrionis, F. D., & Steindler, D. A. (2002). Human cortical glial tumors contain neural stem-like cells expressing astroglial and neuronal markers in vitro. Glia, 39(3), 193-206.

Iijima, R., Ichikawa, T., & Yamazaki, M. (2009). Sialic acid attenuates the cytotoxicity of the lipid hydroperoxides HpODE and HpETE. Carbohydr Res, 344(7), 933-935.

Iijima, R., Takahashi, H., Namme, R., Ikegami, S., & Yamazaki, M. (2004). Novel biological function of sialic acid (N-acetylneuraminic acid) as a hydrogen peroxide scavenger. FEBS Lett, 561(1-3), 163-166.

Ip, J. E., Wu, Y., Huang, J., Zhang, L., Pratt, R. E., & Dzau, V. J. (2007). Mesenchymal stem cells use integrin beta1 not CXC chemokine receptor 4 for myocardial migration and engraftment. Mol Biol Cell, 18(8), 2873-2882.

Jackson, R. J., Fuller, G. N., Abi-Said, D., Lang, F. F., Gokaslan, Z. L., Shi, W. M., et al. (2001). Limitations of stereotactic biopsy in the initial management of gliomas. Neuro Oncol, 3(3), 193-200.

Joost, H. G., & Thorens, B. (2001). The extended GLUT-family of sugar/polyol transport facilitators: nomenclature, sequence characteristics, and potential function of its novel members (review). Mol Membr Biol, 18(4), 247-256.

Kanehisa, M., & Goto, S. (2000). KEGG: kyoto encyclopedia of genes and genomes. Nucleic Acids Res, 28(1), 27-30.

Kanehisa, M., Goto, S., Sato, Y., Kawashima, M., Furumichi, M., & Tanabe, M. (2014). Data, information, knowledge and principle: back to metabolism in KEGG. Nucleic Acids Res, 42(Database issue), D199-205.

Kang, M. K., & Kang, S. K. (2007). Tumorigenesis of chemotherapeutic drug-resistant cancer stem-like cells in brain glioma. Stem Cells Dev, 16(5), 837-847.

Kang, S. W., Lee, S., & Lee, E. K. (2015). ROS and energy metabolism in cancer cells: alliance for fast growth. Arch Pharm Res, 38(3), 338-345.

Kaur, B., Tan, C., Brat, D. J., Post, D. E., & Van Meir, E. G. (2004). Genetic and hypoxic regulation of angiogenesis in gliomas. J Neurooncol, 70(2), 229-243.

Kennedy, D. (2000). Two cheers for new stem cell rules. Science, 289(5484), 1469.

Kennedy, E. P. (1987). Metabolism and function of membrane lipids. Klin Wochenschr, 65(5), 205-212.

Kern, S., Eichler, H., Stoeve, J., Klüter, H., & Bieback, K. (2006). Comparative analysis of mesenchymal stem cells from bone marrow, umbilical cord blood, or adipose tissue. Stem Cells, 24(5), 1294-1301.

Kleihues, P. (2000). World health organization classification of tumors: Pathology and genetics of tumors of the nervous system. In W. K. Cavenee (Ed.). Lyon: International Agency for Research on Cancer, IARC Press.

Kleihues, P., & Ohgaki, H. (1999). Primary and secondary glioblastomas: from concept to clinical diagnosis. Neuro Oncol, 1(1), 44-51.

Kosztowski, T., Zaidi, H. A., & Quiñones-Hinojosa, A. (2009). Applications of neural and mesenchymal stem cells in the treatment of gliomas. Expert Rev Anticancer Ther, 9(5), 597-612.

Koç, O. N., Day, J., Nieder, M., Gerson, S. L., Lazarus, H. M., & Krivit, W. (2002). Allogeneic mesenchymal stem cell infusion for treatment of metachromatic leukodystrophy (MLD) and Hurler syndrome (MPS-IH). Bone Marrow Transplant, 30(4), 215-222.

Kramer, S. (1969). Tumor extent as a determining factor in radiotherapy of glioblastomas. Acta Radiol Ther Phys Biol, 8(1-2), 111-117.

Krewson, C. E., Klarman, M. L., & Saltzman, W. M. (1995). Distribution of nerve growth factor following direct delivery to brain interstitium. Brain Res, 680(1-2), 196-206.

Kroes, R. A., Dawson, G., & Moskal, J. R. (2007). Focused microarray analysis of glyco-gene expression in human glioblastomas. J Neurochem, 103 Suppl 1, 14-24.

Kroes, R. A., He, H., Emmett, M. R., Nilsson, C. L., Leach, F. E., Amster, I. J., et al. (2010). Overexpression of ST6GalNAcV, a ganglioside-specific alpha2,6-sialyltransferase, inhibits glioma growth in vivo. Proc Natl Acad Sci U S A, 107(28), 12646-12651.

Kroes, R. A., Panksepp, J., Burgdorf, J., Otto, N. J., & Moskal, J. R. (2006). Modeling depression: social dominance-submission gene expression patterns in rat neocortex. Neuroscience, 137(1), 37-49.

Laerum, O. D., Bjerkvig, R., Steinsvåg, S. K., & de Ridder, L. (1984). Invasiveness of primary brain tumors. Cancer Metastasis Rev, 3(3), 223-236.

Lal, S., Lacroix, M., Tofilon, P., Fuller, G. N., Sawaya, R., & Lang, F. F. (2000). An implantable guide-screw system for brain tumor studies in small animals. J Neurosurg, 92(2), 326-333.

Lang, F. F., Bruner, J. M., Fuller, G. N., Aldape, K., Prados, M. D., Chang, S., et al. (2003). Phase I trial of adenovirus-mediated p53 gene therapy for recurrent glioma: biological and clinical results. J Clin Oncol, 21(13), 2508-2518.

Langbein, S., Zerilli, M., Zur Hausen, A., Staiger, W., Rensch-Boschert, K., Lukan, N., et al. (2006). Expression of transketolase TKTL1 predicts colon and urothelial cancer patient survival: Warburg effect reinterpreted. Br J Cancer, 94(4), 578-585.

Lapidot, T., Dar, A., & Kollet, O. (2005). How do stem cells find their way home? Blood, 106(6), 1901-1910.

Le Blanc, K., Rasmusson, I., Götherström, C., Seidel, C., Sundberg, B., Sundin, M., et al. (2004). Mesenchymal stem cells inhibit the expression of CD25 (interleukin-2 receptor) and CD38 on phytohaemagglutinin-activated lymphocytes. Scand J Immunol, 60(3), 307-315.

Le Blanc, K., Tammik, C., Rosendahl, K., Zetterberg, E., & Ringdén, O. (2003). HLA expression and immunologic properties of differentiated and undifferentiated mesenchymal stem cells. Exp Hematol, 31(10), 890-896.

Le Calvé, B., Rynkowski, M., Le Mercier, M., Bruyère, C., Lonez, C., Gras, T., et al. (2010). Long-term in vitro treatment of human glioblastoma cells with temozolomide increases resistance in vivo through up-regulation of GLUT transporter and aldo-keto reductase enzyme AKR1C expression. Neoplasia, 12(9), 727-739.

Lee, J., Kotliarova, S., Kotliarov, Y., Li, A., Su, Q., Donin, N. M., et al. (2006). Tumor stem cells derived from glioblastomas cultured in bFGF and EGF more closely mirror the phenotype and genotype of primary tumors than do serum-cultured cell lines. Cancer Cell, 9(5), 391-403.

Lee, O. K., Kuo, T. K., Chen, W. M., Lee, K. D., Hsieh, S. L., & Chen, T. H. (2004). Isolation of multipotent mesenchymal stem cells from umbilical cord blood. Blood, 103(5), 1669-1675.

Lepperdinger, G., Brunauer, R., Jamnig, A., Laschober, G., & Kassem, M. (2008). Controversial issue: is it safe to employ mesenchymal stem cells in cell-based therapies? Exp Gerontol, 43(11), 1018-1023.

Li, Y., Chopp, M., Chen, J., Wang, L., Gautam, S. C., Xu, Y. X., et al. (2000). Intrastriatal transplantation of bone marrow nonhematopoietic cells improves functional recovery after stroke in adult mice. J Cereb Blood Flow Metab, 20(9), 1311-1319.

Lichti, C. F., Liu, H., Shavkunov, A. S., Mostovenko, E., Sulman, E. P., Ezhilarasan, R., et al. (2014). Integrated chromosome 19 transcriptomic and proteomic data sets derived from glioma cancer stem-cell lines. J Proteome Res, 13(1), 191-199.

Lichti, C. F. e. a. (2014). Post-translational Modifications in the Human Proteome. In M.-V. G (Ed.), Genomics and Proteomics for Clinical Discovery and Development. (1 ed., pp. 101-136). Dordrecht: Springer Science and Business Media Dordrecht.

Liu, G., Yuan, X., Zeng, Z., Tunici, P., Ng, H., Abdulkadir, I. R., et al. (2006). Analysis of gene expression and chemoresistance of CD133+ cancer stem cells in glioblastoma. Mol Cancer, 5, 67.

Liu, X., Nie, H., Zhang, Y., Yao, Y., Maitikabili, A., Qu, Y., et al. (2013). Cell surface-specific N-glycan profiling in breast cancer. PLoS One, 8(8), e72704.

Louis, D. N., Ohgaki, H., Wiestler, O. D., Cavenee, W. K., Burger, P. C., Jouvet, A., et al. (2007). The 2007 WHO classification of tumours of the central nervous system. Acta Neuropathol, 114(2), 97-109.

Lunt, S. Y., & Vander Heiden, M. G. (2011). Aerobic glycolysis: meeting the metabolic requirements of cell proliferation. Annu Rev Cell Dev Biol, 27, 441-464.

Ma, J., Murphy, M., O'Dwyer, P. J., Berman, E., Reed, K., & Gallo, J. M. (2002). Biochemical changes associated with a multidrug-resistant phenotype of a human glioma cell line with temozolomide-acquired resistance. Biochem Pharmacol, 63(7), 1219-1228.

Mahmood, A., Lu, D., & Chopp, M. (2004). Marrow stromal cell transplantation after traumatic brain injury promotes cellular proliferation within the brain. Neurosurgery, 55(5), 1185-1193.

Mahmood, A., Lu, D., Wang, L., Li, Y., Lu, M., & Chopp, M. (2001). Treatment of traumatic brain injury in female rats with intravenous administration of bone marrow stromal cells. Neurosurgery, 49(5), 1196-1203; discussion 1203-1194.

Marcheselli, V. L., Hong, S., Lukiw, W. J., Tian, X. H., Gronert, K., Musto, A., et al. (2003). Novel docosanoids inhibit brain ischemia-reperfusion-mediated leukocyte infiltration and pro-inflammatory gene expression. J Biol Chem, 278(44), 43807-43817.

Mareschi, K., Biasin, E., Piacibello, W., Aglietta, M., Madon, E., & Fagioli, F. (2001). Isolation of human mesenchymal stem cells: bone marrow versus umbilical cord blood. Haematologica, 86(10), 1099-1100.

Marshall, S., Bacote, V., & Traxinger, R. R. (1991). Discovery of a metabolic pathway mediating glucose-induced desensitization of the glucose transport system. Role of hexosamine biosynthesis in the induction of insulin resistance. J Biol Chem, 266(8), 4706-4712.

Martin, D. D., Robbins, M. E., Spector, A. A., Wen, B. C., & Hussey, D. H. (1996). The fatty acid composition of human gliomas differs from that found in nonmalignant brain tissue. Lipids, 31(12), 1283-1288.

Matyash, V., Liebisch, G., Kurzchalia, T. V., Shevchenko, A., & Schwudke, D. (2008). Lipid extraction by methyl-tert-butyl ether for high-throughput lipidomics. J Lipid Res, 49(5), 1137-1146.

McComb, R. D., & Bigner, D. D. (1984). The biology of malignant gliomas--a comprehensive survey. Clin Neuropathol, 3(3), 93-106.

McGirt, M. J., Mukherjee, D., Chaichana, K. L., Than, K. D., Weingart, J. D., & Quinones-Hinojosa, A. (2009). Association of surgically acquired motor and language deficits on overall survival after resection of glioblastoma multiforme. Neurosurgery, 65(3), 463-469; discussion 469-470.

Meyer, J. S., & Quenzer, L. F. (2005). Psychopharmacology : drugs, the brain, and behavior. Sunderland, Mass.: Sinauer Associates.

Miletic, H., Fischer, Y., Litwak, S., Giroglou, T., Waerzeggers, Y., Winkeler, A., et al. (2007). Bystander killing of malignant glioma by bone marrow-derived tumor-infiltrating progenitor cells expressing a suicide gene. Mol Ther, 15(7), 1373-1381.

Minniti, G., Scaringi, C., Lanzetta, G., Terrenato, I., Esposito, V., Arcella, A., et al. (2014). Standard (60 Gy) or Short-Course (40 Gy) Irradiation Plus Concomitant and Adjuvant Temozolomide for Elderly Patients With Glioblastoma: A Propensity-Matched Analysis. Int J Radiat Oncol Biol Phys.

Mootha, V. K., Lindgren, C. M., Eriksson, K. F., Subramanian, A., Sihag, S., Lehar, J., et al. (2003). PGC-1alpha-responsive genes involved in oxidative phosphorylation are coordinately downregulated in human diabetes. Nat Genet, 34(3), 267-273.

Moser, B., & Loetscher, P. (2001). Lymphocyte traffic control by chemokines. Nat Immunol, 2(2), 123-128.

Moskal, J. R., Kroes, R. A., & Dawson, G. (2009). The glycobiology of brain tumors: disease relevance and therapeutic potential. Expert Rev Neurother, 9(10), 1529-1545.

Mostovenko, E., Deelder, A. M., & Palmblad, M. (2011). Protein expression dynamics during Escherichia coli glucose-lactose diauxie. BMC Microbiol, 11, 126.

Motaln, H., Schichor, C., & Lah, T. T. (2010). Human mesenchymal stem cells and their use in cell-based therapies. Cancer, 116(11), 2519-2530.

Mukherjee, P. K., Marcheselli, V. L., Serhan, C. N., & Bazan, N. G. (2004). Neuroprotectin D1: a docosahexaenoic acid-derived docosatriene protects human retinal pigment epithelial cells from oxidative stress. Proc Natl Acad Sci U S A, 101(22), 8491-8496.

Nakamizo, A., Marini, F., Amano, T., Khan, A., Studeny, M., Gumin, J., et al. (2005). Human bone marrow-derived mesenchymal stem cells in the treatment of gliomas. Cancer Res, 65(8), 3307-3318.

Nakamura, K., Ito, Y., Kawano, Y., Kurozumi, K., Kobune, M., Tsuda, H., et al. (2004). Antitumor effect of genetically engineered mesenchymal stem cells in a rat glioma model. Gene Ther, 11(14), 1155-1164.

Nduom, E. K., Hadjipanayis, C. G., & Van Meir, E. G. (2012). Glioblastoma cancer stem-like cells: implications for pathogenesis and treatment. Cancer J, 18(1), 100-106.

Neilson, K. A., Ali, N. A., Muralidharan, S., Mirzaei, M., Mariani, M., Assadourian, G., et al. (2011). Less label, more free: approaches in label-free quantitative mass spectrometry. Proteomics, 11(4), 535-553.

Network, C. G. A. R. (2008). Comprehensive genomic characterization defines human glioblastoma genes and core pathways. Nature, 455(7216), 1061-1068.

Newlands, E. S., Stevens, M. F., Wedge, S. R., Wheelhouse, R. T., & Brock, C. (1997). Temozolomide: a review of its discovery, chemical properties, pre-clinical development and clinical trials. Cancer Treat Rev, 23(1), 35-61.

Nieman, K. M., Kenny, H. A., Penicka, C. V., Ladanyi, A., Buell-Gutbrod, R., Zillhardt, M. R., et al. (2011). Adipocytes promote ovarian cancer metastasis and provide energy for rapid tumor growth. Nat Med, 17(11), 1498-1503.

Nilsson, C. L., Berven, F., Selheim, F., Liu, H., Moskal, J. R., Kroes, R. A., et al. (2013). Chromosome 19 annotations with disease speciation: a first report from the Global Research Consortium. J Proteome Res, 12(1), 135-150.

Nishida, S., Endo, N., Yamagiwa, H., Tanizawa, T., & Takahashi, H. E. (1999). Number of osteoprogenitor cells in human bone marrow markedly decreases after skeletal maturation. J Bone Miner Metab, 17(3), 171-177.

Norris, J. L., & Caprioli, R. M. (2013). Analysis of tissue specimens by matrix-assisted laser desorption/ionization imaging mass spectrometry in biological and clinical research. Chem Rev, 113(4), 2309-2342.

O'Brien, J. S., & Sampson, E. L. (1965). Fatty acid and fatty aldehyde composition of the major brain lipids in normal human gray matter, white matter, and myelin. J Lipid Res, 6(4), 545-551.

Oberg, A. L., & Vitek, O. (2009). Statistical design of quantitative mass spectrometry-based proteomic experiments. J Proteome Res, 8(5), 2144-2156.

Ogasawara, Y., Namai, T., Yoshino, F., Lee, M. C., & Ishii, K. (2007). Sialic acid is an essential moiety of mucin as a hydroxyl radical scavenger. FEBS Lett, 581(13), 2473-2477.

Ohgaki, H., & Kleihues, P. (2005). Population-based studies on incidence, survival rates, and genetic alterations in astrocytic and oligodendroglial gliomas. J Neuropathol Exp Neurol, 64(6), 479-489.

Ohtsubo, K., & Marth, J. D. (2006). Glycosylation in cellular mechanisms of health and disease. Cell, 126(5), 855-867.

Onoyama, Y., Abe, M., Yabumoto, E., Sakamoto, T., & Nishidai, T. (1976). Radiation therapy in the treatment of glioblastoma. AJR Am J Roentgenol, 126(3), 481-492.

Orlic, D., Kajstura, J., Chimenti, S., Jakoniuk, I., Anderson, S. M., Li, B., et al. (2001). Bone marrow cells regenerate infarcted myocardium. Nature, 410(6829), 701-705.

Ostrom, Q. T., Gittleman, H., Liao, P., Rouse, C., Chen, Y., Dowling, J., et al. (2014). CBTRUS Statistical Report: Primary Brain and Central Nervous System Tumors Diagnosed in the United States in 2007-2011. Neuro Oncol, 16 Suppl 4, iv1-iv63.

Pardridge, W. M. (2003). Blood-brain barrier drug targeting: the future of brain drug development. Mol Interv, 3(2), 90-105, 151.

Parsons, D. W., Jones, S., Zhang, X., Lin, J. C., Leary, R. J., Angenendt, P., et al. (2008). An integrated genomic analysis of human glioblastoma multiforme. Science, 321(5897), 1807-1812.

Pavlides, S., Whitaker-Menezes, D., Castello-Cros, R., Flomenberg, N., Witkiewicz, A. K., Frank, P. G., et al. (2009). The reverse Warburg effect: aerobic glycolysis in cancer associated fibroblasts and the tumor stroma. Cell Cycle, 8(23), 3984-4001.

Peddie, C. J., Blight, K., Wilson, E., Melia, C., Marrison, J., Carzaniga, R., et al. (2014). Correlative and integrated light and electron microscopy of in-resin GFP fluorescence, used to localise diacylglycerol in mammalian cells. Ultramicroscopy, 143, 3-14.

Pedersen, P. H., Edvardsen, K., Garcia-Cabrera, I., Mahesparan, R., Thorsen, J., Mathisen, B., et al. (1995). Migratory patterns of lac-z transfected human glioma cells in the rat brain. Int J Cancer, 62(6), 767-771.

Pegg, A. E. (1990). Mammalian O6-alkylguanine-DNA alkyltransferase: regulation and importance in response to alkylating carcinogenic and therapeutic agents. Cancer Res, 50(19), 6119-6129.

Perry, D. (2000). Patients' voices: the powerful sound in the stem cell debate. Science, 287(5457), 1423.

Phillips, H. S., Kharbanda, S., Chen, R., Forrest, W. F., Soriano, R. H., Wu, T. D., et al. (2006). Molecular subclasses of high-grade glioma predict prognosis, delineate a pattern of disease progression, and resemble stages in neurogenesis. Cancer Cell, 9(3), 157-173.

Pittenger, M. F., Mackay, A. M., Beck, S. C., Jaiswal, R. K., Douglas, R., Mosca, J. D., et al. (1999). Multilineage potential of adult human mesenchymal stem cells. Science, 284(5411), 143-147.

Pittenger, M. F., & Martin, B. J. (2004). Mesenchymal stem cells and their potential as cardiac therapeutics. Circ Res, 95(1), 9-20.

Ponte, A. L., Marais, E., Gallay, N., Langonné, A., Delorme, B., Hérault, O., et al. (2007). The in vitro migration capacity of human bone marrow mesenchymal stem cells: comparison of chemokine and growth factor chemotactic activities. Stem Cells, 25(7), 1737-1745.

Puchades, M., Nilsson, C. L., Emmett, M. R., Aldape, K. D., Ji, Y., Lang, F. F., et al. (2007). Proteomic investigation of glioblastoma cell lines treated with wild-type p53 and cytotoxic chemotherapy demonstrates an association between galectin-1 and p53 expression. J Proteome Res, 6(2), 869-875.

Quehenberger, O., Armando, A. M., Brown, A. H., Milne, S. B., Myers, D. S., Merrill, A. H., et al. (2010). Lipidomics reveals a remarkable diversity of lipids in human plasma. J Lipid Res, 51(11), 3299-3305.

Rebelatto, C. K., Aguiar, A. M., Moretão, M. P., Senegaglia, A. C., Hansen, P., Barchiki, F., et al. (2008). Dissimilar differentiation of mesenchymal stem cells from bone marrow, umbilical cord blood, and adipose tissue. Exp Biol Med (Maywood), 233(7), 901-913.

Reya, T., Morrison, S. J., Clarke, M. F., & Weissman, I. L. (2001). Stem cells, cancer, and cancer stem cells. Nature, 414(6859), 105-111.

Rong, Y., Durden, D. L., Van Meir, E. G., & Brat, D. J. (2006). 'Pseudopalisading' necrosis in glioblastoma: a familiar morphologic feature that links vascular pathology, hypoxia, and angiogenesis. J Neuropathol Exp Neurol, 65(6), 529-539.

Rutka, J. T., Apodaca, G., Stern, R., & Rosenblum, M. (1988). The extracellular matrix of the central and peripheral nervous systems: structure and function. J Neurosurg, 69(2), 155-170.

Rüster, B., Göttig, S., Ludwig, R. J., Bistrian, R., Müller, S., Seifried, E., et al. (2006). Mesenchymal stem cells display coordinated rolling and adhesion behavior on endothelial cells. Blood, 108(12), 3938-3944.

Salazar, O. M., & Rubin, P. (1976). The spread of glioblastoma multiforme as a determining factor in the radiation treated volume. Int J Radiat Oncol Biol Phys, 1(7-8), 627-637.

Santos, C. R., & Schulze, A. (2012). Lipid metabolism in cancer. FEBS J, 279(15), 2610-2623.

Sawaya, R., Hammoud, M., Schoppa, D., Hess, K. R., Wu, S. Z., Shi, W. M., et al. (1998). Neurosurgical outcomes in a modern series of 400 craniotomies for treatment of parenchymal tumors. Neurosurgery, 42(5), 1044-1055; discussion 1055-1046.

Scherer, H. J. (1940). The forms of growth in gliomas and their practical significance. Brain, 63, 1-35.

Schmidt, A., Ladage, D., Steingen, C., Brixius, K., Schinköthe, T., Klinz, F. J., et al. (2006). Mesenchymal stem cells transmigrate over the endothelial barrier. Eur J Cell Biol, 85(11), 1179-1188.

Schreck, R., Rieber, P., & Baeuerle, P. A. (1991). Reactive oxygen intermediates as apparently widely used messengers in the activation of the NF-kappa B transcription factor and HIV-1. EMBO J, 10(8), 2247-2258.

Schultz, M. J., Swindall, A. F., & Bellis, S. L. (2012). Regulation of the metastatic cell phenotype by sialylated glycans. Cancer Metastasis Rev, 31(3-4), 501-518.

Schulze, W. X., & Usadel, B. (2010). Quantitation in mass-spectrometry-based proteomics. Annu Rev Plant Biol, 61, 491-516.

Schwab, J. M., Chiang, N., Arita, M., & Serhan, C. N. (2007). Resolvin E1 and protectin D1 activate inflammation-resolution programmes. Nature, 447(7146), 869-874.

Scott, D. W., & Patel, R. P. (2013). Endothelial heterogeneity and adhesion molecules N-glycosylation: implications in leukocyte trafficking in inflammation. Glycobiology, 23(6), 622-633.

Segers, V. F., Van Riet, I., Andries, L. J., Lemmens, K., Demolder, M. J., De Becker, A. J., et al. (2006). Mesenchymal stem cell adhesion to cardiac microvascular endothelium: activators and mechanisms. Am J Physiol Heart Circ Physiol, 290(4), H1370-1377.

Selker, R. G., Shapiro, W. R., Burger, P., Blackwood, M. S., Arena, V. C., Gilder, J. C., et al. (2002). The Brain Tumor Cooperative Group NIH Trial 87-01: a randomized comparison of surgery, external radiotherapy, and carmustine versus surgery, interstitial radiotherapy boost, external radiation therapy, and carmustine. Neurosurgery, 51(2), 343-355; discussion 355-347.

Serrano, M., Hannon, G. J., & Beach, D. (1993). A new regulatory motif in cell-cycle control causing specific inhibition of cyclin D/CDK4. Nature, 366(6456), 704-707.

Sethi, M. K., Thaysen-Andersen, M., Smith, J. T., Baker, M. S., Packer, N. H., Hancock, W. S., et al. (2014). Comparative N-glycan profiling of colorectal cancer cell lines reveals unique bisecting GlcNAc and α-2,3-linked sialic acid determinants are associated with membrane proteins of the more metastatic/aggressive cell lines. J Proteome Res, 13(1), 277-288.

Shavkunov, A. S., Wildburger, N. C., Nenov, M. N., James, T. F., Buzhdygan, T. P., Panova-Elektronova, N. I., et al. (2013). The fibroblast growth factor 14·voltage-gated sodium channel complex is a new target of glycogen synthase kinase 3 (GSK3). J Biol Chem, 288(27), 19370-19385.

Shaw, E., Arusell, R., Scheithauer, B., O'Fallon, J., O'Neill, B., Dinapoli, R., et al. (2002). Prospective randomized trial of low- versus high-dose radiation therapy in adults with supratentorial low-grade glioma: initial report of a North Central Cancer Treatment Group/Radiation Therapy Oncology Group/Eastern Cooperative Oncology Group study. J Clin Oncol, 20(9), 2267-2276.

Shinojima, N., Hossain, A., Takezaki, T., Fueyo, J., Gumin, J., Gao, F., et al. (2013). TGF-β mediates homing of bone marrow-derived human mesenchymal stem cells to glioma stem cells. Cancer Res, 73(7), 2333-2344.

Shulga, Y. V., Topham, M. K., & Epand, R. M. (2011). Regulation and functions of diacylglycerol kinases. Chem Rev, 111(10), 6186-6208.

Siegel, G., Kluba, T., Hermanutz-Klein, U., Bieback, K., Northoff, H., & Schäfer, R. (2013). Phenotype, donor age and gender affect function of human bone marrow-derived mesenchymal stromal cells. BMC Med, 11, 146.

Singh, S. K., Clarke, I. D., Terasaki, M., Bonn, V. E., Hawkins, C., Squire, J., et al. (2003). Identification of a cancer stem cell in human brain tumors. Cancer Res, 63(18), 5821-5828.

Singh, S. K., Hawkins, C., Clarke, I. D., Squire, J. A., Bayani, J., Hide, T., et al. (2004). Identification of human brain tumour initiating cells. Nature, 432(7015), 396-401.

Son, B. R., Marquez-Curtis, L. A., Kucia, M., Wysoczynski, M., Turner, A. R., Ratajczak, J., et al. (2006). Migration of bone marrow and cord blood mesenchymal stem cells in vitro is regulated by stromal-derived factor-1-CXCR4 and hepatocyte growth factor-c-met axes and involves matrix metalloproteinases. Stem Cells, 24(5), 1254-1264.

Sowers, J. L., Johnson, K. M., Conrad, C., Patterson, J. T., & Sowers, L. C. (2014). The role of inflammation in brain cancer. Adv Exp Med Biol, 816, 75-105.

Steingen, C., Brenig, F., Baumgartner, L., Schmidt, J., Schmidt, A., & Bloch, W. (2008). Characterization of key mechanisms in transmigration and invasion of mesenchymal stem cells. J Mol Cell Cardiol, 44(6), 1072-1084.

Stenderup, K., Justesen, J., Clausen, C., & Kassem, M. (2003). Aging is associated with decreased maximal life span and accelerated senescence of bone marrow stromal cells. Bone, 33(6), 919-926.

Stevens, M. F., & Newlands, E. S. (1993). From triazines and triazenes to temozolomide. Eur J Cancer, 29A(7), 1045-1047.

Studeny, M., Marini, F. C., Champlin, R. E., Zompetta, C., Fidler, I. J., & Andreeff, M. (2002). Bone marrow-derived mesenchymal stem cells as vehicles for interferon-beta delivery into tumors. Cancer Res, 62(13), 3603-3608.

Studeny, M., Marini, F. C., Dembinski, J. L., Zompetta, C., Cabreira-Hansen, M., Bekele, B. N., et al. (2004). Mesenchymal stem cells: potential precursors for tumor stroma and targeted-delivery vehicles for anticancer agents. J Natl Cancer Inst, 96(21), 1593-1603.

Stupp, R., Hegi, M.E., Gilbert, M.R., & Chakravarti, A. (2007). Chemoradiotherapy in malignant glioma: standard of care and future directions. J Clin Oncol, 25(26), 4127-3416.

Stupp, R., Hegi, M. E., van den Bent, M. J., Mason, W. P., Weller, M., Mirimanoff, R. O., et al. (2006). Changing paradigms--an update on the multidisciplinary management of malignant glioma. Oncologist, 11(2), 165-180.

Stupp, R., Mason, W. P., van den Bent, M. J., Weller, M., Fisher, B., Taphoorn, M. J., et al. (2005). Radiotherapy plus concomitant and adjuvant temozolomide for glioblastoma. N Engl J Med, 352(10), 987-996.

Subramanian, A., Tamayo, P., Mootha, V. K., Mukherjee, S., Ebert, B. L., Gillette, M. A., et al. (2005). Gene set enrichment analysis: a knowledge-based approach for interpreting genome-wide expression profiles. Proc Natl Acad Sci U S A, 102(43), 15545-15550.

Svennerholm, L. (1968). Distribution and fatty acid composition of phosphoglycerides in normal human brain. J Lipid Res, 9(5), 570-579.

Tsai, T. H., Wang, M., Di Poto, C., Hu, Y., Zhou, S., Zhao, Y., et al. (2014). LC-MS profiling of N-Glycans derived from human serum samples for biomarker discovery in hepatocellular carcinoma. J Proteome Res, 13(11), 4859-4868.

Tsao, M. N., Mehta, M. P., Whelan, T. J., Morris, D. E., Hayman, J. A., Flickinger, J. C., et al. (2005). The American Society for Therapeutic Radiology and Oncology (ASTRO) evidence-based review of the role of radiosurgery for malignant glioma. Int J Radiat Oncol Biol Phys, 63(1), 47-55.

Tusher, V. G., Tibshirani, R., & Chu, G. (2001). Significance analysis of microarrays applied to the ionizing radiation response. Proc Natl Acad Sci U S A, 98(9), 5116-5121.

Ueki, K., Ono, Y., Henson, J. W., Efird, J. T., von Deimling, A., & Louis, D. N. (1996). CDKN2/p16 or RB alterations occur in the majority of glioblastomas and are inversely correlated. Cancer Res, 56(1), 150-153.

Ujifuku, K., Mitsutake, N., Takakura, S., Matsuse, M., Saenko, V., Suzuki, K., et al. (2010). miR-195, miR-455-3p and miR-10a(*) are implicated in acquired temozolomide resistance in glioblastoma multiforme cells. Cancer Lett, 296(2), 241-248.

van Meer, G., Voelker, D. R., & Feigenson, G. W. (2008). Membrane lipids: where they are and how they behave. Nat Rev Mol Cell Biol, 9(2), 112-124.

Vander Heiden, M. G., Cantley, L. C., & Thompson, C. B. (2009). Understanding the Warburg effect: the metabolic requirements of cell proliferation. Science, 324(5930), 1029-1033.

Varki, A. (1993). Biological roles of oligosaccharides: all of the theories are correct. Glycobiology, 3(2), 97-130.

Varki, A. (2009). Essentials of glycobiology (2nd ed.). Cold Spring Harbor, N.Y.: Cold Spring Harbor Laboratory Press.

Verhaak, R. G., Hoadley, K. A., Purdom, E., Wang, V., Qi, Y., Wilkerson, M. D., et al. (2010). Integrated genomic analysis identifies clinically relevant subtypes of glioblastoma characterized by abnormalities in PDGFRA, IDH1, EGFR, and NF1. Cancer Cell, 17(1), 98-110.

Vizcaíno, J. A., Côté, R. G., Csordas, A., Dianes, J. A., Fabregat, A., Foster, J. M., et al. (2013). The PRoteomics IDEntifications (PRIDE) database and associated tools: status in 2013. Nucleic Acids Res, 41(Database issue), D1063-1069.

Wang, X., Devaiah, S. P., Zhang, W., & Welti, R. (2006). Signaling functions of phosphatidic acid. Prog Lipid Res, 45(3), 250-278.

Warburg, O. (1925). Uber den Stoffwechsel der Carcinomzelle. Klin. Wochenschr., 4, 534–536.

Warburg, O. (1956). On the origin of cancer cells. Science, 123(3191), 309-314.

Wedge, S. R., Porteous, J. K., Glaser, M. G., Marcus, K., & Newlands, E. S. (1997). In vitro evaluation of temozolomide combined with X-irradiation. Anticancer Drugs, 8(1), 92-97.

Wellen, K. E., & Thompson, C. B. (2012). A two-way street: reciprocal regulation of metabolism and signalling. Nat Rev Mol Cell Biol, 13(4), 270-276.

Wesseling, P., Ruiter, D. J., & Burger, P. C. (1997). Angiogenesis in brain tumors; pathobiological and clinical aspects. J Neurooncol, 32(3), 253-265.

Wexler, S. A., Donaldson, C., Denning-Kendall, P., Rice, C., Bradley, B., & Hows, J. M. (2003). Adult bone marrow is a rich source of human mesenchymal 'stem' cells but umbilical cord and mobilized adult blood are not. Br J Haematol, 121(2), 368-374.

Wildburger, N. C., Ali, S. R., Hsu, W. C., Shavkunov, A. S., Nenov, M. N., Lichti, C. F., et al. (2015). Quantitative proteomics reveals protein-protein interactions with fibroblast growth factor 12 as a component of the voltage-gated sodium channel 1.2 (nav1.2) macromolecular complex in Mammalian brain. Mol Cell Proteomics, 14(5), 1288-1300.

Wildburger, N. C., Lichti, C.F., LeDuc, R.D., Schmidt, M., Kroes, R.A., Moskal, J.R., and Nilsson, C.L. (2015). Quantitative Proteomics and Transcriptomics Reveals Metabolic Differences in Homing and Non-Homing Human Glioma Stem Cell Xenografts and Stromal Cells. EuPa Open Proteomics, *Accepted with Revisions.*

Wildburger, N. C., Wood, P. L., Gumin, J., Lichti, C. F., Emmett, M. R., Lang, F. F., et al. (2015). ESI-MS/MS and MALDI-IMS Localization Reveal Alterations in Phosphatidic Acid, Diacylglycerol, and DHA in Glioma Stem Cell Xenografts. J Proteome Res, *In Press.*

Wood, P. L. (2012). Lipidomics of Alzheimer's disease: current status. Alzheimers Res Ther, 4(1), 5.

Wood, P. L. & Shirley, N.R. (2013). Lipidomics Analysis of Postmortem Interval: Preliminary Evaluation of Human Skeletal Muscle. Metabolomics, 3, 127.

Wright, R. D., & Cooper, D. (2014). Glycobiology of leukocyte trafficking in inflammation. Glycobiology, 24(12), 1242-1251.

Wu, G. D., Nolta, J. A., Jin, Y. S., Barr, M. L., Yu, H., Starnes, V. A., et al. (2003). Migration of mesenchymal stem cells to heart allografts during chronic rejection. Transplantation, 75(5), 679-685.

Xie, Q., Mittal, S., & Berens, M. E. (2014). Targeting adaptive glioblastoma: an overview of proliferation and invasion. Neuro Oncol, 16(12), 1575-1584.

Yang, W. S., Chang, J. W., Han, N. J., & Park, S. K. (2011). Darbepoetin alfa suppresses tumor necrosis factor-α-induced endothelin-1 production through antioxidant action in human aortic endothelial cells: role of sialic acid residues. Free Radic Biol Med, 50(10), 1242-1251.

Yasuda, J., Eguchi, H., Fujiwara, N., Ookawara, T., Kojima, S., Yamaguchi, Y., et al. (2006). Reactive oxygen species modify oligosaccharides of glycoproteins in vivo: a study of a spontaneous acute hepatitis model rat (LEC rat). Biochem Biophys Res Commun, 342(1), 127-134.

Yong, R. L., Shinojima, N., Fueyo, J., Gumin, J., Vecil, G. G., Marini, F. C., et al. (2009). Human bone marrow-derived mesenchymal stem cells for intravascular delivery of oncolytic adenovirus Delta24-RGD to human gliomas. Cancer Res, 69(23), 8932-8940.

Young, F. E. (2000). A time for restraint. Science, 287(5457), 1424.

Yu, C. Y., Mayampurath, A., Hu, Y., Zhou, S., Mechref, Y., & Tang, H. (2013). Automated annotation and quantification of glycans using liquid chromatography-mass spectrometry. Bioinformatics, 29(13), 1706-1707.

Yuan, X., Curtin, J., Xiong, Y., Liu, G., Waschsmann-Hogiu, S., Farkas, D. L., et al. (2004). Isolation of cancer stem cells from adult glioblastoma multiforme. Oncogene, 23(58), 9392-9400.

Zhang, J., Stevens, M. F., Laughton, C. A., Madhusudan, S., & Bradshaw, T. D. (2010). Acquired resistance to temozolomide in glioma cell lines: molecular mechanisms and potential translational applications. Oncology, 78(2), 103-114.

Zhang, W., Ge, W., Li, C., You, S., Liao, L., Han, Q., et al. (2004). Effects of mesenchymal stem cells on differentiation, maturation, and function of human monocyte-derived dendritic cells. Stem Cells Dev, 13(3), 263-271.

Zhang, W., Trachootham, D., Liu, J., Chen, G., Pelicano, H., Garcia-Prieto, C., et al. (2012). Stromal control of cystine metabolism promotes cancer cell survival in chronic lymphocytic leukaemia. Nat Cell Biol, 14(3), 276-286.

Zhuo, Y., & Bellis, S. L. (2011). Emerging role of alpha2,6-sialic acid as a negative regulator of galectin binding and function. J Biol Chem, 286(8), 5935-5941.

Zülch, K. J. (1979). Histological typing of tumours of the central nervous system. Geneva: World Health Organization.

VITA

Norelle Christine Wildburger was born on March 27th 1988 in Dallas, Texas. She is the daughter of Hans Anton and Susan Marie Wildburger. She obtained a Bachelor of Science in Neuroscience from Baylor University *magna cum laude* in May of 2010. In August 2010 she enrolled in the Neuroscience Graduate Program at the University of Texas Medical Branch Galveston to begin her doctoral research. Norelle is the recipient of the 2014 UTMB Team Award and the 2015 Dr. and Mrs. Seymour Fisher Academic Excellence Award in Neuroscience.

EDUCATION

B.Sc. Neuroscience, May 2010, Baylor University, Waco, Texas

- Minors in Biology and Classics
- Graduate of the Baylor Interdisciplinary Core (BIC) program of the Baylor Honors College

PUBLICATIONS

1. **Wildburger, N.C.**, Wood, P.L., Gumin, J., LeDuc, D.R., Lichti, C.F., Emmett, M.R., Lang, F.F., and Nilsson, C.L. ESI-MS/MS and MALDI-IMS Localization Reveal Alterations in Phosphatidic Acid, Diacylglycerol, and DHA in Glioma Stem Cell Xenografts. *Journal of Proteome Research, In Press.*

2. **Wildburger, N.C.**, Ali, S.R., Hsu, W-C.J., Shavkunov, A.S., Nenov, M.N., Lichti, C.F., LeDuc, R.D., Mostovenko, E., Panova-Elektronova, N., Emmett, M.R., Nilsson, C.L., and Fernanda Laezza. Quantitative Proteomics Reveals Protein-Protein Interactions with Fibroblast Growth Factor12 as a Component of the Nav1.2 Macromolecular Complex in Mammalian Brain. *Molecular and Cellular Proteomics*, 14, 1288-1300.

3. James, T.F., Nenov, M.N., **Wildburger, N.C.,** Lichti, C.F., Luisi, J., Vergara, F., Panova-Elektronova, N.I., Nilsson C.L., Rudra, J., Green, T.A., Labate, D., and Laezza, F. (2015). The Nav1.2 channel is regulated by GSK3. *Biochim Biophys Acta,* 1850, 832-844.

4. Lichti, C.F., **Wildburger, N.C**., Emmett, M.R., Mostovenko, E., Shavkunov, A.S., et al. Genomics and Proteomics for Clinical Discovery and Development. 1 ed. Marko-Varga G, editor. Dordrecht: Springer Science and Business Media Dordrecht; 2014. Chapter 6, Post-translational Modifications in the Human Proteome; p.101-136.

5. *Shavkunov, A.S, ***Wildburger, N.C.**, Buzhgyan, T., Panova, N. Veselenak, R., Bourne, N., and Laezza, F. (2013). The Fibroblast Growth Factor14:Voltage-gated Sodium Channel

Complex is a New Target of Glycogen Synthase Kinase 3 (GSK3). *Journal of Biological Chemistry*, 288, 19370-19385.

*These authors contributed equally

6. **Wildburger, N.C.** & Laezza, F.L. (2012). Control of neuronal ion channel function by glycogen synthase kinase-3: new prospective for an old kinase. *Frontiers in Molecular Neuroscience*. 5:80.

7. **Wildburger, N.C.**, Lin-Ye, A., Baird, M.A., Lei, D., and Bao. J. (2009). Neuroprotective effects of blockers for T-type calcium channels. *Molecular Neurodegeneration*; doi:10.1186/1750-1326-4-44.